Thesis
Graduation research Structural Engineering - Concrete structures

Analysis of the capacity of a reinforcement detail in a soil-mix wall

An experimental and numerical approach

Author:
BSc. I. Dik

University supervisors:
Prof.dr.ir. D.A. Hordijk
Dr.ir.drs. C.R. Braam
Dr.ir. P.C.J. Hoogenboom

Company supervisors:
Ir. J. Meijdam
Ir. J.C.P. van Bezooijen

September 15, 2017

TU Delft

DURA VERMEER

Preface

This thesis is the result of the graduation research performed for the master of Structural Engineering, specialization Concrete Structures, of the faculty of Civil Engineering at the Technical University of Delft. The research is facilitated by Dura Vermeer and supported by the TU Delft. Additionally guidance has been provided by Nicolas Denies, Flor de Cock, Bart Lameire and Noël Huybrechts from the Wetenschappelijk en Technisch Centrum voor het Bouwbedrijf (WTCB) and the Belgische Vereniging Aannemers Funderinswerken (ABEF) during the literature study.
The testing phase consisted of physical tests on two sets of samples. The tests were performed on drilled cores provided by Winmix BV and on a batch of lab made samples. These tests were assisted by Maiko van Leeuwem, Ton Blom and Albert Bosman.
For the modelling phase finite element software Atena was used. Atena is a software developed by Cervenka Consulting and is often used for modelling of reinforced concrete structures. Yuguang Yang has provided helpful support on the use of the software.
Regular guidance was given by company supervisors Jeroen Meijdam and Joost van Bezooijen. Aside from advice and insights on the content of the research they provide the required hardware to be able run the software properly.
Prof.dr.ir. D.A. Hordijk, dr.ir.drs. C.R. Braam and Dr.ir. P.C.J. Hoogenboom have supported the project as university supervisors.

September 15, 2017

Inge Dik

Abstract

Soil-mix walls are subsoil walls, which are constructed by in situ mixing of soil with cement and water. The technique was initially used as a ground improvement technique and is now being developed as construction method for walls with a structural purpose. Currently these walls are reinforced with large steel profiles, which requires a large quantity of steel. Replacing the profiles with bar reinforcement might lead to a decrease in required material quantity and thus a reduction of material costs.

There are multiple aspects which influence the possibilities and limitations of bar reinforced soil-mix walls. These include predictability of the material quality, durability and cooperation between soil-mix and the reinforcement. The aim of this project was to contribute to this research by analysing one of the influential aspects. The specific goal of this research project was to analyse the capacity of a reinforcement detail within a soil-mix wall and define the governing failure mechanism. The research combined an experimental and numerical approach to the subject.

The critical detail was chosen based on the Huybrechts et al. (2016), Ganne et al. (2010), Dörendahl et al. (2004) and contact with soil-mix experts. To model this detail in a finite element model, in 2D and 3D, material parameters were derived from Denies et al. (2012a), Denies et al. (2014), Denies et al. (2015a) and performed physical tests. The 2D models represented the most critical sections of the detail based on the theoretical stress distribution. The geometrical parameters of the reinforcement design were varied in the models to provide insight in the influence of the design on the capacity.

The model results were used to define an preliminary set of design guidelines for the reinforcement cage, related to the depth of the wall. Since only the capacity of the detail is considered, these guidelines are not sufficient for a complete design of a bar reinforced soil-mix wall and can only serve as an initial indication.

In conclusion, the reinforcement detail is most sensitive to failure due to vertical splitting and has sufficient capacity for acceptable wall depths. As stated before there are multiple aspects relevant to the feasibility of bar reinforced soil-mix walls. The predictability of the material quality, the bond with the reinforcement and the durability of the soil-mix strongly influence the final capacity and behaviour of the wall. Therefore it is important to perform further research on these, and other, aspects to conclude on the total structural integrity of an entire bar reinforced soil-mix wall.

Contents

List of Figures

List of Tables

1

Introduction

The context of this graduation research was suggested by Dura Vermeer, the research objective within this context was specified further in collaboration with the TU Delft. The soil-mix technique is an interesting subject for a contractor like Dura Vermeer. The application of this technique is still relatively new and Dura Vermeer has only done a few projects where this technique has been applied. Gaining more insight in the method and possible improvements, could be beneficial.
From a scientific perspective it is interesting to get acquainted with a new technique and simultaneously contribute to the development of the construction method. Considering the novelty of the soil-mix technique, the expectation is that there is plenty of room for improvements and new findings.
This thesis report provides the reader with background information on the soil-mix technique and will elaborate on the relevance of the research that has been conducted over the past months. Starting with a summary of the current knowledge on the technique in chapter 2 the reader will get acquainted with the soil-mix technique.
The research was divided into two main phases, the testing phase and the modelling phase. The purpose of the testing phase was to gain more insight in the properties of soil-mix material. The information acquired during the testing phase combined with the data available from the literature study provided knowledge required to create a material model which could represent the behaviour of soil-mix in a finite element model.
The aim, method and results of the testing phase are described in chapter 3. The incorporation of the test results into the model are addressed in chapter 4. Subsequently chapter 4 elaborates on the set-up of the models and the relevant results. The results are translated to preliminary design guidelines in section 4.5. Chapter 5 addresses the discussion points of the research methods and the results. Chapter 6 summarizes the conclusions of the research and provides the answers to the research questions. The final chapter, chapter 7, suggests subjects for follow up research.
The appendices support the report with additional information on the modelling software, the model input, testing procedure and the results.

1.1 Scope

When introducing a new technique there is always room for improvement. For example: increase quality, decrease costs, simplify the construction procedure, increase durability and so on. Every aspect of the technique should be optimized where possible, the optimization is an ongoing process. This research aims to contribute to the improvement of the soil-mix technique by analysing an alternative way of reinforcement: bar reinforcement. In concrete structures bar reinforcement is the most common type of reinforcement, but its application in soil-mix walls has not yet been researched. Currently CSM walls are typically reinforced with steel IPE or HEA profiles. Multiple parties (Dura Vermeer, WTCB & ABEF) have shown interest in the possibilities with bar reinforced CSM walls. When considering the application of bar reinforcement in CSM walls, multiple aspects are of relevance:

- Force transfer at reinforcement details
- Bond between steel and soil-mix
- Influence of local weaknesses
- Durability of the soil-mix
- Property range of the soil-mix

The feasibility of bar reinforced soil-mix walls depends on these and other aspects. This research focussed on the force transfer between the soil-mix and steel at the reinforcement details.
When reinforced with steel profiles the compression stresses in the soil-mix are able to transfer to continuous flanges of the steel profiles along the entire height of the walls. Bar reinforcement solely provides these stresses with the support of slender longitudinal reinforcement bars and the discretely distributed stirrups along the height. Due to the slender reinforcement and the reduced presence of steel in the structure the forces will be distributed differently throughout the structure. The main point of concern is the corner of the reinforcement stirrup. This corner, or node is where the compressive stresses are transferred to the reinforcement bars. This corner is further referred to as 'the detail'. Due to the discretely distributed stirrups the orientation of the stresses reaching the detail are not only tilted in the horizontal plane (compression arc), they also have a vertical component (compression diagonal). Toward the detail these stresses are redistributed to concentrated stresses around the reinforcement. The force transfer within the wall is described in more detail in chapter 2. The capacity of this detail is crucial to the structural integrity of the entire structure, which is the foundation for the research questions.

Research question

What is the capacity a reinforcement detail in a bar reinforced soil-mix wall?

Sub-questions

Which sections of the detail are critical for the capacity of the detail?

What material parameters should be used to model the behaviour of soil-mix material with a finite element model?

How can the geometry of the detail and the loading configuration on the detail be represented in a finite element model?

Is it possible to derive design guidelines from the model?

The goal of the research was to analyse the capacity of the reinforcement detail. The maximum capacity was then used to provide limits on the loading configurations a soil-mix wall may be subject to when reinforced with bar reinforcement. This is related to the depth of the wall. Guidelines for this exterior dimension are valuable for further research in relation to the feasibility and advantages of soil-mix walls with bar reinforcement. Additionally guidelines have been drafted for the reinforcement design of a soil-mix wall related to the depth limitations. The guidelines address the spacing between the bars, the length of the stirrups and the radius of curvature at the corners.

To answer the main research question, several sub-questions were drafted.
First of all it is important to analyse the theoretical force distribution in the wall. Based on this analysis

the first sub-question can be addressed. How are the forces transferred near the detail and which sections are the most critical? This question is answered in chapter 2
The second question is related to the representation of soil-mix in a finite element model. To accurately represent its behaviour, the material model should be based on the correct parameters. These parameters are partially based on available literature (Denies et al., 2012a), (Denies et al., 2015a), (Denies et al., 2014) and are complemented by data acquired from multiple tests performed for the purpose of this research, described in chapter 3.
Accurately modelling the behaviour of a detail is dependent on the input parameters of the material and the geometry. Other large influences are the applied load configuration and the defined boundary conditions. The load configuration has to be a valid simplification of the actual load stress distribution in the wall, this concerns the dimension of the loading plane, the orientation and the magnitude of the applied load. These quantities have been determined based on acceptable ranges of the relevant dimensions. These dimensions being the depth of the wall, the weight of the soil-mix and the dimensions of the reinforcement stirrups. The boundary conditions have to represent the restrictions provided by the reinforcement and the surrounding soil-mix material. The set-up and the results of the modelling phase are addressed in chapter 4.
The model results are used to find the stress trajectories in the detail, determine the failure load and analyse the crack development. By varying multiple parameters of the model geometrically, the results are used to draft preliminary design guidelines for bar reinforced soil-mix walls. These guidelines can be found in section 4.5.

1.2 Relevance

Recently the application of soil-mix walls has increased significantly. The use of this technique originated from soil improvement techniques and is being developed to serve structural purposes as well. In 2016 a group of Belgian and Dutch researchers and engineers developed a set of guidelines for the design and construction of soil-mix walls (Huybrechts et al., 2016). These guidelines focus on soil-mix walls reinforced with large steel profiles (IPE or HEA). These profiles are extremely stiff and can carry the entire load acting on the wall. The soil-mix acts as a medium to transfer the soil and water pressures to the steel elements. By using such steel profiles as reinforcement, the strength and stiffness of the structure is easily guaranteed. However, it might be a significant over-dimensioning of the structure.

As stated previously this research focussed on the application of bar reinforcement in soil-mix walls, instead of the currently applied profile reinforcement. The expectation is that, if bar reinforcement proves to be a suitable method of reinforcing soil-mix walls, the amount of steel in soil-mix walls and thus the material costs can be reduced significantly. To support this hypothesis, a comparison has been made between the theoretical capacity of bar reinforced soil-mix panels and the (experimental) capacity of profile reinforced soil-mix panels, (Denies et al., 2015a) and (Denies et al., 2015c). The comparison was made for both for bending and shear forces.
The theoretical bending capacity of the bar reinforced wall is determined by using the well known formula for concrete structures loaded in pure bending, equation 1.1 and 1.2. Figure 1.1 provides a visualization of the method used for the determination of the theoretical bending moment capacity. For durability considerations the concrete cover is chosen to be relatively high (50 mm). A larger coverage reduces the risk of cracks reaching the reinforcement bars.

$$N_{sm} = \alpha X_u b \frac{f_{cd}}{\gamma_m} \tag{1.1}$$

$$M_{Rd,max} = (d - \beta X_u) N_{sm} \tag{1.2}$$

With:

N_{sm}	Force capacity of the soil-mix compression zone [kN]
α	Factor to account for non-uniform stress distribution (0.75) [-]
X_u	Height compression zone [mm]
b	Width compression zone [mm]
$\frac{f_{cd}}{\gamma_m}$	Characteristic compressive strength soil-mix [MPa]

$M_{Rd,max}$ Bending moment capacity [kNm]
d Effective depth wall (total depth minus (cover - 0.5ϕ)) [mm]
β Distance factor (0.39) [-]

As shown in table 1.1 the bending capacities found by the experiments done by Denies et al. (2015a), Denies et al. (2015c) and Denies et al. (2015b) are met when using bar reinforcement, even with a lower amount of steel per stretching meter.

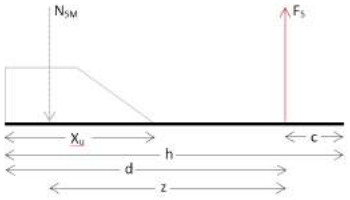

Figure 1.1: Visualisation of bending moment capacity calculation method

Table 1.1: Quantification of the amount of steel used with bar reinforcement and profile reinforcement with similar bending moment capacities per stretching meters

	Bar reinforcement (Theoretical values)			*Profile reinforcement (experimental values)*[1]			*Ratio bar/profile*	
$f_{cd}[MPa]$	N_{sm} $[kN]$	$M_{Rd,max}$ $[kNm]$	A_s $[mm^2]$	**Type**	$M_{Rd,max}$ $[kNm]$	A_s $[mm^2]$	M_{Rd}%	A_s%
2	224	92.4	515	IPE240	82.1	3910	113%	26%
4	448	184.9	1030	IPE330	186.5	6260	99%	33%
6	672	277.3	1546	IPE360	242.0	7270	115%	43%
7	862	348.3	1984	HEA240	246.9	7680	141%	52%
8	896	369.7	2061	IPE400	340.2	8450	109%	49%

Table 1.2: Quantified amount of shear reinforcement to account for shear forces compared to the capacity of the steel profiles

	Profile reinforcement (Theoretical values)			*Bar reinforcement (Theoretical values for 10 mm bars)*		*Ratio bar/profile*
$f_{cd}[MPa]$	**Type**	V_{Rd} $[kNm]$	A_s $[mm^3]$	*spacing* $[mm]$	A_s $[mm^3]$	A_s%
2	IPE240	178.5	3910000	158	1541325	39%
4	IPE330	288.7	6260000	98	2492680	40%
6	IPE360	336.8	7270000	84	2908281	40%
7	HEA240	212.8	7680000	132	1837553	24%
8	IPE400	412.3	8450000	68	3560003	42%

Aside from the bending capacity, the wall also has to resist shear forces. The steel profiles are stiff and are capable of resisting large shear forces. When using bar reinforcement, stirrups are required to account for the shear forces. Table 1.2 shows the amount of transversal reinforcement required to reach the same shear capacity as the profiles, determined by using equation 1.3. For these calculations the bond between the soil-mix and the reinforcement bars is assumed to be sufficient.

$$V_{Rd} = \frac{A_{sw} \cdot f_{ywd} \cdot z \cdot cot\theta}{s} \tag{1.3}$$

With:

V_{Rd}	Shear capacity [kN]
A_{sw}	Reinforcement area [mm^2]
f_{ywd}	Yield strength steel [MPa]
z	Efficient depth wall (total depth minus coverage on both sides) [mm]
θ	Orientation of the compression diagonal [°]
s	Vertical spacing between the stirrups [mm]

The shear reinforcement is compared in volumes of mm^3 per meter depth and 1.1 meter width (centre to centre distance of the steel profiles) of the wall, since the orientation of the profile and shear reinforcement is different.

Combining both reinforcement directions results in the steel quantities given in table 1.3. This table presents the amount of steel required when using bar reinforcement as a percentage of the amount of steel that would be used with profile reinforcement to construct a wall with the same capacity. It shows that the amount of steel can be reduced with 30%, whilst still reaching an equal structural capacity. The expectation was that the amount of steel could be reduced when applying bar reinforcement. These results support this hypothesis and prove the relevance of this research.
Note that this is only an approximation of the required amount of bar reinforcement. For an accurate structural design, parameters related to the cooperation between the two materials and the influence of cracking behaviour have to be optimized.

Table 1.3: Quantities of bar reinforcement compared to the amount of steel in IPE/HEA profiles

Amount of bar reinforcement		
$\boldsymbol{f_{cd}[MPa]}$	$\boldsymbol{A_s required\%}$	$\boldsymbol{A_s saved\%}$
2	65%	35%
4	66%	34%
6	66%	34%
7	39%	61%
8	69%	31%

2

Literature

The project started with an elaborate study of the available information on the topic of soil-mix walls. This included searching the web for freely accessible literature, but also contacting experts in the field for their knowledge and insights on the subject.
The Belgian research institution WTCB (Wetenschappelijk en Technisch Centrum voor het Bouwbedrijf) provided multiple articles on the topic of soil-mix. The topics of these papers range from the description of multiple construction techniques (Denies et al., 2012b) to detailed numerical analysis of small soft inclusions in the material (Vervoort et al., 2012). Their research is leading in the subject of soil-mix walls, which makes their cooperation valuable.
Dura Vermeer shared knowledge and experience which was gained during the construction of a parking garage in The Hague, where they applied soil-mix walls.
Combining all the information acquired during the literature study and the expert contacts resulted in the definition of the scope of the research and its relevance, which can both be found in the chapter 1. This chapter provides an overview of the literature study and is used to answer the first sub-question:

Which sections of the detail are critical for the capacity of the detail?

2.1 Background

The past decades the use of soil-mix walls has seen a strong increase in the Netherlands, following in the footsteps of our southern neighbours in Belgium. The technique used to be applied solely as a soil improvement method. Recently it has become more common to apply the technique for structural purposes, such as for water or ground retaining or for vertical bearing capacity. The rapid advancement of this method is not surprising, since the soil-mix technique has multiple advantages compared to traditional methods for construction of structural walls below the ground surface:

- A large contribution of the material comes from the soil at the construction site, therefore it doesn't require soil removal and has a lower environmental impact.
- Soil-mix technique is vibration free, which allows for the method to be executed in areas sensitive for vibrations (either for technical reasons or hindrance of local residents).
- Less space is required for construction equipment and less material has to be transported to and from the site.

Nevertheless, slurry walls and sheet pile walls are still more common in geo-engineering. Both are well known structures used for ground and water retaining. Slurry walls can serve as structural elements as well. These structures are still frequently used, since there are disadvantages to the use of soil-mix walls as well. There are a lot of uncertainties in the achieved quality of the material and the long term behaviour of the structure is mostly unknown. The list below gives an overview of multiple critical aspects of the soil-mix technique.

- Heterogeneous mix quality
- Unknown level of water tightness
- Influence of polluted soil
- Uncertain durability
- Risk of soft inclusions (local weak spots)
- Cooperation with reinforcement (bond strength)
- Unknown crack development
- Less accuracy in the positioning of the walls

2.1.1 Construction method

An understanding of the construction method provides insight in the argumentation behind the mentioned advantages and disadvantages to the technique.
The construction method consists of several steps, which are repeated in an alternate pattern to create an underground wall system. A soil-mix wall can either be created with column or panel shaped elements or as a continuous trench. The following steps describe the construction process of Cutter Soil Mix (CSM) walls, a panel wall. The exact method differs per contractor. This process follows the execution steps followed by contractor Franki Foundations (FrankiFoundations, 2016).

1. Dry cutting of approximately 1 m to check the verticality of the shaft.
2. Slowly lowering the cutter-mixing tool to the required depth while simultaneously loosening the soil and injecting a cement-grout.
3. Retracting the cutter-mixing tool after reaching the maximum depth. Whilst moving upwards the loosened soil is mixed with a predetermined cement mixture, creating the CSM panel (figure 2.1).
4. Position of the reinforcement, I-Profiles
5. The panels are created in an alternately order, where each panel slightly overlaps with the adjacent panels. Secondary panels are built after the completion of the primary panels, see figure 2.2

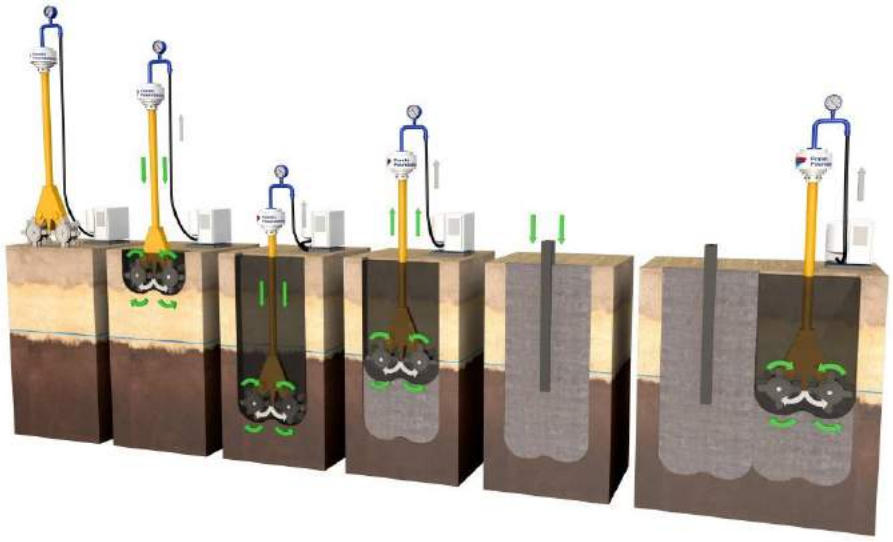

Figure 2.1: Production process of soil-mix panel walls (FrankiFoundations, 2016)

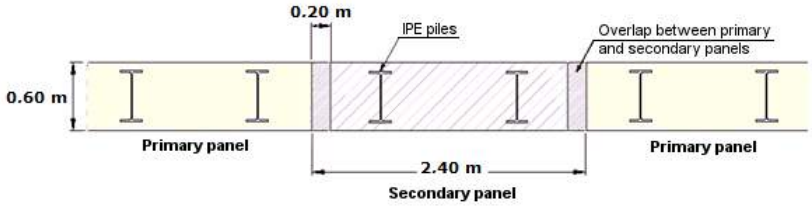

Figure 2.2: Construction order of panel system wall

2.1.2 Material properties

As a result of the mixing procedure a wall is created which consists of soil, cement and water. This combination is similar to a concrete mixture, yet the properties of the soil-mix material cannot be assumed equal to those of concrete. The summation below briefly describes some of the factors that influence the material properties of the soil-mix.

Material ratio A concrete mixture is carefully designed and contains a specific ratio of aggregate sizes, cement, water and possibly other additives. It is not possible to achieve such detail in the design of a soil-mix mixture. Only the w/c-ratio and the quantity of that mixture added to the soil can be controlled, which is not sufficient to create concrete-like properties. The distribution of aggregate sizes, shapes and other soil properties are wholly dependent on the present soil profile at the construction site.

Heterogeneity At the basis of the soil-mix composition is the soil at the construction site. Often there are several different soil layers which will be combined in the soil-mix wall. Small layers will be mixed through the wall, but large layers are likely to cause heterogeneity of the material properties in the wall.
The heterogeneity doesn't only occur within one panel, but might also be observed along the length of the entire wall.

Inclusions The construction process is completely below ground level, which means that visual inspection is impossible. It is likely that the mixing process does not achieve a sufficient mixing degree

and as a result the wall can contain soft inclusions. Such inclusions can impact the local soil-mix properties.

Although the use of soil-mix as a structural element is still in its young years, research has already been conducted on its properties by with a structural purpose of the material in mind. Denies et al. (2012a) provides the results of a study on the mechanical characterization of soil-mix.

The values in figure 2.3 show that the ultimate compression strength (UCS or f_c) of the soil-mix material is significantly lower than that of concrete. Additionally the range of the UCS is very large, even within one soil type. Other basic material properties (elastic modulus (E) and tensile strength (f_t) have been related to the compressive strength based on multiple test results.

	Sandy soils		Silty soils		Clayey soils	
	DSM columns	**CSM systems**	**DSM columns**	**CSM systems**	**DSM columns**	**CSM systems**
Minimal UCS values	1.32 MPa	1.28 MPa	0.93 MPa	0.66 MPa	0.44 MPa	0.65 MPa
Maximal UCS values	39.90 MPa	32.07 MPa	31.17 MPa	12.63 MPa	33.23 MPa	12.69 MPa

Figure 2.3: Extreme Ultimate Compression Strength (UCS) values for various soil types (Denies et al., 2012a)

$E = 1000 \cdot f_c$

$f_t = 0.1 \cdot f_c$

However it should be noted that these are rough approximations and show a significant range as well. An overview of the results of the tests on mechanical characterisation (Denies et al., 2012a) can be found in appendix I.

Based on these results it is difficult to accurately predict the properties that will be realised throughout a wall at a given construction site. Knowledge on the realized properties can be acquired by monitoring soil-mix structures and analysing the resulting data. Creating a database will allow researchers and contractors to gain more insight in the actual performance of the material. Such a database and several processes of monitoring have recently been suggested by Huybrechts et al. (2016).

The quantification of both the strength and the stiffness of an entire wall depends on the cooperation between the steel and the soil-mix material. Research has been done to analyse the cooperation between the two materials (Denies et al., 2012a), but a decisive answer to this problem has not yet been found. It has been proven that both the stiffness and the strength of a profile reinforced soil-mix wall is higher than those of the steel beams only. So it is certain that there is a contribution of the soil-mix material to the composite behaviour.

2.1.3 Structural integrity

The structural integrity of a soil-mix wall is different to that of regular reinforced concrete walls. Firstly the material is weak, especially when considering tensile strength. Secondly the quality cannot be guaranteed throughout the entire structure. The traditional reinforcement method of steel profiles, results in a force distribution within the wall along a pressure arc. The arc distributes all the forces acting on the wall to the steel profiles through compression, avoiding tensile stresses in the weak soil-mix material. The steel profiles transfer these forces to the foundation of the wall, due to their high stiffness the steel profiles are able to transfer high loads without large deformations. Huybrechts et al. (2016) provides numerical proof for the presence of a compression arc in soil-mix walls reinforced with steel profiles. Figure 2.4a visualises the compression arc that transfers the load on the wall to the steel reinforcement profiles. Figure 2.4b shows the result of the numerical analysis done by Huybrechts et al. (2016) to demonstrate the existence of the compression arc.

Assuming a similar tendency for the force distribution in a soil-mix wall reinforced with bar reinforcement (figure 2.5a), the compression arcs will distribute the compressive stresses to the reinforcement as shown in figure 2.5b (this figure represents the section of a bar reinforced soil-mix wall shown in figure 2.5a). The main difference between the two methods of reinforcement is the continuity of the profile

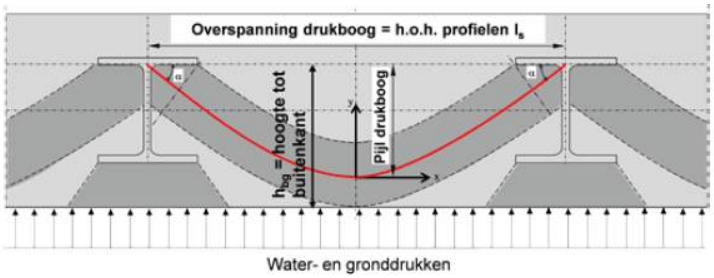

(a) Schematized force distribution through a compression arc to the steel profiles

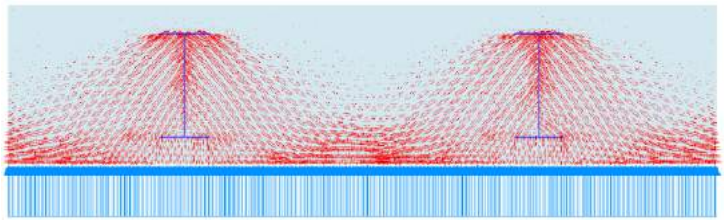

(b) Modelled force flow within a CSM wall reinforced with steel profiles, supporting the compression arc force distribution

Figure 2.4: Compression arc force distribution (Huybrechts et al., 2016)

reinforcement compared to the discretely distributed stirrups along the height of the wall. As a result, the stresses from the compression arcs (figure 2.6 top view) have to be redistributed vertically to concentrated stresses at the stirrup corners. This stress path is further referred to as the compression diagonal (figure 2.6 side view). All stresses are transferred to the stirrup corner, which is therefore chosen as the critical detailed to be analysed in this research (figure 2.7).
Within the detail the stress is distributed both horizontally and vertically. The degree of redistribution depends on the geometry of the reinforcement. The horizontal redistribution is influenced by the radius of curvature of the stirrups. With a smaller radius the available area for the transfer of forces between the compression arc and the reinforcement decreases, which requires more redistribution of the stresses (figure 2.8a). This section is further referred to as section AA'. The vertical redistribution depends on the spacing between the stirrups. With a greater vertical distance between the stirrups (spacing), the redistribution is more severe (see figure 2.9a). This section is further referred to as section BB'.
Both stress distributions lead to tensile stresses perpendicular to the direction of stress distribution. Since the tensile strength of soil-mix is extremely low, these sections are critical to the structural integrity of the entire wall. Therefore these sections will be analysed in chapter 4 as 2D models.

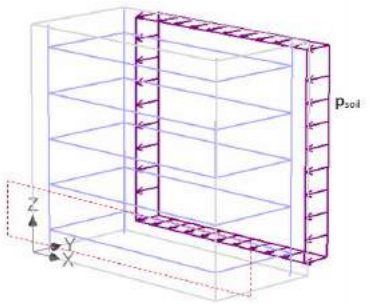

(a) Bar reinforced soil-mix wall

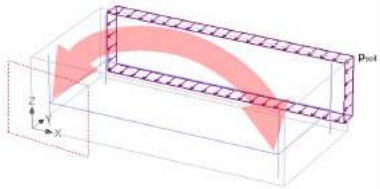

(b) Section single stirrup, 3D compression arc

Figure 2.5: Pressure arc from 3D perspective

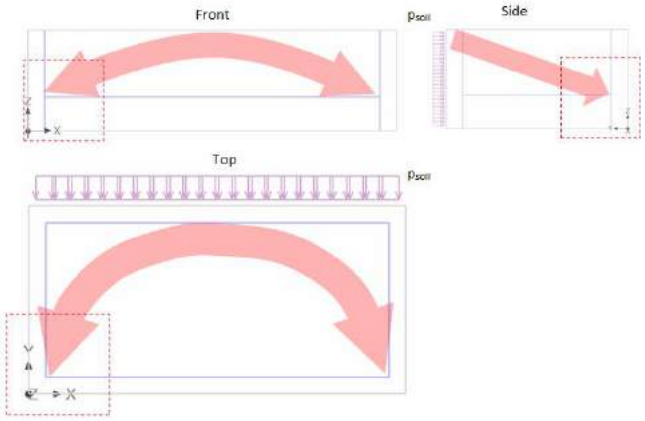

Figure 2.6: Stress distribution to bar reinforcement, 2D

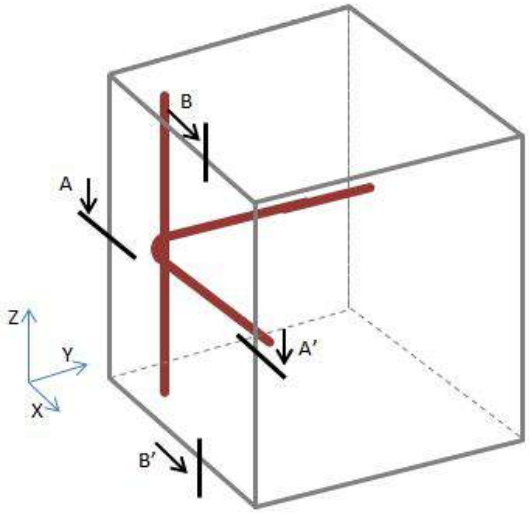

Figure 2.7: Critical detail, indication the location of the critical sections

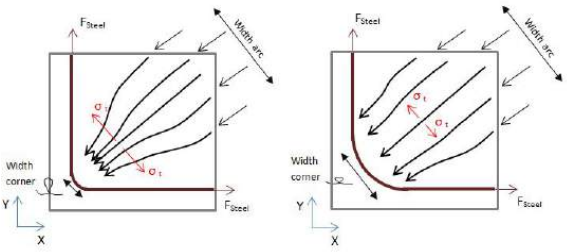

(a) Radius of curvature

Figure 2.8: Critical stress distribution

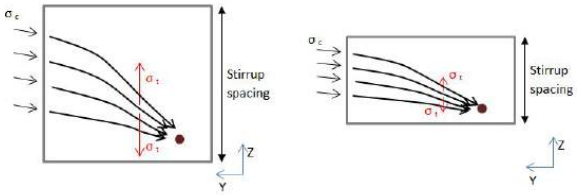

(a) Vertical spacing

2.2 Applications

Soil-mix walls have been applied in multiple projects in The Netherlands and Belgium. Table 2.1 provides an overview of several projects that included the application of soil-mix walls.

Table 2.1: Overview of projects that included the construction of CSM walls (Huybrechts et al., 2016)

Location	**Project**	**Company**	**Type**	**Comments**
The Hague *The Netherlands*	Parkinggarage Toernooiveld	Dura Vermeer (Wedam B.V.)	CSM IPE450 c.t.c. 0.73 m	Temporary ground and water retaining purpose Depth of 18.5 m Dense sand with small loam and clay layer
Assen *The Netherlands*	Drents museum	Franki foundations group	CSM HEB320 c.t.c. 1.0 m	Temporary ground and water retaining and constructive purpose Depth of 18.0 m Dense sand till +1.0 N.A.P. with loam below
Venlo *The Netherlands*	Floriadebridge	Wedam B.V.	CSM Reinforcement unknown	Temporary ground retaining purpose Permanent constructive purpose Depth of 9.5 m Slightly densed sand with low loam content Reached $f_c = 12[MPa]$
Noordwijkerhout *The Netherlands*	Parkinggarage Coremolen	Winmix B.V.	CSM Unknown profile reinforcement	Permanent ground retaining purpose Temporary water retaining purpose Depth of 15.0 m Slightly densed sand Reached $f_c = 10[MPa]$
Leuven *Belgium*	IMEC Tower	Lameire	CSM IPE360	Temporary ground retaining purpose Permanent water retaining purpose Light loamy sands to quite dense sand Depth of 17.5 m
Roeselare *Belgium*	De Munt	Soiltech	CSM IPE330	Temporary ground retaining purpose Permanent water retaining and constructive purpose Sandy loam to loamy sand Depth of 17.0 m
Aalst *Belgium*	Hopmarkt	Soiltech	CSM Unknown reinforcement	Temporary ground and water retaining purpose Sandy loam to loamy sand Depth of 18.5 m
Mol *Belgium*	Bike tunnel	Smet F&C	TSM (Column wall) IPE160 & IPE220	Temporary ground retaining purpose Permanent constructive purpose Quartenairy sand Depth appr. 7.0 m (variable) Reached $f_c = 19[MPa]$

3

Testing

To eventually create a representative material model, enough information had to be acquired on the material properties of soil-mix. To supplement the data available in the literature, the testing phase was included. During the testing phase multiple soil-mix specimens were subjected to a threefold of physical tests, a compression test, splitting test and a displacement controlled compression test. The purpose of these tests was to gain more insight in the behaviour of soil-mix under these loading conditions and, where possible, find relations between the tested parameters. The results in combination with the available literature have been used to answer the second sub-question:

What material parameters should be used to model the behaviour of soil-mix material with a finite element model?

The tests were performed on two different sets of samples. One set consisted of cores drilled from actual soil-mix walls, these were provided by Winmix BV. The other set contained cubes and cuboids, which were made in the lab for the purpose of this research. The mixture used for these samples was based on the recipe used by Dura Vermeer on their project in The Hague. As an addition to the destructive tests, the mixture used for the lab samples was also subject to several pre-hardening tests. These tests determine the density, workability and air content of the material.
Additionally the testing phase provides knowledge on the physical appearance of the material, the structure, the failure mechanism and any other striking visual aspects.

3.1 Aim

For a better understanding of the behaviour of soil-mix, knowledge on its material properties is required. One of the most important behavioural properties is the stress-strain relation. This relation determines the physical response of a structure to a certain load, it's maximum capacity and the type of failure that can be expected. Since the material properties of soil-mix vary a lot, it is likely that there will also be a deviation in the results when considering the stress-strain relation of the material. Therefore it is valuable to be able to relate the stress-strain relation to other parameters of the material, such as the compressive strength or ideally properties of the soil used for the mix. These relations are investigated by performing physical test on multiple soil-mix specimens of the same mixture. The aim of these tests is to investigate these properties and increase the knowledge on the behaviour of soil-mix as a construction material. For this purpose the experiment consists of three different tests, a uni-axial compression test, a splitting test and a displacement controlled test. Figure 3.1 gives a schematic representation of each of these tests.
Furthermore, performing physical tests on soil-mix elements increases the insight in the material properties and its behaviour, for example the governing failure mechanism, crack development and the physical appearance of the material. This experience aids in the interpretation and validation of modelled results.

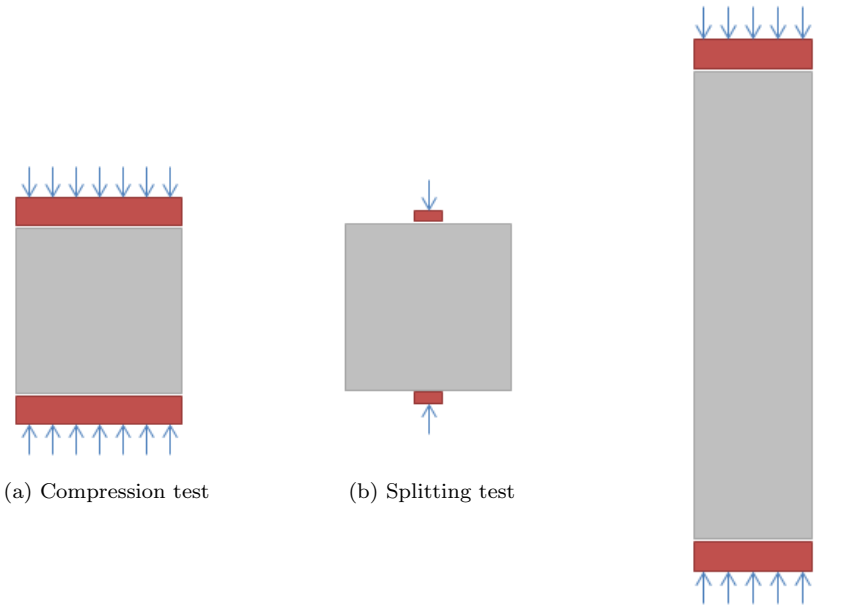

(a) Compression test (b) Splitting test (c) Displacement test

Figure 3.1: Mechanical schemes of experiments

3.2 Procedure

Two sets of samples have been tested. The first consists of samples drilled from soil-mix walls constructed by WinMix BV. The second set are samples produced in the concrete lab at the faculty of civil engineering of the TU Delft. Both sets have been subjected to multiple tests, compression, splitting and displacement controlled tests. Aside from these destructive tests, the mixture used for the lab samples was used for several non-destructive tests. Table 3.1 provides an overview of which tests have been conducted on which set of specimens. Appendix II shows the time schedule of the tests.

Table 3.1: Overview of tests that have been performed on the different specimens at different hardening stages. ✓indicates which test has been performed with which specimens.

		Lab made specimens				Winmix
		After mixing	**7 days**	**14 days**	**28 days**	**Specimens**
Non destructive tests	*Slump*	✓				
	Density	✓	✓	✓	✓	✓
	Air content	✓				
Compression test	f_c		✓	✓	✓	✓
Splitting test	f_t		✓	✓	✓	✓
Displacement test	ϵ_{peak}				✓	✓
	σ_{max}				✓	✓
	$\epsilon_{failure}$				✓	✓
	$E_{initial}$				✓	✓
	E_{tan}				✓	✓
	$Other specific \quad \sigma, \epsilon$				✓	✓
All tests	*Crack pattern*		✓	✓	✓	✓
	Visual	✓	✓	✓	✓	✓
	Influence of time		✓	✓	✓	✓

3.2.1 Preparation: Set 1 – Winmix samples

This set consisted of 13 cylindrical samples, see figure 3.2a, taken from a wall at one of their project sites. These samples were leftovers from the batch used for quality control by TNO. The cores were sawn to create samples of different heights which were suitable for the destructive tests. Small samples for the compression tests ($h \approx 100mm$), medium sized samples for the splitting tests ($h \approx 200mm$) and large samples for the displacement controlled tests ($h \approx 400mm$), see figure 3.2b for the sawn samples. The diameters vary between 94 and 104 mm, with one exception of 145 mm. It is certain the samples were all taken from the same construction site. Unfortunately the specifics of the mixture were unknown. Therefore, the results of the experiments done with this set only serve as a way to analyse the behaviour of completely hardened soil-mix specimens. The properties found by the experiments can't be linked to characteristics of the mixture.

(a) Unprocessed drilled cores

(b) Sawn drilled cores provided

Figure 3.2: Cores provided by Winmix BV

3.2.2 Preparation: Set 2 – Lab made samples

The second set consisted of 18 cubes and 3 cuboids made in the lab. The cubes were used for the compression and splitting tests at different hardening stages and the cuboids for the displacement controlled tests. Accounting for the volume necessary to perform additional tests on the wet mixture and 25 % of waste, table 3.2 describes the total required amount of material.

The challenge with this approach is to get a representative soil-mix, without using the actual methods used to create soil-mix walls. Dura Vermeer supplied information on the mixture used in one of their

Table 3.2: Required volume

Required mixture volume		
18x Cube 150x150x150 mm	60.8	L
3x Prism 100x100x400 mm	12.0	L
Air content	10.0	L
Net. Total	82.8	L
Waste (25%)	20.7	L
Total	***103.4***	***L***

projects, a parking garage in The Hague. This information was the foundation for the mixture recipe used for the lab samples and contained data on the following aspects.

- Grain distribution of multiple soil layers
- Dry and wet weight soil
- Cement type: HS-Blitzdämmer 738S
- 425 kg cement $per\, m^3$ soil
- Water-binder mass ratio of 1:1

This information combined with the available materials at the lab lead to the mixture recipe found in table 3.3. Table 3.3b shows the grain distribution used in the mixture. An unexpected specification is the water-binder ratio of 1:1. This is a high ratio, which is uncommon for concrete (typical water-binder ratio between 0.4 and 0.7). However in this case the large amount of water is combined with an aggregate material of very fine nature (fineness modulus of 1.16, see appendix III). This means that there is more aggregate surface available to absorb the water.
The information provided by Dura Vermeer is based on the use of saturated soil, the water level at their construction site is at ground level. However, the aggregate material available at the TU Delft is dry. Therefore extra water is required to create an initially saturated soil. The estimated amount of additional water was used to determine the other material quantities in the recipe. Based on visual inspection of the material, the final amount of water used for saturating the soil is 12L.
Another important aspect is the used cement. Dura Vermeer used HS Blitzdämmer 738S, but unfortunately this cement type was not readily available at the TU Delft. Instead regular Portlandcement I/42.5N was used for this batch. The entire production process of mixing, casting and curing is described in appendix III.

Table 3.3: Mixture composition of the lab samples

(a) Mixture recipe

Material	**Amount**			
	Volume		*Mass*	
Soil				
Sand	70	L	183	kg
Extra water*	10	L	10	kg
Additive			***68***	***kg***
Water	34	L	34	kg
Cement	11	L	34	kg
Total	**125**	**L**	**261**	**kg**
*Estimate of amount of water required to saturate soil. Actual amount used is 12 L				

(b) Grain distribution

Grain size	**Mass (%)**	**Mass (kg)**
$2mm < \ldots$	2.5%	4.6
$1mm < \ldots < 2mm$	0.3%	0.6
$0,5mm < \ldots < 1mm$	0.9%	1.7
$0,250mm < \ldots < 0,50mm$	15.1%	27.8
$0,125mm < \ldots < 0,250mm$	69.5%	127.5
$\ldots < 0,125mm$	11.6%	21.3
Total	**100.0%**	**183.4**

3.2.3 Methods

The approach to the tests was equal for both sets. Only the processing of the results differs slightly, since the shapes and sizes of the specimens in both sets are different.

Compression Test
The compression tests were performed on specimens which were placed between two steel plates. These plates exert a uniform pressure on the specimen. The pressure was increased gradually until failure. The expected final compressive strength of the material was in the range of 5 to 20 MPa (Denies et al., 2012a). To avoid instant failure of the specimen, the applied load per step could only be a fraction of the material capacity. The loading speed was set to 3 kN/s, which was an acceptable loading speed for both sets of specimens. The compression test resulted in a maximum compressive strength and provided insight in the crack pattern of the material.

Splitting test
The tensile capacity of soil-mix is approximated at 10% of the compressive strength (Denies et al., 2012a), in this case between 0.5 and 2.0 MPa. In a splitting test a compression load is applied locally on the specimen, creating a tensile zone in the middle of the sample. To do so, small strips are placed between the loading plates and the specimen. These strips transfer the compressive forces from the plates to a slender strip on the specimen. Formula 3.1 converts the applied load to the tensile stress in the middle.

$$T = \frac{2P}{\pi LD} \tag{3.1}$$

With:

P	Applied load (N)
L	Specimen length (mm)
D	Specimen diameter (mm)
T	Tensile stress (MPa)

This results in expected failure of the specimen at a load between 6 kN and 56 kN (Denies et al., 2012a). To prevent instant failure, the loading speed is set to 1.1 kN/s.
The lab samples are cubes, but the formula is based on a cylindrical specimen. Nevertheless, the same formula can be applied, since the additional material in the cube doesn't contribute to the tensile capacity in the centre (see figure 3.3). The splitting test was used to derive the tensile strength and analyse the cracking pattern.

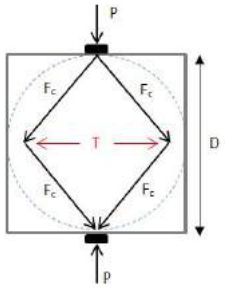

Figure 3.3: Forces in a splitting test

Displacement test
This test is performed to acquire the stress strain relation of the material. A displacement controlled test requires sensors, Linear Variable Differential Transformer (LVDT), which measure the strain of the specimen in the area where the stress distribution is uniform. Each element subjected to a displacement test is equipped with four longitudinal LVDT sensors, one located on each side of the sample. With this method the load is specified as displacement instead of force/pressure. Both the displacement (strain)

and applied force (stress) have to be monitored at every step. A displacement controlled test can only be performed on a relative large specimen, since it requires a sufficiently large zone with a uniform stress distribution. Near the surfaces on which the load is applied the stress distribution is disturbed, along a height approximately equal to the width of the specimen. As a rule of thumb, the minimum height to depth ratio is 4 for displacement controlled test specimens. Two of the Winmix samples were large enough to be used for this test. The set with lab samples contained three larger prism's which were used for the displacement controlled test.
The magnitude of the load step is dependent on the expected maximum compressive strength and modulus of elasticity. The modulus of elasticity is estimated at $1000 \cdot f_c$. This suggests that failure is expected at a strain of approximately 0.001, which corresponds with a displacement of $0.4\,mm$ for a specimen with a length of $400mm$. Based on these assumptions, the initial load step is set at a maximum of $0.01\,mm$.
The displacement controlled test is able to monitor the stress-strain relation, instead of solely the maximum capacity. This data is used for analysing the deformation behaviour of the material. The stress-strain relation is used to determine the secant elastic modulus (E_{sec}). This is the fictitious stiffness of the material when simplifying the deformation to linear behaviour, from the origin of the curve to the maximum load peak ($E_sec = \frac{f_{c,max}}{\epsilon at f_{c,max}}$).
In addition to the longitudinal strains, the lateral strains have been monitored as well for the cuboid specimens. Due to shape restriction this was not done with the cylindrical specimens.

Equipment
The tests have been performed in the concrete laboratory of the faculty of Civil Engineering at the TU Delft. The lab has the required production, loading and monitoring equipment. The equipment which is usually used for the displacement test was unavailable for the Winmix samples. Therefore a loading bench was constructed in a steel frame for this purpose. The set up for the displacement controlled test on the Winmix samples is visually presented in appendix IV.

3.3 Results

Multiple measurements were done on the Winmix samples, the wet mixture used for the lab samples and on the set lab samples at different hardening stages. This section provides a summary of the results of these tests and the conclusions that can be drawn based on these results. Appendix V provides a more detailed overview of the results.

3.3.1 Set 1 – Winmix samples

The samples provided by Winmix were sawn to create six samples for the compression test, seven for the splitting test and two for the displacement controlled test. Figure 3.4 shows each of these tests being executed.
The results from the compression and splitting tests are presented in table 3.4a and 3.4b. The tables both present the density, failure load and corresponding failure stress for each tested specimen. The tensile stress at failure was calculated according to formula 3.1. The compressive stress was determined by combining the failure load with the surface area of the sample.
The elements used for the compressive tests had a low height to diameter ratio (H/D=1), whereas the typical ratio for a compression test on a cylinder is H/D=2. However, multiple reports show that the influence of H/D=1 with a diameter of approximately 100 mm on the strength of the specimen is close to nil (Carroll et al., 2016) and (Unknown., 2010). Therefore, the impact of the specimen size is neglected.
The maximum compressive stresses show a wide range of values, whereas the tensile strengths lie closer together. Nevertheless, the minimum and maximum tensile strength also differ with a factor two. The higher compressive strengths seem to be related to the density of those stronger specimens, which are significantly heavier than the others. Such a link is not evident for the tensile stresses.

The elements used for the displacement tests had a similar appearance as the samples which had lower compressive strength. Based on this observation the strength of these elements was assumed between 2 and 6 MPa. This estimation was used to determine the loading speed of the test. In contrast to the results found by Vervoort and Van Lysebetten (2012), both elements display brittle failure instantly after

reaching the maximum capacity. Sample 2 even displayed explosive failure. It didn't display evident warning cracks before total failure occurred. The material properties resulting from these tests are found in table 3.5 and figure 3.5. As expected the compressive strengths of these specimens coincide with the values of the weaker strengths found from the compressive tests. The elastic moduli (table 3.5) lie within the range of values that can be expected based on compressive strengths (Denies et al., 2012a). However, it is striking that both values differ with a factor two. As the wide range of values found with the compression and splitting tests, these results show that the heterogeneity of the material is an aspect to take into account.

(a) Compression test

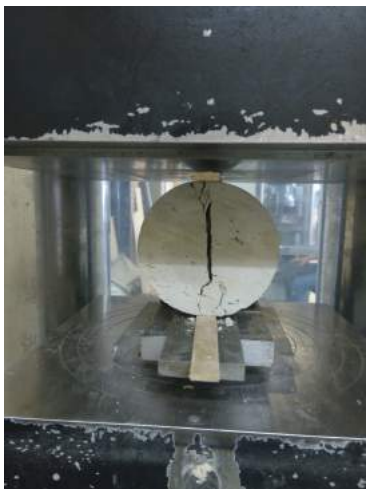

(b) Splitting test

(c) Displacement test

Figure 3.4: Tests on Winmix samples

Table 3.4: Test results Winmix samples

(a) Compression tests

Sample	$\rho[kg/m^3]$	$F_{max}[kN]$	$\sigma[MPa]$
1	1533,2	24,4	3,5
2	1574,3	17,7	2,6
3	1510,1	26,2	3,8
4	1698,7	44,1	5,2
5	1967,2	96,6	11,4
6	1960,0	108,1	12,7

(b) Splitting tests

Sample	$\rho[kg/m^3]$	$F_{max}[kN]$	$\sigma_t[MPa]$
1	1652,8	39,4	1,10
2	1891,1	26,2	0,80
3	1874,4	29,8	1,09
4	1940,6	47,7	1,46
5	1626,4	18,2	0,69
6	1758,7	48,3	1,48
7	1807,4	29,3	1,20

Table 3.5: Results Winmix samples displacement tests

Sample	$f_c[MPa]$	$E_{sec}[MPa]$
1	3.57	5 500
2	5.47	10 200

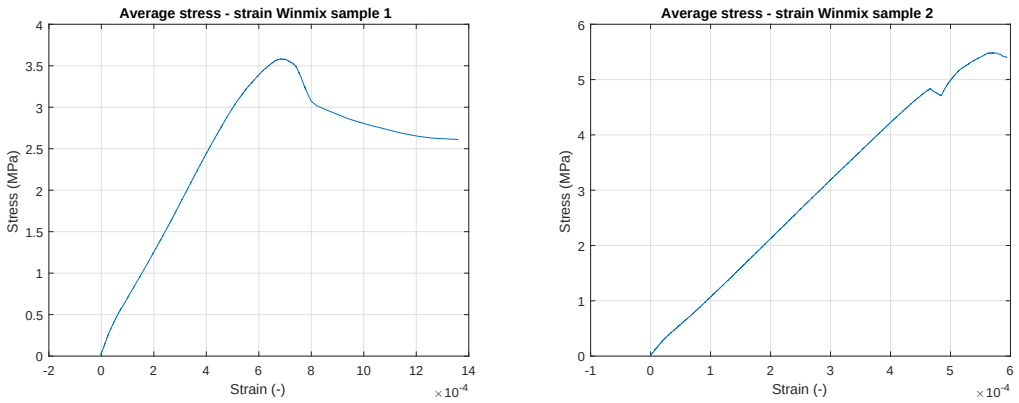

(a) Sample 1 (d = 100 mm) (b) Sample 2 (d = 150 mm)

Figure 3.5: Stress-strain relations Winmix samples

Visual remarks

Aside from the quantitative results, the visual appearance of the samples is also valuable for interpreting the quality of the specimens and the results. For example, the difference in the compressive strengths of the samples is in line with the expectations based on visual inspection of the specimens. Specimen 5 and 6 had a smoother surface than the other specimens and a denser appearance. Additionally these specimens were darker of colour, which could be an indication of a higher cement content in these specific samples. Specimens with a higher cement content are likely to have greater strength.

Another interesting aspect related to the cement content of the material, is the dusty feel it has to it. Each sample is covered with a thin layer of dust like particles. Due to the high cement content which is typical for soil-mix, it is likely that not all of the fine particles reacted with the water. Which resulted in free fine particles in the material.

Also the specimens each had a heterogeneous appearance, which is a result from the on site production process and the environmental conditions. The specimens either contain soft inclusion, unmixed soil, or even large chunks of rock.
Appendix V presents photographs of several test specimens.

3.3.2 Set 2 – Lab made samples

This section provides an overview of the most relevant experimental results. A detailed overview of the results can be found in appendix V.

Fresh soil-mix

The first tests in set 2 are done on the wet mixture. These tests include determining the density, the workability and the air content of the mixture. Appendix III describes the process of these tests. Table 3.6 shows the results of the tests done before casting the mixture and comments on the meaning of these results.

The fineness modulus is related to the particle sizes in the grain distribution of the soil. A FM of 1.16 is a low value, which implies that the aggregates in the mixture are very fine. Fine sands have more surface area to absorb water, which results in a higher water demand. The water cement ratio of this mixture is 1:1, which is relatively high compared to typical ratios used in concrete mix (between 04 and 0.7). However, the workability of the mix is low, which means it is a dry mixture. This coincides with the low fineness modulus. Despite the low fineness modulus and the low workability, the mixture showed a lot of bleeding after casting. Bleeding occurs when free water in the mix is pushed upwards by heavier particles. Since the mixture seemed to be dry, the occurrence of a lot of bleeding was unexpected. Figure 3.6 shows the bleeding of a fresh specimen. The relatively large amount of bleeding might be

Table 3.6: Measurements on soil-mix before casting

Property	**Value**	**Notes**
Fineness modulus (FM)	1.16	Low value, which implies very fine aggregate particles in the mixture. Fine particles require more water to create a workable mix.
Density (ρ)	$2031\,kg/m^3$	The value lies in the range of light weight concrete
Slump (workability)	$20\,mm$	Low slump value. Workability category S1, dry mixture
Air content	3%	Relatively low air content.

related to the low air content of the mixture. For regular concrete, as well as for lightweight concrete, the optimal air content lies between 4 and 7 %. A low air content has a negative effect on the durability and workability of the material. However, during the construction process of actual soil-mix walls air is pumped in along with the water cement suspension (to guarantee its fluidity). Which likely increases the air content relative to the lab produced mixture. The density of the mixture lies within the range for lightweight concretes.

A difference between the appearance of the lab made samples and the Winmix samples, is the het-

Figure 3.6: Bleeding of a specimen after casting

erogeneity of the mix. Each sample of the Winmix set either contained soft inclusions or chunks of hard rock. The lab mixture however, is entirely homogeneous. This difference is due to the production processes. The lab made samples are produced in a controlled environment. Made from certified components, which were mixed evenly. Actual soil-mix is entirely dependant on the soil composition on site, which is bound to contain disturbances. Exactly replicating the product achieved by on site production of soil-mix would require deliberate 'pollution' of the mix. Creating a heterogeneous mix is usually undesirable and thus there is no experience with creating such mixtures in lab conditions. As a result, the test results are expected to have a smaller deviation than the results from the Winmix cores.

Hardened soil-mix

The samples were tested at multiple hardening stages, after 7, 14 and 28 days. At each stage both the compressive and the tensile capacity of the material were tested. After 28 days the displacement controlled tests were performed. Tables 3.7, 3.8 and 3.9 provide the results from the compression and splitting tests. For concrete hardening of the mixture typically reaches 65% of its final strength after 7 days, 90 % after 14 days and 99% after 28 days. These reference values roughly correspond with the hardening process found in the soil-mix specimens. Which indicates that even though the composition of soil-mix is different to that of concrete, the hardening process is similar.

Table 3.7: Test results of the compression and splitting tests after 7 days of hardening (22-05-2017)

Compression test					
Sample	$Mass[kg]$	$h[mm]$	$\rho[kg/m^3]$	$F_{max}[kN]$	$\sigma_{max}[MPa]$
1	6,520	14,30	2026,4	65,5	2,9
2	6,700	14,50	2053,6	83,7	3,7
3	6,795	14,70	2054,4	70,9	3,2
Splitting test					
Sample	$Mass[kg]$	$h[mm]$	$\rho[kg/m^3]$	$F_{max}[kN]$	$\sigma_{max}[MPa]$
1	6,650	14,45	2045,4	16,4	0,482
2	6,700	14,50	2053,6	18,6	0,544
3	6,600	14,15	2073,0	16,4	0,492

Table 3.8: Test results of the compression and splitting tests after 14 days of hardening (29-05-2017)

Compression test					
Sample	$Mass[kg]$	$h[mm]$	$\rho[kg/m^3]$	$F_{max}[kN]$	$\sigma_{max}[MPa]$
1	6,605	14,15	2074,6	98	4,36
2	6,675	14,50	2046,0	100,9	4,48
3	6,670	14,45	2051,5	109,6	4,87
Splitting test					
Sample	$Mass[kg]$	$h[mm]$	$\rho[kg/m^3]$	$F_{max}[kN]$	$\sigma_{max}[MPa]$
1	6,640	14,65	2014,4	21,9	0,634
2	6,755	14,60	2056,3	11,0	0,320
3	6,730	14,75	2027,9	19,7	0,567

Table 3.9: Test results of the compression and splitting tests after 28 days of hardening (12-06-2017)

Compression test					
Sample	$Mass[kg]$	$h[mm]$	$\rho[kg/m^3]$	$F_{max}[kN]$	$\sigma_{max}[MPa]$
1	6,665	14,65	2022,0	-	-
2	6,670	14,65	2023,5	111,2	4,94
3	6,655	14,60	2025,9	140	6,22
Splitting test					
Sample	$Mass[kg]$	$h[mm]$	$\rho[kg/m^3]$	$F_{max}[kN]$	$\sigma_{max}[MPa]$
1	6,645	14,65	2015,9	23,5	0,681
2	6,720	14,75	2024,9	22,8	0,656
3	6,660	14,60	2027,4	23,3	0,677

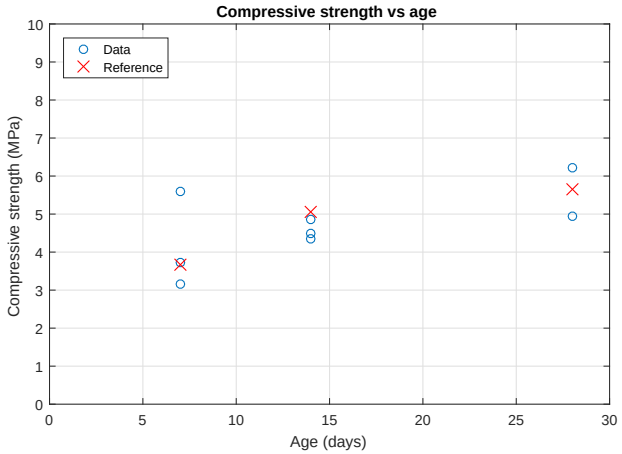

Figure 3.7: Development of the compressive strength

Displacement tests

The displacement tests on the lab samples set differ slightly from the tests done on the large Winmix core samples. The equipment used for these tests was controlled with the strain measured on the sample, instead of the applied displacement. This prevented brittle failure of the specimen. Complementary to the longitudinal strains, the transversal strain of these specimens was monitored as well. Figure 3.8a shows a specimen with attached LVDT's in both directions. Measuring transversal displacement was not possible with the Winmix cores, since these cores were cylindrical attaching the LVDT's was too tedious. The transversal strain LVDT's provided additional data, which was used to determine the poisson's ratio of the material. Figure 3.8b shows the specimen after testing and figure 3.9 shows the resulting average stress-strain relation for each specimen.

NOTE: The loading machine malfunctioned during the first test. The load was rapidly increased,

(a) Before testing

(b) After testing

Figure 3.8: Displacement test lab sample

instead of applying the specified strain steps. Nevertheless, the strains were monitored. The stiffness measured on this sample is high compared to the other two and the critical strain is significantly lower. Which could be caused by the rapid loading. An additional explanation can be found by looking at the measurements of all sensors in appendix V.4. The difference between the separate measurements indicates that the specimen was not solely subject to compression, but also to bending. This lead to different behaviour of the material, which explains the deviation of results compared to the other two samples. Due to the malfunctioning of the equipment test 2 and 3 were conducted 11 days later (23-06-2017). Since the strength of the material is nearly fully developed after 28 days, these additional 11 days are

expected not to influence the compressive strength of the samples.

The resulting compressive strength, secant elastic modulus (E_{sec}) and initial elastic modulus (E_{in})

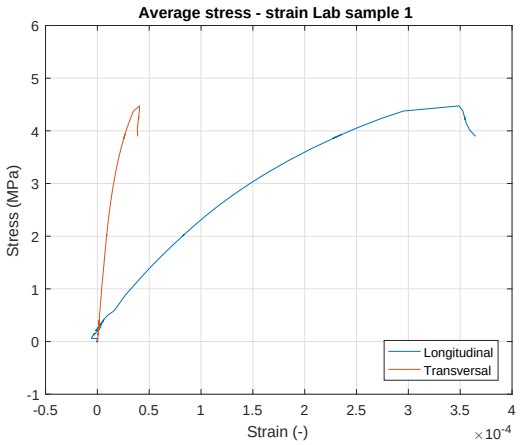

(a) Sample 1

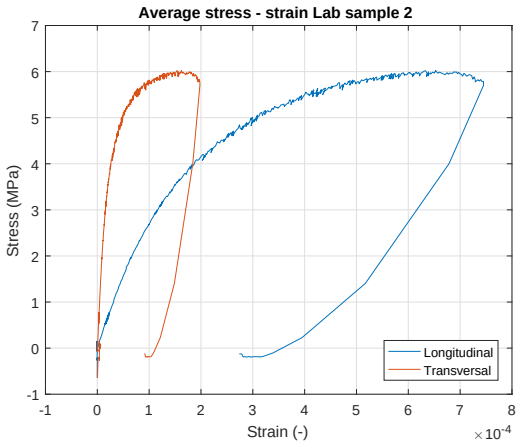

(b) Sample 2

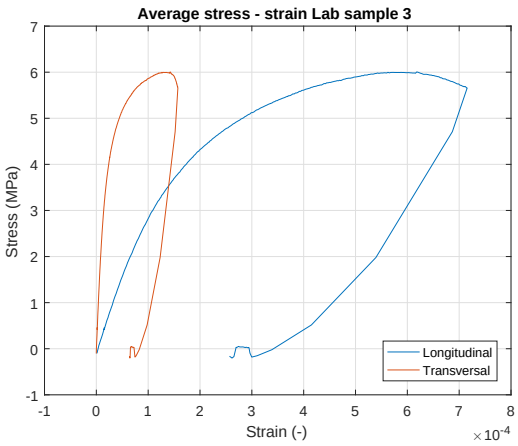

(c) Sample 3

Figure 3.9: Stress-strain relation lab samples

are presented in table 3.10. The secant elastic moduli are rough estimations, since the strain controlled test doesn't show a clear peak value for maximum compressive capacity. The initial elastic moduli are determined from the stiffness at the origin of the stress-strain curve.
The measured compressive strengths have the same order of magnitude as those measured from the Winmix samples. The elastic moduli seem to be significantly higher. However, when considering the wide range in elastic moduli in both the Winmix set as well as the lab set, the properties of the lab samples coincide with actual soil-mix parameters. These results show that there is a great uncertainty in the material properties of soil-mix. Even when the mixture is produced in a controlled environment and (appears) to be homogeneous, the properties vary.

To be able to determine the plastic strain at the compressive strength (ϵ_{cp}), required for the material model in Atena), the initial stiffness is determined. When unloading a specimen, its deformation is released with the initial stiffness. The remaining strain gives an approximation of ϵ_{cp} (figure 3.10). The last property derived from the displacement controlled tests is the poisson ratio. This parameter showed less variation. The weighted average of the poisson ratio throughout the loading process is given in table 3.10.

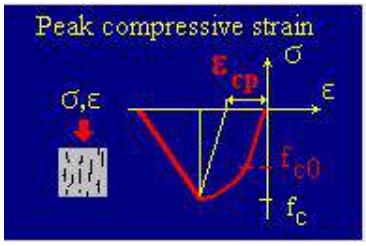

Figure 3.10: Determining ϵ_{cp} (Cervenka et al., 2016)

Table 3.10: Results lab samples displacement tests

Sample	$f_c[MPa]$	$E_{sec}[MPa]$	$E_{in}[MPa]$	$\epsilon_{cp}[-]$	ν
1	4.47	12700	31 100	$2.06 \cdot 10^{-4}$	0.11
2	6.02	9700	35 000	$4.48 \cdot 10^{-4}$	0.14
3	6.00	10300	35 000	$4.14 \cdot 10^{-4}$	0.13

Visual remarks
Like the Winmix specimens the lab samples were also covered in a thin layer of dust like particles, indicating that not all of the fine particles have reacted with the water. The layer of small particles indicates not all of the cement reacted with the water, whereas the bleeding suggests that the amount of water present in the mix was abundant.
The samples also contained small air bubbles and no large aggregates, just like the Winmix specimens. Such similarities prove that the lab mixture can be seen as a representable soil-mix.

3.4 Verification

Executing physical tests on actual soil-mix specimens gave insight in the properties of the material. Both on its quantifiable properties as well as its visual appearance. The combination of core samples taken from actual soil-mix walls and samples made in the lab provided valuable information. Visually both sets showed multiple similarities; absence of large aggregates, dusty feel (indicating the presence of un-bonded cement particles) and the presence of air bubbles. This validates the acceptability of the lab made samples. The acceptability is important, since the production process of the lab specimens differed significantly from the regular production process of soil-mix walls.
The sets could have been compared even in more detail if information on the mixture composition of the Winmix cores was available. Unfortunately, this data was not provided. Despite the absence of the mixture recipe, the Winmix samples do show the wide range that can be found within one project site. This is in line with the results presented in Denies et al. (2012a). Also the quantified results were used to analyse the relation between the measured parameters (compressive strength, tensile strength, elastic modulus and density). Since the results show that there is no strong correlation between any of the parameters. The most evident relation is the increase in strength with the increase of the density. Unfortunately, no samples with a high density were suitable for the displacement tests, hence the relation between density and stiffness could not be addressed. The test results are within the property range found by Denies et al. (2012a) (see appendix I).
The lab samples represent an approximation of the soil-mix walls constructed by Dura Vermeer in The Hague. The following aspects were slightly altered due to availability of the materials.

- The grain distribution used for the samples was based on the soil samples taken from the project site. The fractions available at the TU Delft however were less detailed. Therefore the final grain distribution contains the cumulated fractions from the detailed distribution.

- The cement used for the actual mix (HS-Blitzdämmer 738S) was unavailable, Portland cement I/42.5N was chosen to replace it.
- The mixture recipe was based on saturated sands. The sand fractions used for the lab samples consist of dry particles. To replicate the mixture these particles had to be saturated. This is an empirical process and is unlikely to result in exactly the same moisture content as found in the actual soil.

These deviations imply that the mixture is not an exact copy of the mixture used by Dura Vermeer. The used mix is a soil-mix with a slightly different composition. As stated previously the visual and physical appearance of the lab samples showed similarities with the Winmix samples. These similarities validate the acceptability of the lab samples as soil-mix samples. The measured parameters from these samples have a smaller range than the Winmix samples. Since these samples have been produced in a controlled environment and are made with a homogeneous mix composition these results are in line with the expectations. In contrast with the Winmix samples there is a more clear relation between each of the measured parameters. The measured tensile strengths are close to 10% of the maximum compressive strength, which was the guideline drafted by Denies et al. (2012a). The stiffness can be approximated by 1500 times the compressive strength, which is 1.5 times the average value given in Denies et al. (2012a). With the low compression strength the results are still within the given range ($908 f_c^{0.8} - 2056 f_c^{0.8}$). Considering all aspects the test results are acceptable and can be used to supplement the data on material properties found in the literature. All data was combined and implemented in the material model. The material model was used in the finite element model to resemble the soil-mix behaviour.

3.5 Implementation material model

The results acquired from the testing phase combined with the material properties found in the available literature have been used to quantify the material model in Atena. Atena is finite element software which is often used for modelling of reinforced concrete structures (Cervenka et al., 2016). The material model used to represent the soil-mix is based on the 'Non Linear Cementitious 2' model. This model is suitable for the representation of rock and concrete like materials (Cervenka et al., 2011). The input parameters listed in table 3.11a have been specified based on the available data. The other parameters are predefined by the software and based on the specified compressive strength, these are listed in table 3.11b. Since there is no data on these parameters, these are left to the default values.

Both the performed experiments and the available literature indicated that the properties of soil-mix

Table 3.11: Parameters of the Non Linear Cementitious 2 material model - Atena

(a) Defined by data

User defined	
Elastic modulus	E_c
Poisson's ratio	ν
Specific weigth	ρ
Compressive strength	f_c
Tensile strength	f_t
Plastic strain at strength f_c	ϵ_{cp}
Aggregate size	ϕ

(b) Software default values from f_c

Atena default values	
Fracture energy	G_f
Reduction of f_c due to cracks	r_c^{lim}
Crack shear stiffness factor	S_F
Exc., Def.the shape of the failure surface	-
Direction of plastic flow	β
Coefficient of thermal expansion	α
Fixed crack model coefficient	-
Critical compressive disp. (loc. band)	w_d

have a wide range for all basic material parameters. It is not feasible to model every combination of possible material properties, therefore a single material definition is drafted for the modelling phase. To find the best representation of the soil-mix and simultaneously get acquainted with the Atena software, a calibration was done based on experiments described in the literature (Denies et al., 2014) (Denies et al., 2015a). This calibration can be found in appendix VI. The result of the calibration combined with the experimental results form the foundation for the soil-mix material model definition.

The data set used by Denies et al. (2012a) is significantly more extensive than the experimental results

acquired from the test performed for this research. Therefore, that data is used for the main material characteristics (compressive strength, tensile strength and elastic modulus). For the feasibility of the research the material model is based on the properties of soil-mix of average quality. Combined with the data from the physical test the parameters presented in table 3.12a are derived for the material model. For a proper representation of the detail in a finite element model spring elements have been incorporated in the model (chapter 4). The spring properties (table 3.12b) are based on the test results from the displacement tests on the Winmix samples. The aim of the model is to analyse the stress distribution within the detail to the reinforcement, therefore the springs are represented by the properties of a relatively weak soil-mix. Stiff elements tend to carry large parts of the load, therefore these springs represent a weak type of soil-mix to prevent significant stress distribution to these springs.

Property values		
Elastic modulus (E)	5 000	MPa
Poisson's ratio (υ)	0.135	-
Specific weigth (ρ)	0.02	MN/m^3
Compressive strength (f_c)	5.0	MPa
Tensile strength (f_t)	0.5	MPa
Plastic strain at strength f_c (ϵ_{cp})	$4.3 \cdot 10^{-4}$	-
Critical compressive disp. (w)	$5.0 \cdot 10^{-4}$	m
Fracture energy (G_f)	1.754	MN/m
Reduction of f_c due to cracks (r_c)	0.8	-
Crack shear stiffness factor	20.0	-
Aggregate size	0.20	mm
Exc., Def.the shape of the failure surface	0.52	-
Direction of plastic flow (β)	0.00	-
Coefficient of thermal expansion (α)	$1.2 \cdot 10^{-5}$	$1/K$
Fixed crack model coefficient	1.00	-

(a) Properties material model soil-mix

$\boldsymbol{\sigma[MPa]}$	**Rel. disp [-]**
0.03	$5.00 \cdot 10^{-4}$
0.00	0.00
-3.06	$-5.15 \cdot 10^{-4}$
-3.54	$-7.22 \cdot 10^{-4}$
-3.11	$-7.99 \cdot 10^{-4}$
-2.82	$-9.86 \cdot 10^{-4}$

(b) Spring properties

Table 3.12: Quantified material parameters finite element model

4

Model

The literature study and the testing phase are the foundation for the modelling phase. Both have provided information to define the material model. Additionally the literature study gave insight in the most critical sections of the detail. These critical sections have been modelled in 2D to analyse the stress distribution, the possible failure mechanisms and the failure load. To analyse the influence of multi-axial loading conditions, a 3D model of the detail was built as well.
To construct these models the third sub-question had to be answered.

How can the geometry of the detail and the loading configuration on the detail be represented in a finite element model?

The models are computed for multiple different geometrical configurations, representing differences in the reinforcement design (radius of curvature of the corner, the length of the stirrup and vertical spacing between the stirrups). The results of the 2D models have been compared to the 3D model to check whether or not the failure mechanisms and maximum loads agree. This comparison is used to determine the governing failure mechanism. The resulting failure mechanisms are then used to determine a set of preliminary guidelines which can be consulted when designing a bar reinforced soil-mix wall. These guidelines are presented in section 4.5.

4.1 Global analysis

As addressed in section 2.1.3 the corner of the reinforcement stirrups is a crucial node for the structural integrity of a soil-mix wall. Consequently this is the detail which is analysed in the modelling phase. An accurate representation of the geometry and the loading configuration on this detail are important for the acceptability of the model. Therefore the modelling of the reinforcement node is based on the global stress distribution throughout an entire soil-mix wall. From the force distribution on a global scale, the loading conditions on the reinforcement detail were determined.

4.1.1 Loading soil-mix wall

A soil-mix wall is typically loaded with both active and passive soil and water pressure. The wall is retained by an anchor or anchors along the depth of the wall and the floor slab at the bottom (see figure 4.1). The vertical force distribution of these forces to the foundation are analysed by modelling the wall as a strut and tie model, consisting of the compression diagonals in the soil-mix and reinforcement bars as tensile ties. A MatrixFrame model was constructed with standard beam elements, to find the orientation of the compression diagonals in the wall. The model is a representation of a wall with limited height. A higher wall would require multiple anchors and would show a repetitive pattern of the strut and tie pattern in the short wall.

The model is simplified. The structure is loaded only by the active soil pressure, the embedded part

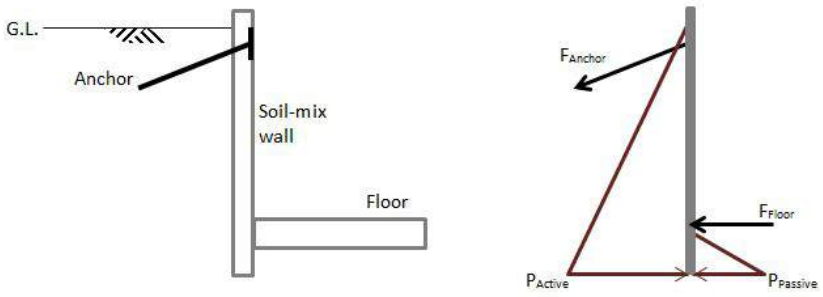

Figure 4.1: Schematic loading on soil-mix wall

of the wall is represented by the supports at the bottom of the framework. A single anchor is modelled as a horizontal support just below the top of the structure. This way the model will result in a force distribution within the wall, which can be used to determine the orientation of the loading at the critical detail. The strut and tie model and the corresponding results are presented in figure 4.2a. The critical node is highlighted with the red circle. This node is loaded by a compression force from above and transfers those forces to tensile stresses in both the horizontal stirrup and the longitudinal bar.

The model only represents a short wall, in order to find the global stress distribution within the wall and the position of the critical node. The magnitude of the forces within the wall depend on the depth of the wall, in combination with the amount and positioning of the anchors. A deeper wall requires more anchors to prevent large deformations of the wall. As an estimation, the maximum compressive force on the critical detail varies between 50 and 200 kN respectively based on a MatrixFrame model representing a wall depth of 5 and 25 m depth. The wall of 5 m was supported by 2 anchors and the wall of 25 m deep was supported by 10 anchors. Note that this is only a rough approximation of the magnitude of the forces, which will not be used for further reference.

In reality the compressive stresses also have a component in the direction perpendicular to the plane modelled with MatrixFrame. This component results from the distribution of the stresses along the width of the wall, the compression arc (figure 4.2b). The stress distribution along such a compression arc has been proven by Huybrechts et al. (2016).

For validation of the vertical force distribution in the wall, several strut and tie configurations have been analysed. These configurations can be found in appendix VIII. These options lead to tensile forces in

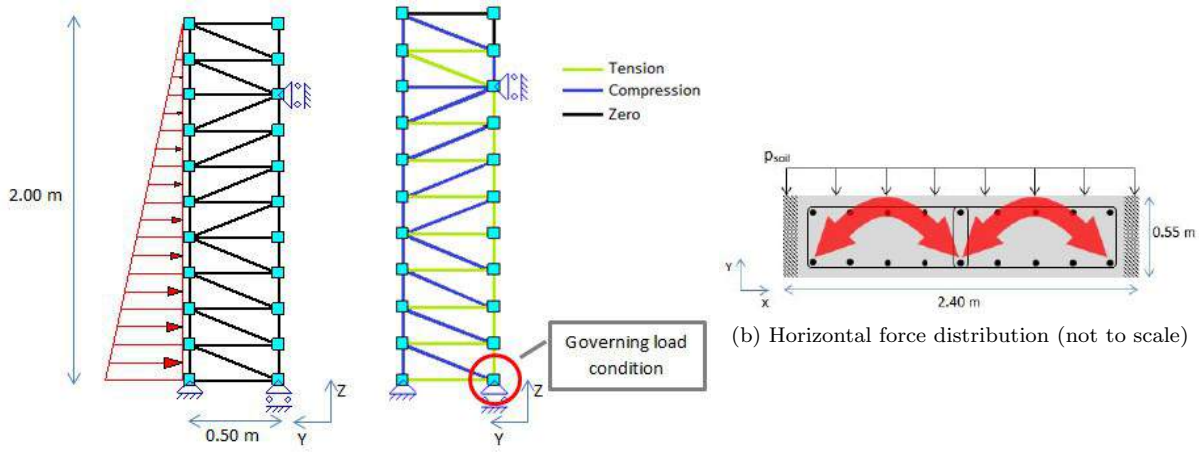

(a) MatrixFrame analysis vertical force distribution

(b) Horizontal force distribution (not to scale)

Figure 4.2: Global force distribution with a soil-mix wall

the diagonals[1], which is both unfavourable and unlikely, since these diagonals represent soil-mix with a low tensile capacity.

4.1.2 Critical node - hypothesis

In the soil-mix surrounding the reinforcement in the detail these stresses have to be redistributed and transferred to the reinforcement bars. This redistribution occurs both in a vertical and a horizontal plane (figure 4.3 and 4.4). Eventually all stresses are concentrated at the stirrup corner at the 'free' side of the wall (figure 4.2a). Both the stresses from the diagonal (figure 4.4 side view) and the arc (figure 4.4 top view) are distributed along a certain width when reaching the detail. Redistribution of stresses to higher concentrations leads to tensile stresses in the perpendicular direction, due to the curvature in the stress trajectories. Since the tensile capacity of soil-mix is low, tensile stresses are undesirable. Therefore it is important to analyse the distribution of the stresses near the detail and analyse the critical sections where tensile stresses might occur. Figure 4.5 shows the positions of both the critical horizontal (AA') and vertical section (BB'). The next paragraphs describe the hypothesis concerning the expected stress distribution and failure mechanism of each section.

[1]The one tensile diagonal in the final results is negligible and is thus acceptable.

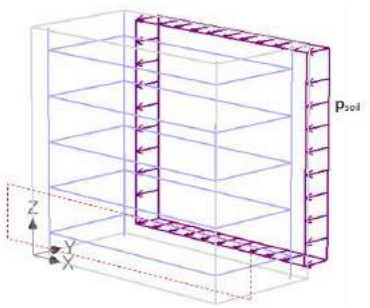

(a) Bar reinforced soil-mix wall

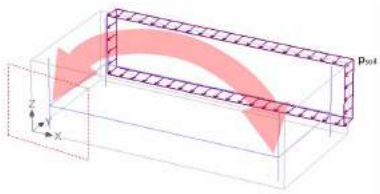

(b) 3D compression arc, single stirrup (arc not to scale)

Figure 4.3: Pressure arc from 3D perspective

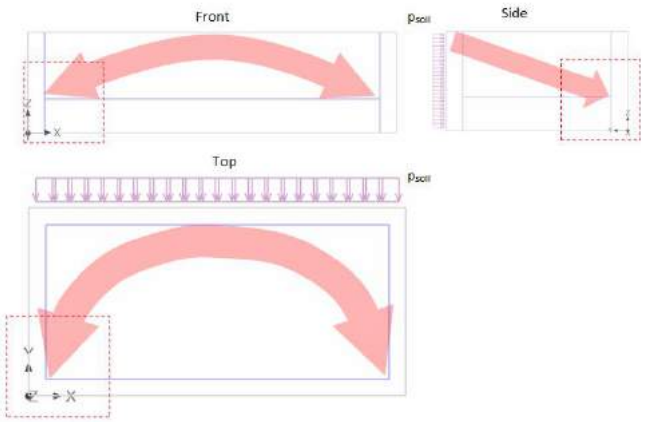

Figure 4.4: Stress distribution to bar reinforcement, 2D (arc not to scale)

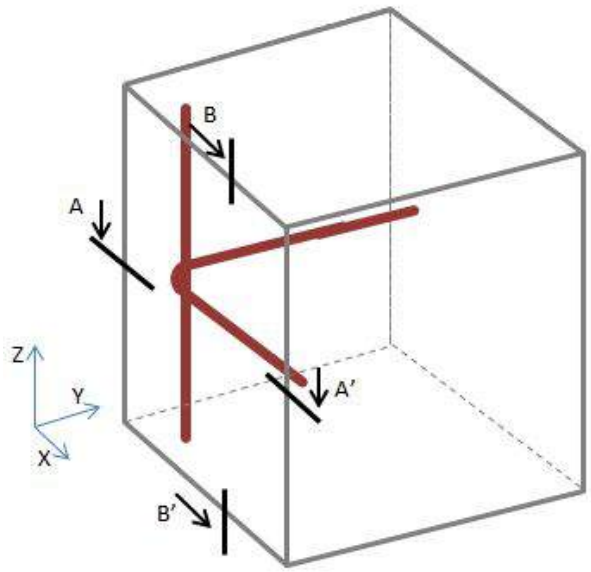

Figure 4.5: Positions of critical 2D sections of the detail

Section AA'

Cross section AA' shows the stirrup corner in the horizontal plane, which corresponds with the dashed square in the top view in figure 4.4. This is the plane in which the stresses of the compression arc are transferred to the stirrup reinforcement. The compressive stresses in the soil-mix are compensated at the stirrup corner. Since the width of the corner is generally smaller than that of the compression arc, the stresses are more concentrated on the inside of the corner. When compressive stresses are distributed to a higher concentration, tensile stresses occur in the perpendicular direction. These tensile stresses will cause splitting failure when the maximum capacity is reached. Figure 4.6a shows the stress trajectories expected in the cross section and figure 4.6b the corresponding crack orientation, these cracks will be further referred to as diagonal cracks. The ratio between the width of the compression arc and the effective width inside of the stirrup corner has a strong influence on the tensile stresses occurring due to the stress redistribution. A larger effective width inside the corner results in lower tensile stresses. The effective width of the corner is increased by increasing the radius of curvature of the corner.
Aside from the detailing of the corner of the stirrup, the length to depth ratio also influences the load distribution near the detail. A more slender stirrup, means an increased angle for the orientation of the load. Stresses with a relatively steeper orientation require more redistribution in the cross section to be transferred to the reinforcement. This might decrease the capacity of the detail.
Note that this model only considers the stress distribution in a horizontal plane. Since only a thin slice is modelled, vertical redistribution minimized. Also the use of plain strain elements prevents strain in the direction perpendicular to the plain. Which implies that vertical splitting cracks can not occur in this model.

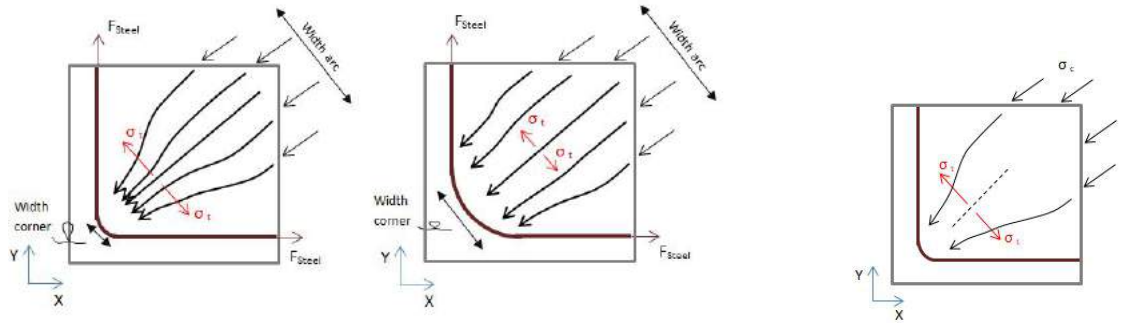

(a) Stress distribution (b) Cracks

Figure 4.6: Cross section AA' (horizontal)

Section BB'

Cross section BB' is taken in the vertical plane, corresponding with the dashed square in the side view in figure 4.4. In this plane the stresses from the compression diagonals are redistributed to the reinforcement in the vertical plane. Similar to cross section AA', the trajectories of the compressive stresses are redistributed to concentrated stresses at the reinforcement bar. This redistribution leads to tensile stresses in the perpendicular direction, which might cause splitting of the material (cracks parallel to the loading direction, see figure 4.7b). These cracks will be further referred to as vertical splitting cracks. In this case the tensile stresses can be reduced by decreasing the vertical spacing between the stirrups. This would decrease the initial width of the compression diagonal and therefore decrease the angle in the trajectories required for redistributing the forces (see figure 4.7a).

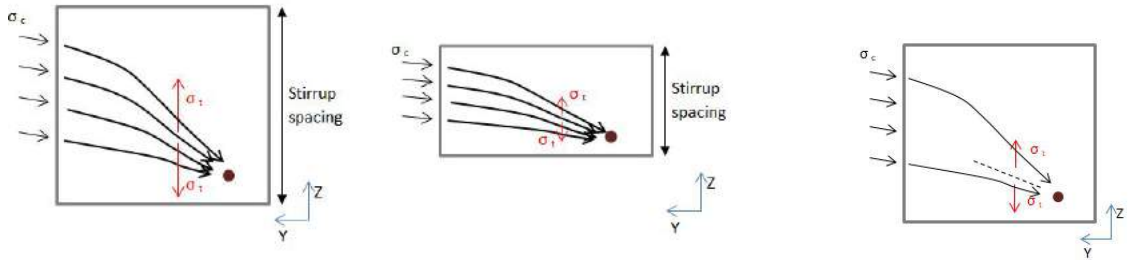

(a) Stress distribution (b) Cracks

Figure 4.7: Cross section BB' (vertical)

3D

The 3D model should show a combination of both failure mechanisms of the 2D models. Based on the failure loads resulting from the 2D models the governing failure mechanism can be determined, either diagonal cracking (like section AA'), vertical splitting (like section BB') or a combination of both. The failure mechanism occurring in the 3D model is additional information concerning the failure mechanism which is likely to be governing. The stresses on the detail are simultaneously redistributed in both the horizontal and the vertical plane. As a result the horizontal redistribution will influence the location of vertical splitting cracks and vice versa, depending on whichever mechanism is governing.

4.2 Model set-up

From the framework model (vertical forces) and the compression arc theory (horizontal forces) the governing load conditions on a reinforcement node are found. This is where the compression diagonal meets tensile ties in both the vertical and horizontal direction on the 'free' side of the wall (figure 4.1) just above the floor slab. Additionally this reinforcement node is loaded by the compression arc in the horizontal plane, leading to a critical loading configuration on the reinforcement detail.
Both the vertical diagonal and the arc load the detail with compressive stresses under a certain angle and distributed over a certain height and width. The dimensions and orientation of these loading planes depend on the geometry of the reinforcement cage, being the length (w), depth (d) and the vertical spacing between the stirrups. Other reinforcement dimensions which influence the force distribution within the detail are the radius of curvature and the diameter of the reinforcement bar, but these don't influence the external loading configuration on the detail. A summation of all parameters influencing the load configuration is given in table 4.1.

Table 4.1: Wall and reinforcement dimensions influencing the loading conditions on the detail

Dimension	**Range**
Depth wall (h)	$550mm$
Cover (c)	$50mm$
Stirrup length (w)	$400–1100mm$
Stirrup depth (d)	$450mm$
Stirrup spacing (vertical)	$50–250mm$
Radius of curvature (r)	$2\phi - 10\phi$
Diameter reinforcement	$10mm$

4.2.1 2D Model

The 2D models analyse the critical section in the horizontal plane (section AA') and in the vertical plane (section BB'). The set-up of both models is described in the paragraphs below.

Section AA'

The length (w) of the stirrup in combination with the height of the compression arc (stirrup depth plus cover on one side , $d+c = 500mm$) determine the orientation (α) of the compression arc at the corner, as can be seen in figure 4.8. The arc is assumed to follow a parabolic shape, resulting in a load orientation at the corner[2] of $tan\alpha = 2(d+c)/0.5w$. This gives the following range for the orientation $61° < \alpha < 78°$. The width of the compression arc is estimated at $0.5(d+c) = 250mm$ (figure 4.8). This estimation is based on Dörendahl et al. (2004). The width is constant and perpendicular to the curvature of the arc. For the effective width of the arc on the detail the arc width is divided by $\sin(\alpha)$.

The supports of the models should restrict the rigid body movements of the element, simulating the

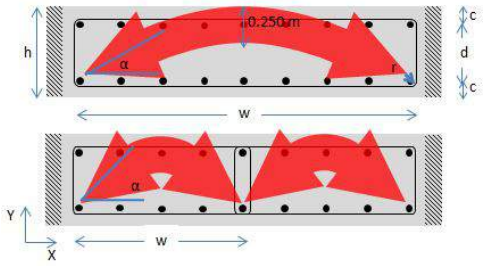

Figure 4.8: Parameters and orientation of the compression arc (not to scale)

effect of the surrounding soil-mix and embedded reinforcement. Cross section AA' models the transfer of horizontal stresses in the soil-mix to tensile forces in the reinforcement. To model these supports the ends of the reinforcement are clamped in a stiff element, whilst not allowing any slip at these points. The stiff elements are then provided with supports in both directions. The support perpendicular to the orientation of the reinforcement is only present to avoid lateral movement of the reinforcement. It shouldn't lead to any support reactions, since the reinforcement is not able to transfer shear forces. This implies that clamping the reinforcement bars lead to the restriction of two degrees of freedom. To create a statically determined model one additional support is required. Therefore the element is supported in y-direction at the entry point of the reinforcement oriented in the x-direction, see figure 4.9.

Aside from the supports of the reinforcement bars, the detail is surrounded by soil-mix which prevents large deformations and rotations. These restrictions are modelled by the application of line springs resembling the surrounding soil-mix. The spring properties have been defined in chapter 3. As mentioned these springs have a low stiffness, to avoid unrealistic stress concentrations at the springs.

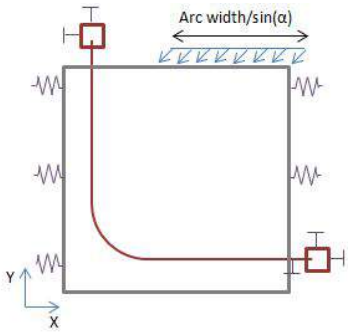

Figure 4.9: Cross section AA' - supports (confined)

Section BB'

The vertical loading on the reinforcement detail depends on the spacing between the stirrups. With smaller spacing, the vertical component of the diagonal force decreases. The estimated spacing ranges from 50 to 250 mm as seen in table 4.1. The horizontal distance which the diagonal crossed is equal to

[2]The orientation of the load changes slightly along the width of the arc, but this is within the range of 2°. Therefore this approximation is sufficiently accurate.

the depth of the wall minus the concrete cover on one side (h-c), which is 500 mm. Which results in an orientation angle of $\tan\beta = spacing/500$ with the horizontal line. This angle lies within the following range $6° < \beta < 26°$.
The height along which these stresses are present, is initially equal to the spacing between the stirrups. Stresses acting outside the spacing are transferred to other stirrups. Closer to the detail the height will decrease, since the stresses are redistributed to concentrate around the reinforcement bar. The detail represents approximately half of the depth of the wall, therefore the height of the compression diagonal is set at half of the spacing at the edge of the detail.
The slice contains the cross section of a stirrup bar. The stirrup is loaded in tension, which provides resistance against in plane movements. This is modelled by restricting displacement in both the x- and y direction. Since it is a vertical cross section of a small part of a wall, the element has soil-mix atop and underneath it. The material below provides support against vertical movement as well as rotational stability (third degree of freedom). The influence of the material below is crucial to the stress distribution within the detail, therefore it cannot be neglected. The material below is included in the model as a line spring, with spring properties based on the stress-strain relation found with the displacement controlled lab tests. The soil-mix above the element does not provide support, but it does result in additional compressive forces in the material due to its self-weight. The magnitude of these stresses however is small and is therefore neglected. Figure 4.10 shows the supports of the model.

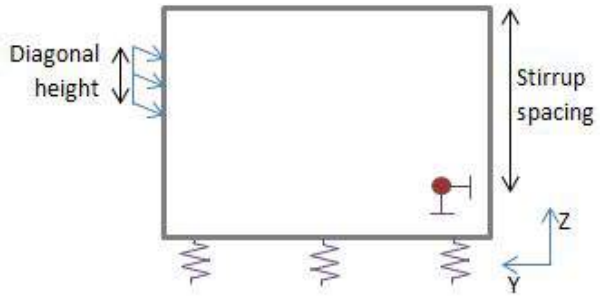

Figure 4.10: Cross section BB' - supports

4.2.2 3D Model

The 3D model contains both the longitudinal reinforcement bar as well as the stirrup corner. It is loaded with pressure with components in both the horizontal and the vertical direction. The orientation of these stresses is a combination of the horizontal and vertical angle specified earlier. Since the corner is supported by soil-mix below, this side is supported with surface springs. These springs account for the retaining capacity of the supporting material and avoid large rotational displacements. The reinforcement bars are clamped outside of the detail, to allow for stresses to develop in the bars (see figure 4.11). The entry point of the bar at the utter right and top are also restricted in the lateral (Y) direction, to restrict all six degrees of freedom. The clamps represent the part of the reinforcement embedded in the soil-mix outside of the detail dimensions to which the reinforcement stresses are transferred in reality[3]. The 3D model is able to account for the multi-axial loading state of the detail and the stress distribution from compression in the soil-mix to tensile stresses in the reinforcement. Additionally it also provides displacements and cracks in multiple directions.

4.2.3 Geometry

The model of the detail has to represent the behaviour of the reinforcement in reaction to the loading conditions described in the previous section. This implies that the geometrical dimensions of the detail

[3]Theoretically the support from the reinforcement bars should be sufficient to avoid rotational movement. However the shear capacity of single bars is only low, which explains the necessity of the spring supports.

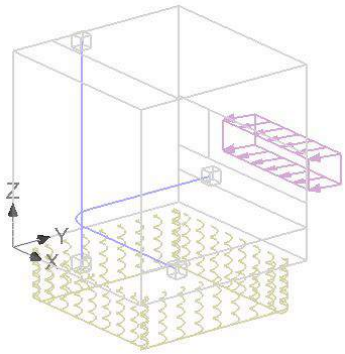

Figure 4.11: 3D model - supports

have to be large enough to apply the described load configurations. Figure 4.12 gives a visual representation of the 2D models, both the vertical and the horizontal slice of the detail. The outer dimensions of these elements and the coverage are constant values. The radius of curvature of the reinforcement, the height of the section, the orientation and the magnitude of the loading are variable. The depth and

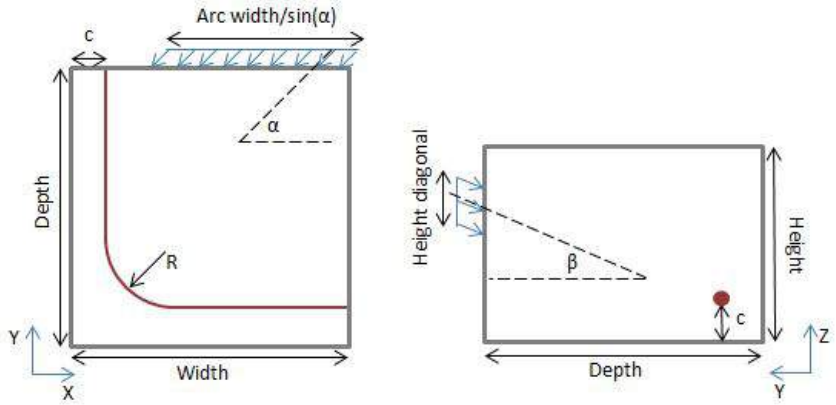

Figure 4.12: Geometrical parameters 2D models

the width of the model are set at 300 mm. These dimensions are sufficiently large to include both the coverage and the arc width.
The height of the detail varies and depends on the chosen spacing between the stirrups. Since the diagonal reaches the node from above, the reinforcement bar is positioned at the bottom of the cross section. To avoid unrealistic failure a small layer of soil-mix is positioned below the reinforcement bar. Additionally the element is supported with springs at the bottom edge, the springs represent the soil-mix below the section. The spring properties are based on the stress-strain relation which resulted from the displacement controlled test performed on multiple physical soil-mix samples (chapter 3). The influence of the height of the detail (which is directly related to the height of the compression diagonal), is analysed by using three different values for the height (50, 150 and 250 mm). The height of the diagonal is chosen to be equal to half the spacing and is varied from 25 to 125 mm with three steps of 50 mm. This is done because the detail only represents half of the depth of the wall. The assumption is made that the stresses have already been partially redistributed at the edge of the detail.
The coverage of the reinforcement bars is set at 50 mm. Compared to concrete reinforcement this is rather high. This is done because durability is a crucial point of soil-mix structures. The cracking behaviour of the material is largely unknown, but based on the weak properties of the material it is expected to be sensitive to cracking. A low coverage in combination with high risk of cracking leads to high risk corrosion of the reinforcement steel. So to increase the probability of a durable structure, the coverage is increased relative to typical concrete coverage.
The radius of curvature strongly influences the stress distribution within the horizontal cross section.

A smaller radius of curvature leads to a stronger deflection in the stress trajectories and on its turn higher tensile stresses. The influence of the radius is analysed by varying the value between two and ten times the diameter of the reinforcement bars. These values are based on the guidelines for curvature of reinforcement in concrete, which suggests a radius of curvature equal to five times the bar diameter (5ϕ) (Eurocode2, 2011). This analysis is meant to lead to a minimum or ideal value for the radius of curvature.
The orientation of the loading is based on the dimensions of the stirrups. Which was elaborately discussed in the previous section. The orientations of the loads will be varied, to find the optimal reinforcement design. The orientation of the vertical diagonal is directly related to the stirrup spacing and thus the height of the element.
The bar diameter is set at 10 mm. Due to the low bond strength between the soil-mix and steel, the best cooperation is achieved by applying multiple bars with a smaller diameter instead of a few large bars. By doing so the contact area between the two materials is increased, which also increases the total bond capacity. Based on this theory only 10 mm bars are used in these models.
Both 2D models represent a slice of the 3D model, which is described in the next section. The slices are used to analyse the stress distribution. To find the most likely failure mechanism in both the horizontal and the vertical plane. The thickness of the horizontal slice (AA') is set at 50 mm. This slice represents the redistribution of the horizontal stresses, to analyse the possible failure in this plane. With a thickness of 50 mm, the actual angle of the stresses required to reach the reinforcement range with 5° both up and down (perpendicular to the plane). This is relatively small which approximates the solely horizontal stresses and limits the chance on vertical splitting cracks.
The thickness of the vertical slice (BB') is set at 20 mm. This slice represents a vertical plane with concentrated stresses from the compression diagonal as well as from the compression arc. Since the stresses are not distributed uniformly along the reinforcement bar, only a 20 mm thick slice is considered for this analysis. Also, the cross section of the reinforcement bar in the slice is assumed to be fixed in place. If the thickness was to be increased, this would not be an accurate representation of reality.
The thickness of the element is important when determining the applied loads.
The 2D models have been meshed with blocks of 0.01 m. The 3D model has been meshed with a tetra mesh of 0.04 m. Due to additional geometrical joints necessary for the input of the load and boundary conditions it was not possible to mesh the 3D model with bricks. A smaller mesh size leads to both higher accuracy and more required calculation capacity. The chosen mesh sizes for the 2D and 3D models are based on an optimization of accuracy and calculation time.
Table 4.2 gives an overview of all final geometrical parameters, including an indication on which parameters have been altered throughout the modelling process to analyse their influence.

Table 4.2: Final geometrical parameters models

Dimension	**Range**	**No. of steps**
Depth	300 mm	-
Width	300 mm	-
Height	100–300 mm	3
Coverage	50 mm	-
Width arc	250 mm	-
Height diagonal	25 – 125 mm	3
Radius	$2\phi - 10\phi$	4
α	$61° - 78°$	3
β	$6° - 26°$	3
Diameter reinforcement	10 mm	-
Thickness (AA')	50 mm	-
Thickness (BB')	20 mm	-
Mesh size 2D (brick)	0.01 m	-
Mesh size 3D (tetra)	0.04 m	-

4.3 Results

Running the simulation of each model for the relevant geometrical parameters resulted in the governing failure mechanisms and the corresponding loads. The load steps preceding the ultimate step show how the cracks propagate until failure. The sections below provide the results for each 2D model and the 3D model. The colour scales in the 2D model use red for maximum compression and blue for maximum tension with blue, the 3D model uses an inverted colour scale.
To assess the capacity of each model the following load levels were analysed.

- Load when the initial crack occurs, which corresponds with the location predicted in the hypothesis ($F_{cr,in}$)
- Failure load, at which the cracks are fully developed and the model fails (F_{cr})

To validate the modelled results, they have been compared to the hypothesis on the failure mechanism described in section 4.1.2. Additionally the results of section BB' have been compared to hand calculations of strut and tie models (Eurocode2, 2011) which represent a simplification of the stress distribution within the section[4].
The maximum capacities acquired from the modelled results are interpreted in such a way that the can be used to draft preliminary design guidelines for bar reinforced soil-mix walls. This has been done in section 4.5.

4.3.1 2D Model

Section AA'
Combining the geometrical and physical data into a 2D model representing the horizontal cross section AA' resulted in the model input as shown in figure 4.13. This figure shows the input for the model used to calculate the stress distribution with a radius of 7ϕ and a load orientation of 60°(related to a stirrup length of 1100 mm). The other models have a different load orientation and/or radius of curvature.
Figure 4.14 shows the influence of the orientation of the load angle for the radius of curvature equal to

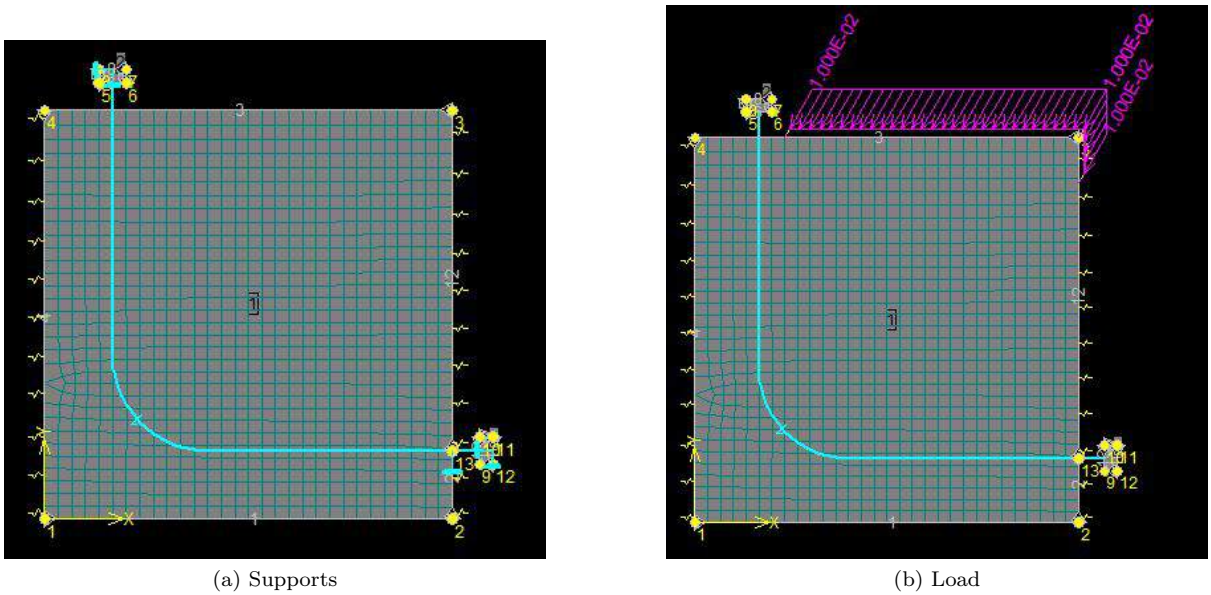

(a) Supports (b) Load

Figure 4.13: Input 2D model vertical section AA'

2ϕ. It shows that the cracks develop parallel to the load orientation, so with a larger angle for steeper

[4] A similar comparison for section AA' was not possible. Due to the constant redistribution of stresses within the section, it was not possible to design one representative strut and tie model for comparison.

load orientations. Figures 4.15 to 4.17 show the modelling results of section AA' for the remaining radii of curvature. The figures present the failure mechanisms of the cross sections, by displaying the developed cracks and the corresponding maximum principal stresses ($\sigma_{principal,max}$) and vertical stresses (σ_{zz}). The stress scale is included in the figures. The vertical stresses show that the section is in compression perpendicular to the plain. This is caused by the tendency of the section to expand in this direction. However those deformations are restricted by the plain strain elements used to model the section. Without this restriction the model would likely display tensile stresses in the z-direction, leading to vertical splitting cracks. With larger radii, the compressive stresses (σzz) are smaller and more spread out. This is in line with the expectations of more concentrated forces with small radii of curvature.
The location of the initial cracks and the crack propagation confirm the expectations. As predicted the sections which included a reinforcement bar with a small radius of curvature had a lower capacity than the ones with a large radius. Increasing the ratio up to 7ϕ even avoids diagonal cracks all together. Those sections fail due to reaching the bearing capacity of the soil-mix near the entry points of the reinforcement or on the outer edge of the stirrup corner. This is where excessive displacements occurred, which lead to divergence of the computations. The maximum capacities of the cross sections are presented in table 4.3. This table gives the applied load at the occurrence of the initial splitting crack and the maximum applied load at failure. With large radii splitting cracks do not occur, therefore these rows are empty in the table.
The results indicate that the detail is more sensitive to splitting failure when stirrups with a small radius of curvature have been applied. The orientation of the applied load has a small influence on the failure load. A load with a steeper orientation of 70° and 80° (corresponding with a stirrup length of respectively 750 an 400 mm) seem to have the highest risk of failure. These stress distributions contain more regions of critical stress, which makes them more sensitive to failure.

Table 4.3: Splitting and failure load for section AA'

Radius	**2ϕ**								
Stirrup length	**1100 [mm]**			**750 [mm]**			**400 [mm]**		
First crack	Step 34	23.8	[kN]	Step 35	19.4	[kN]	Step 52	16.6	[kN]
Failure	Step 85	35.7	[kN]	Step 130	39.5	[kN]	Step 150	41.9	[kN]

Radius	**5ϕ**								
Stirrup length	**1100 [mm]**			**750 [mm]**			**400 [mm]**		
First crack	Step 85	40.1	[kN]	Step 69	32.4	[kN]	Step 354	30.3	[kN]
Failure	Step 167	58.5	[kN]	Step 140	53.0	[kN]	Step 96	54.6	[kN]

Radius	**7ϕ**								
Stirrup length	**1100 [mm]**			**750 [mm]**			**400 [mm]**		
First crack	-			-			-		
Failure	Step 124	59.7	[kN]	Step 136	55.6	[kN]	Step 98	57.3	[kN]

Radius	**10ϕ**								
Stirrup length	**1100 [mm]**			**750 [mm]**			**400 [mm]**		
First crack	-			-			-		
Failure	Step 115	54.5	[kN]	Step 129	55.5	[kN]	Step 20	55.7	[kN]

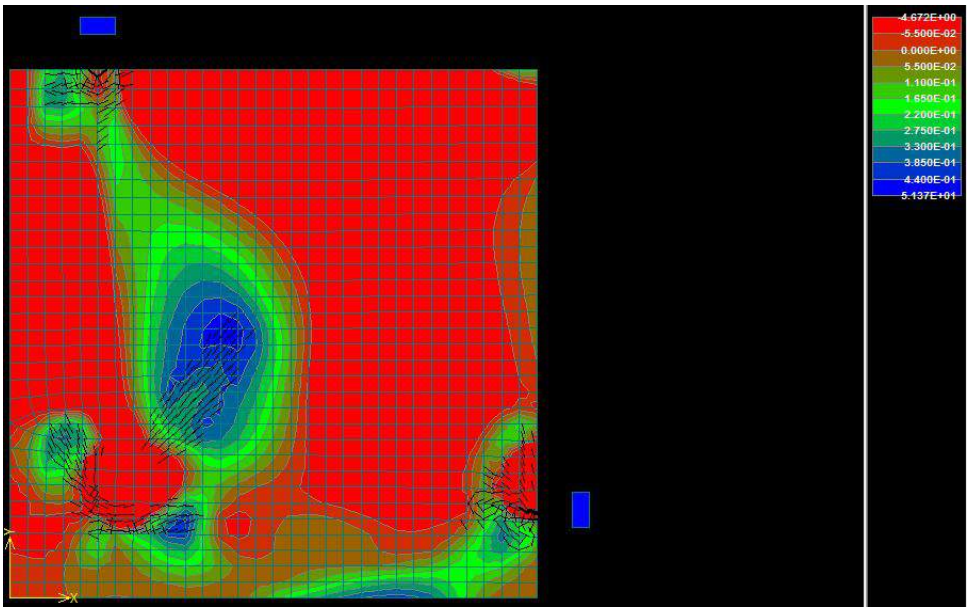

(a) $\alpha = 60°$, step 60

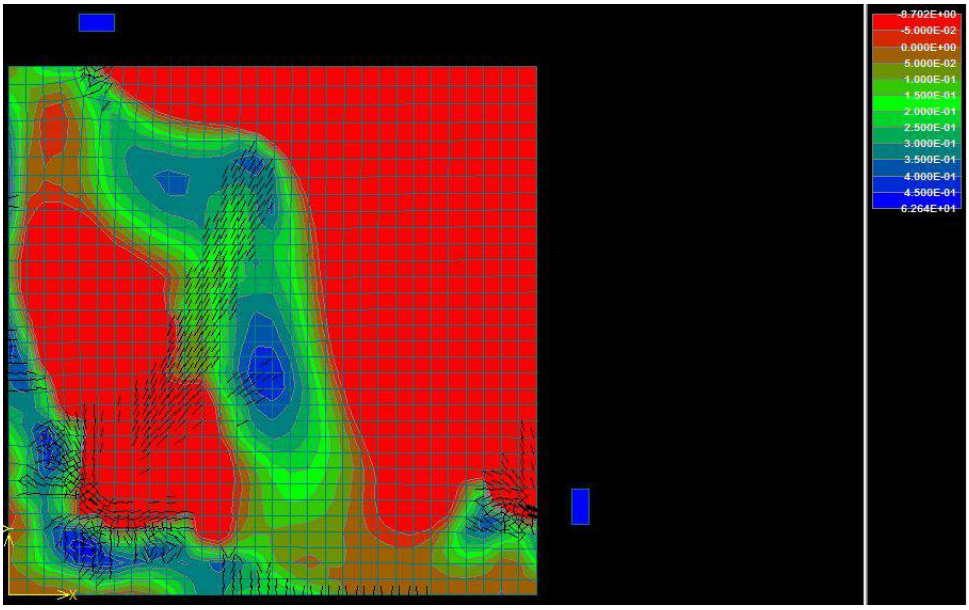

(b) $\alpha = 80°$, step 100

Figure 4.14: Results horizontal section AA' (radius 2ϕ), $\sigma_{principal,max}$

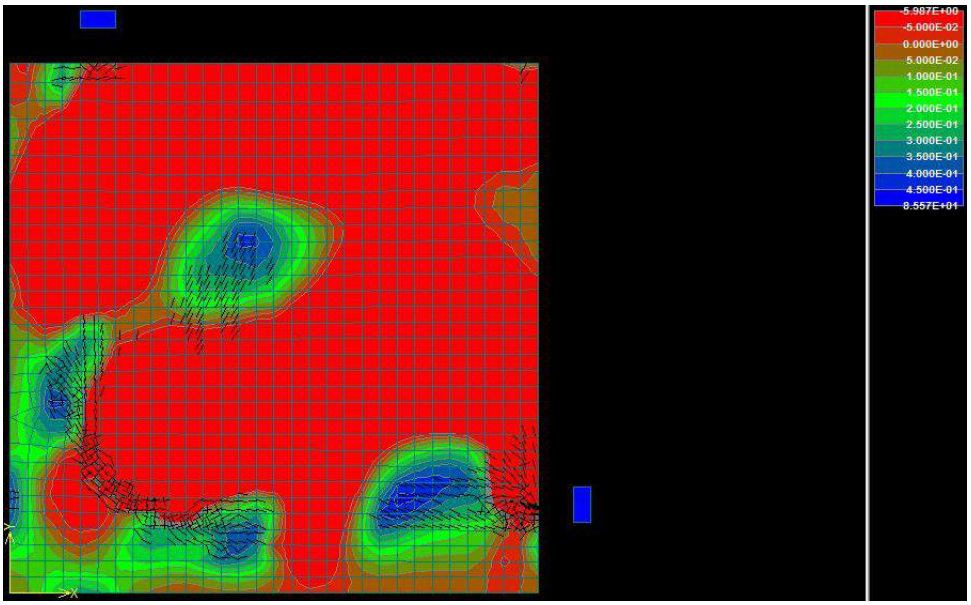

(a) $\alpha = 60°$, step 120, $\sigma_{principal,max}$

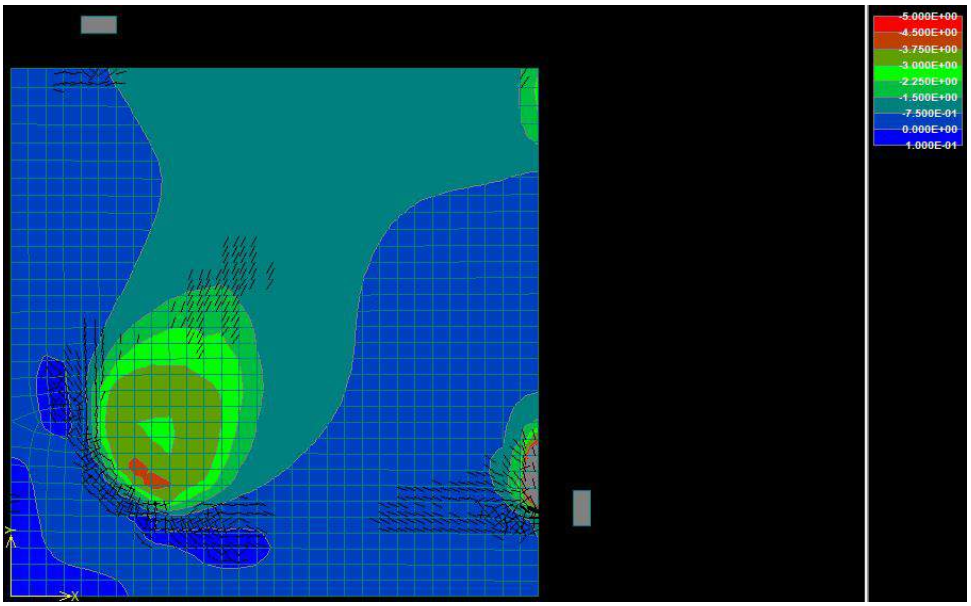

(b) $\alpha = 60°$, step 120, σ_{zz}

Figure 4.15: Results horizontal section AA' (radius 5ϕ)

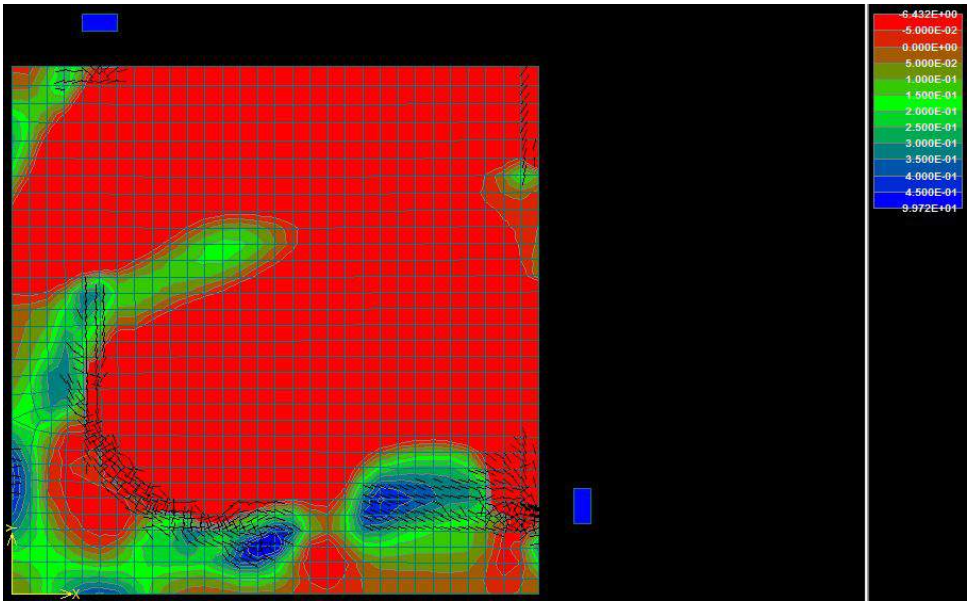

(a) $\alpha = 60°$, step 124, $\sigma_{principal,max}$

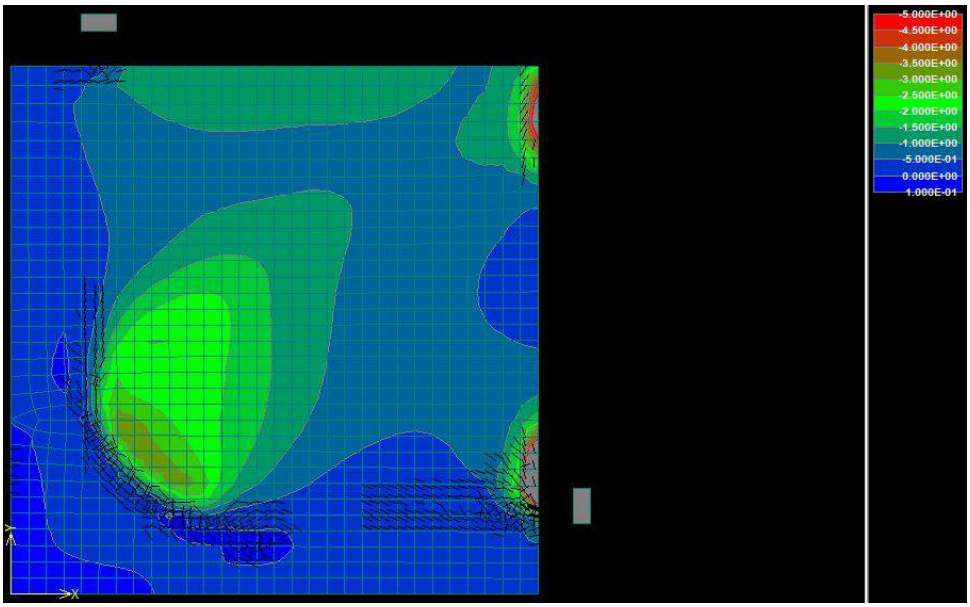

(b) $\alpha = 60°$, step 124, σ_{zz}

Figure 4.16: Results horizontal section AA' (radius 7ϕ)

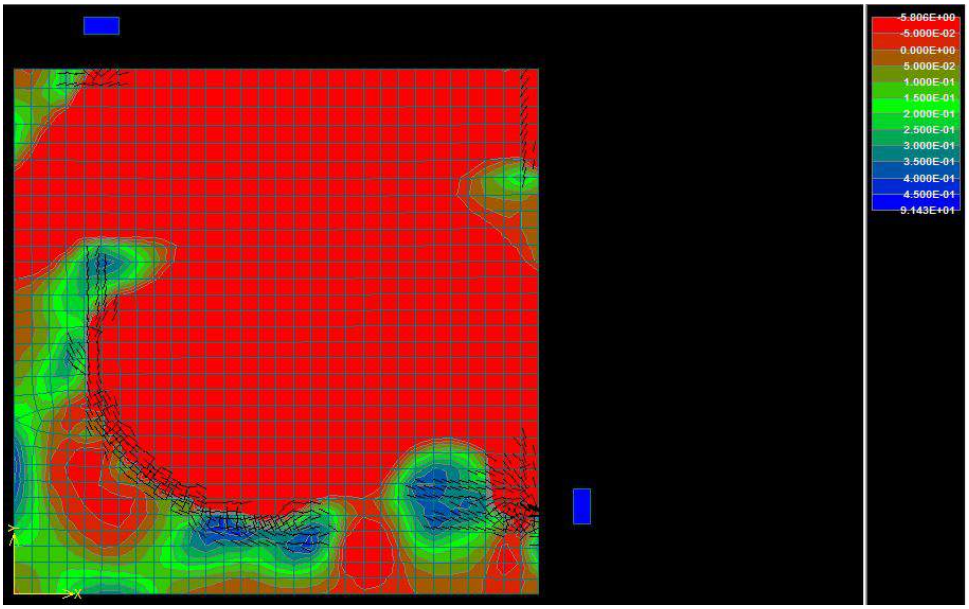

(a) $\alpha = 60°$, step 115, $\sigma_{principal,max}$

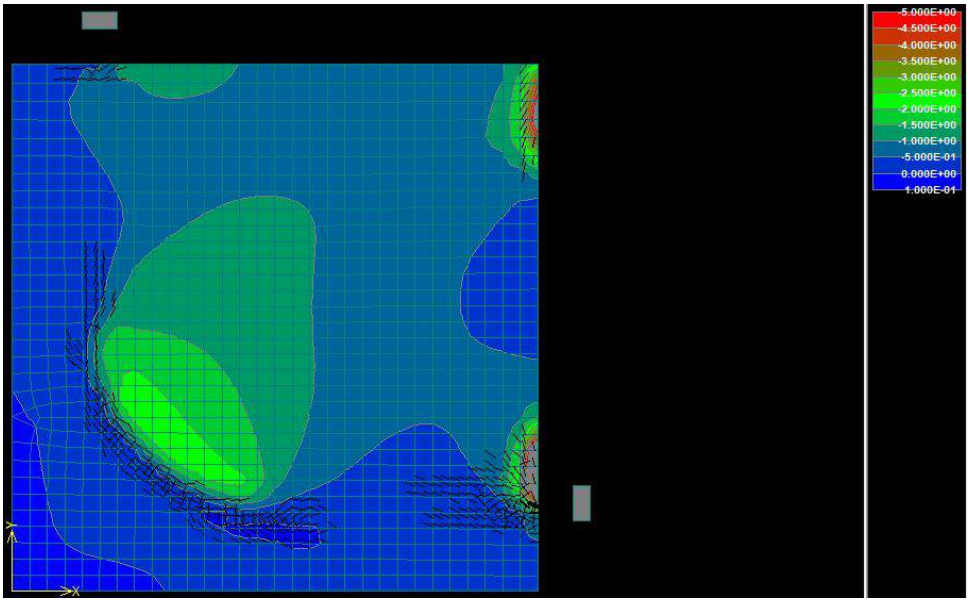

(b) $\alpha = 60°$, step 115, σ_{zz}

Figure 4.17: Results horizontal section AA' (radius 10ϕ)

Section BB'

Most relevant to the stress distribution within the vertical cross section BB' is the spacing between the stirrups. The spacing determines the orientation and the width of the compression diagonal in the section. The section was analysed for a spacing of 50, 150 and 250 mm. Figure 4.18 shows the geometrical input of the model with a spacing of 150 mm. The input for the models representing a spacing of 50 and 250 mm are similar to the input for a spacing of 150 mm. The difference is the total height of the section and the length along which the load is applied.

The results of the model confirmed the hypothesis, since the crack propagation confirms the expectations

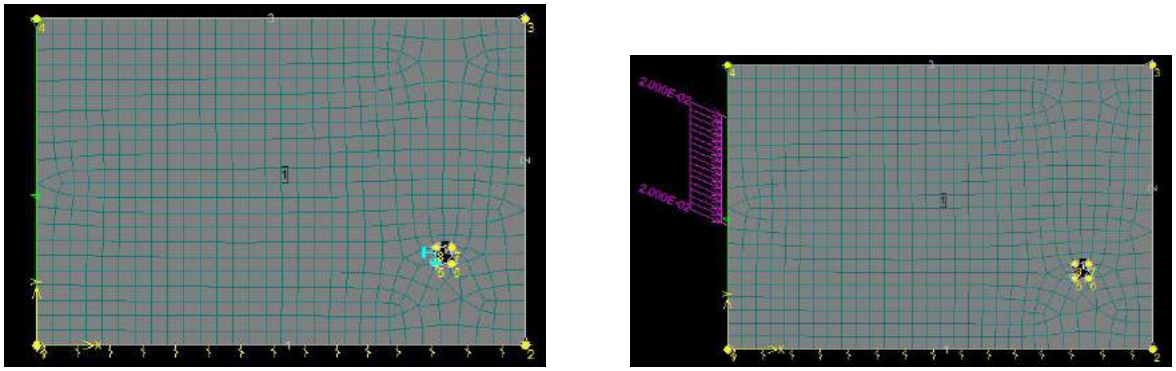

(a) Supports (b) Load

Figure 4.18: Input 2D model vertical section BB'

described in section 4.1.2. The cracks develop parallel to the loading direction and originate at the reinforcement bar[5]. Figures 4.19 to 4.21 present the results of the models at multiple stages of crack development. The applied load at the initial crack ($F_{cr,in}$) and at failure (F_{cr}) is specified in table 4.4. It shows that the larger the spacing, the more sensitive the model is to splitting cracks (lower stresses).

Table 4.4: Applied loads at initial cracking and at failure in section BB'

Spacing	50 mm			150 mm			250 mm		
		$\boldsymbol{F[kN]}$	$\boldsymbol{\sigma[MPa]}$		$\boldsymbol{F[kN]}$	$\boldsymbol{\sigma[MPa]}$		$\boldsymbol{F[kN]}$	$\boldsymbol{\sigma[MPa]}$
First crack	step 3	1,5	3	step 4	1,8	1,2	step 4	1,8	0,7
Failure	step 10	4,6	9,2	step 11	6,6	4,4	step 11	5,5	2,2

[5]When the spacing is reduced to 50 mm, the cracks initiate near the load application as well. Due to the concentrated character of the applied load the stresses tend to spread out, which results in tensile stresses near the edge of the section.

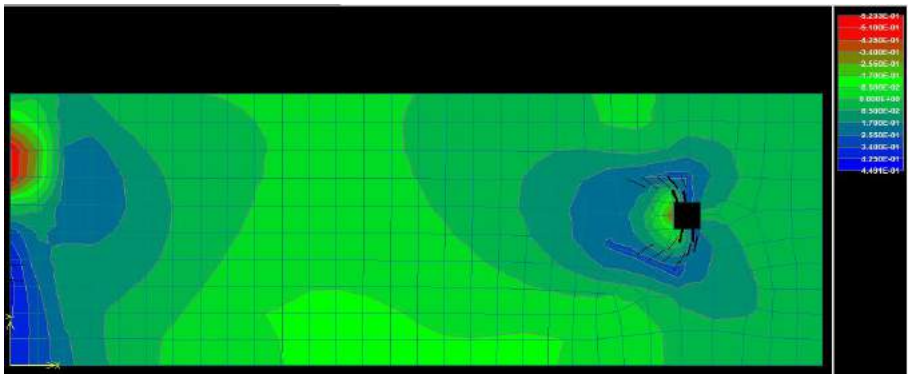

(a) Step 3

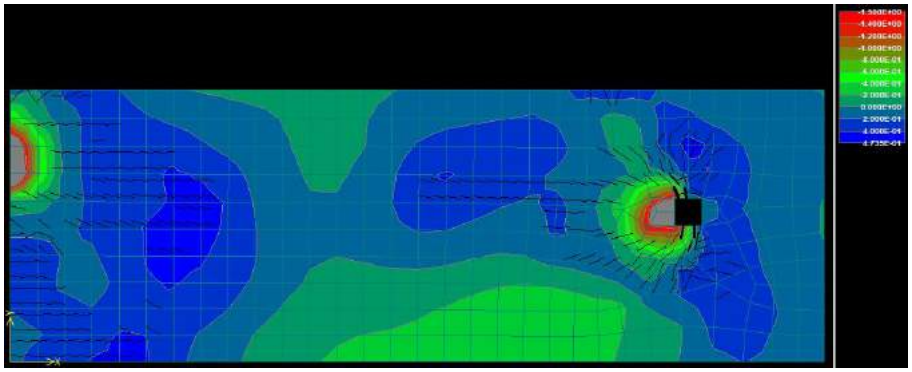

(b) Step 9

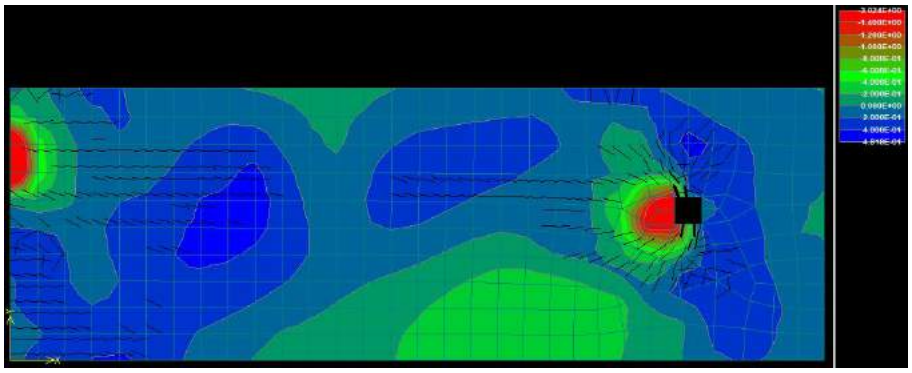

(c) Step 10

Figure 4.19: Results vertical section BB' (spacing 50 mm), $\sigma_{principal,max}$

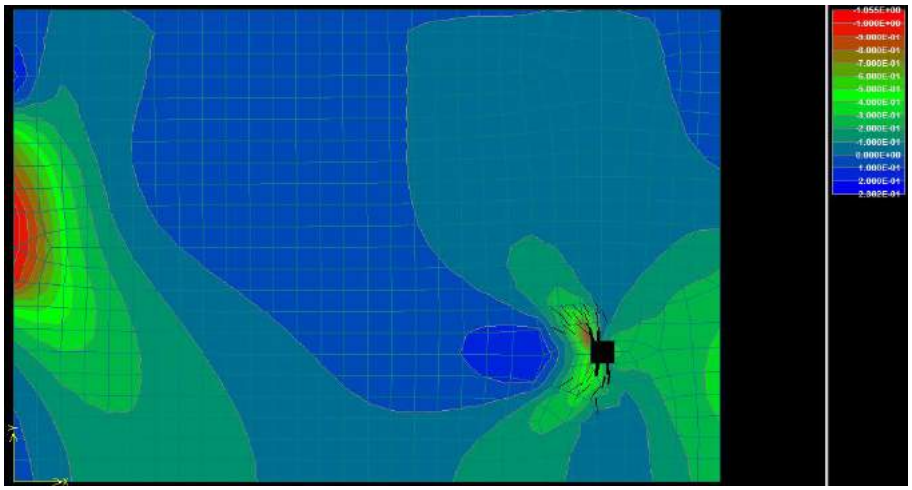

(a) Step 4

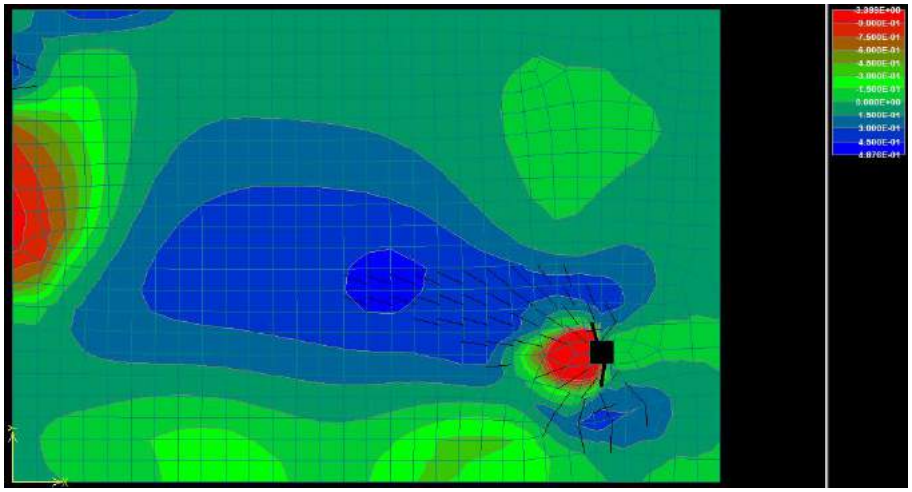

(b) Step 9

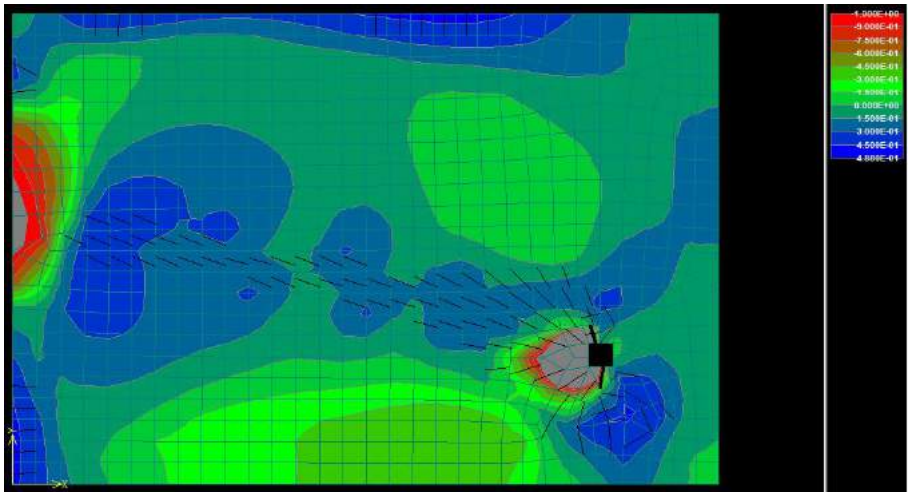

(c) Step 11

Figure 4.20: Results vertical section BB' (spacing 150 mm), $\sigma_{principal,max}$

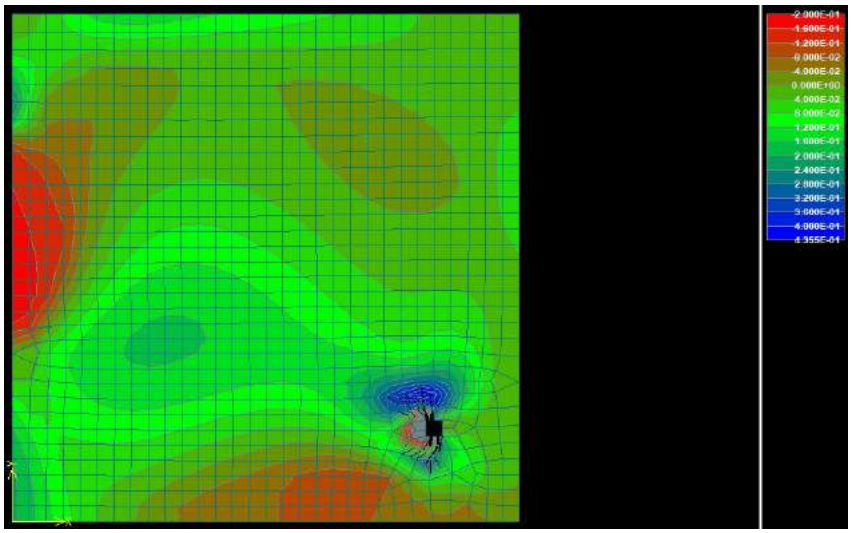

(a) Step 4

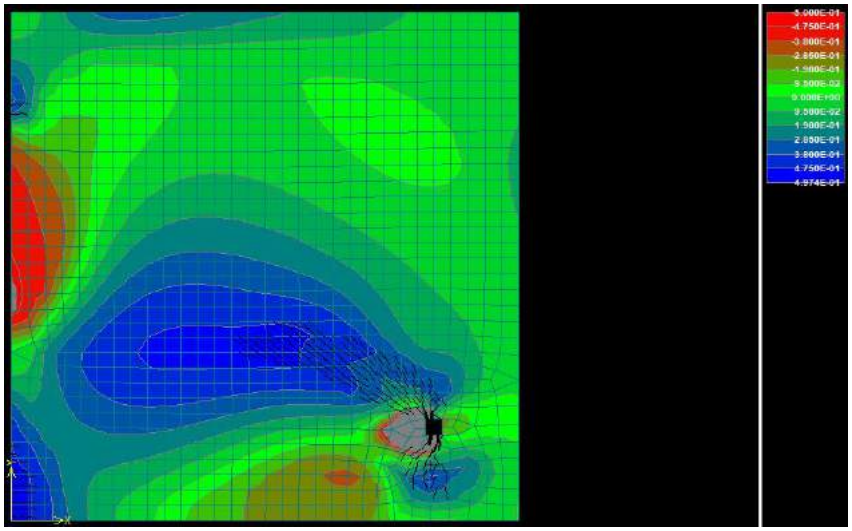

(b) Step 10

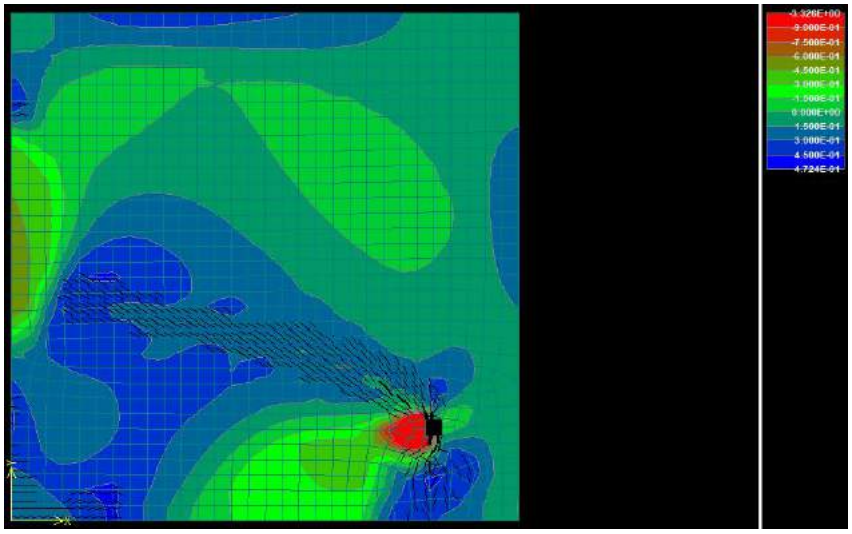

(c) Step 11

Figure 4.21: Results vertical section BB' (spacing 250 mm), $\sigma_{principal,max}$

For additional verification these results have been compared to hand calculations which simplify the model to a strut and tie model. Eurocode2 (2011) describes a method to calculate the forces in a strut and tie model. In the case of section BB', compression is applied as distributed stresses. Which implies that half of the strut and tie model suggested in Eurocode2 (2011) is sufficient. The effective width of the compressive stress (25 - 125 mm) is smaller than the height of the model (h). Therefore the following equation is valid for determining the force in the tensile tie (Eurocode2, 2011). The resulting ratio (r_t) between the tensile and compressive force is presented in table 4.5.

$$F_t = \frac{1}{4}\frac{b-a}{b}F_c \tag{4.1}$$

When translated to stresses, the tensile force can give an indication on the state of crack propagation.

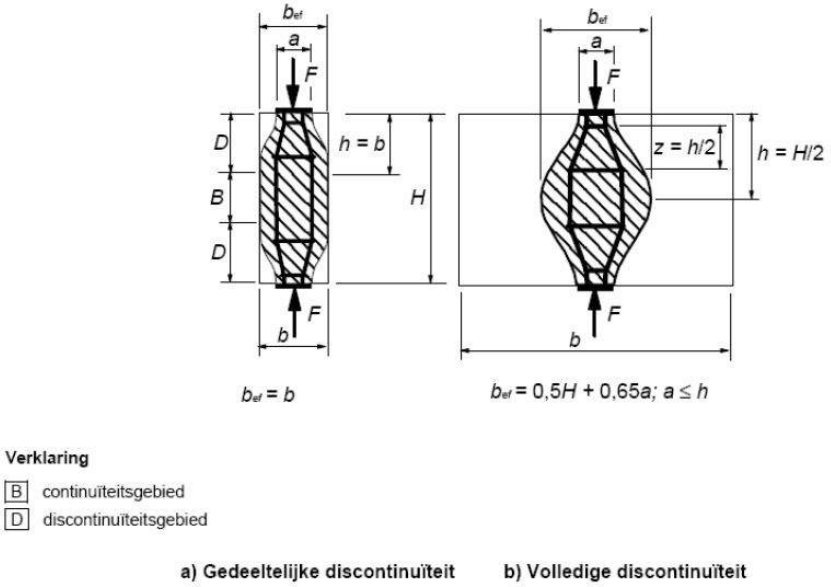

Figure 4.22: Strut and tie model (Eurocode2, 2011)

The results corresponding with an early stage of crack development have been compared to expected values according to the strut and tie simplification. The results are shown in table 4.6. The tensile force which followed from the strut and tie model was combined with the tensile strength (0.50 MPa) and the thickness of the elements (20 mm) to find the length along which the maximum capacity is reached. The last two columns show the length along which cracks have developed, the expected length based on the strut and tie model and the length found in the model results. The two values are similar, which validates the modelled results.

Table 4.5: Ratio between applied compressive force and tensile force from the strut and tie model

	$F_t = r_t \cdot F_c$		
Spacing [mm]	50	150	250
Factor r_t [-]	0.15	0.22	0.23

Table 4.6: Comparison between modelled results and strut tie simplification

Spacing	**Total load [kN]**	σ_c **[MPa]**	F_t **[kN]**	**Cracked length [mm]**	**Modelled cracked length [mm]**
50 mm	4.50	9.00	0.68	68	60
150 mm	5.40	3.60	1.17	117	120
250 mm	5.00	2.00	1.15	115	140

4.3.2 3D Model

The 2D models have proven that the failure mechanisms which were expected based on the stress trajectories, are likely to occur in the detail. The maximum capacity of cross section BB' is significantly lower than that of cross section AA' (appendix XI presents an overview of the total forces on the detail derived from the model results), which indicates that this failure mechanism is likely to be governing. However, it is important to realise that the actual problem addresses a multi-axial stress state. The applied stresses from both the compression arc and diagonal are simultaneously transferred to the reinforcement both vertically and horizontally. Which means that the stress distributions analysed in the separate cross sections are likely to influence each other. The expectation is that the horizontal distribution of stresses decides the location of failure due to vertical splitting (like in section BB').To analyse the influence of the multi-axial stress state, the detail has been constructed as a 3D model.
The 3D model is based on the same physical and geometrical parameters as the 2D models and is restricted by similar boundary conditions. In addition to the 2D models, the 3D model contains a segment of the longitudinal reinforcement on the inside of the stirrup corner. Both segments of reinforcement (stirrup and longitudinal bar) have been clamped outside of the detail to represent the reinforcement embedded in the surrounding soil-mix. This longitudinal bar is likely to influence the capacity of the detail regarding vertical splitting (seen in section BB').
The interpretation of a three dimensional model is more complicated than the interpretation of a model representing a single plane. To analyse the stress distribution within the three dimensional model, two cross sections have been specified to analyse the stresses in relevant planes. These sections have were taken parallel to the stirrup at equal height (XY plane section AA', figure 4.23a) and parallel to the YZ-plane at the start of the curvature of the stirrup (section BB', figure 4.23b).

(a) Section AA' (b) Section BB'

Figure 4.23: Relevant planes 3D model

The stress distributions in the two cuts were compared to the 2D results. Both stress distributions (figure 4.24 to 4.26) show similar stress distributions as found in the 2D models. The cut representing section AA' shows that the highest values of $\sigma_{principal,max}$ are concentrated in a similar way, as seen in the 2D model of the section. This is caused by the horizontal redistribution of the stresses. In contrast to the 2D model, the governing component of these stresses is mainly vertical[6] (σ_{zz}). In contrast to the 2D results of the model of section AA', σ_{zz} shows tension. This is because the vertical splitting cracks are not restricted in the 3D model, as was the case in the 2D model. The governing vertical tensile stresses imply that the governing failure mechanism corresponds with section BB', failure due to vertical splitting cracks. This is confirmed by the results of the 2D results. The failure load of cross section BB' is lower and is therefore expected to have the strongest influence on the 3D failure mechanism. Appendix X provides a visualization of the failure plane observed in the 3D model.

As expected the capacity of the 3D model is higher than estimated by the 2D model of section BB'. The increase in capacity is related to the presence of the longitudinal reinforcement bar in the 3D model. This bar accounts for vertical tensile stresses and thus delays the failure mechanism occurring in section BB'. Table 4.7 presents the capacities of each model configuration and the corresponding governing failure mechanism. The capacities are based on the applied loads at the occurrence of the initial splitting cracks ($F_{in.cr}$) and at full development of the splitting cracks (F_{cr}).
As expected from the 2D models, the 3D models representing a spacing of 50 mm are more sensitive to the failure mechanism of section AA'. This is due to the limited stress redistribution in the vertical plane. The model representing a radius of 10ϕ and a spacing of 50 mm is an exception to the predetermined failure mechanisms. This model fails due to excessive deformations at the top entry point of the reinforcement.
Due to a larger mesh size of the 3D model, the cracks in the model are more disperse. Like in the 2D model there are many cracks near the entry points of the reinforcement bars. This is an indication of a poor representation of the reinforcement embedded in the surrounding soil-mix.

Table 4.7: Detail capacity based on the 3D model and corresponding planes of the occurring failure mechanisms

Radius	**2ϕ**			**5ϕ**			**7ϕ**			**10ϕ**		
Spacing [mm]	**50**	**150**	**250**	**50**	**150**	**250**	**50**	**150**	**250**	**50**	**150**	**250**
$F_{in.cr}[kN]$	32.3	38.8	32.2	41.4	47.4	44.0	53.7	55.4	44.0	37.4	43.1	44.0
$F_{cr}[kN]$	50.0	58.6	44.0	58.6	70.7	52.0	74.4	71.5	55.8	73.3	63.8	47.0
Plane governing failure mechanism	*AA*	*BB*	*BB*	*AA*	*BB*	*BB*	*AA*	*BB*	*BB*	*X*	*BB*	*BB*

[6]The actual direction of the principal stress is perpendicular to the loading direction in the vertical plane, angle β. So the principal stress direction ranges from 65° to 85° with the XY-plane

(a) Section AA', $\sigma_{principal,max}$

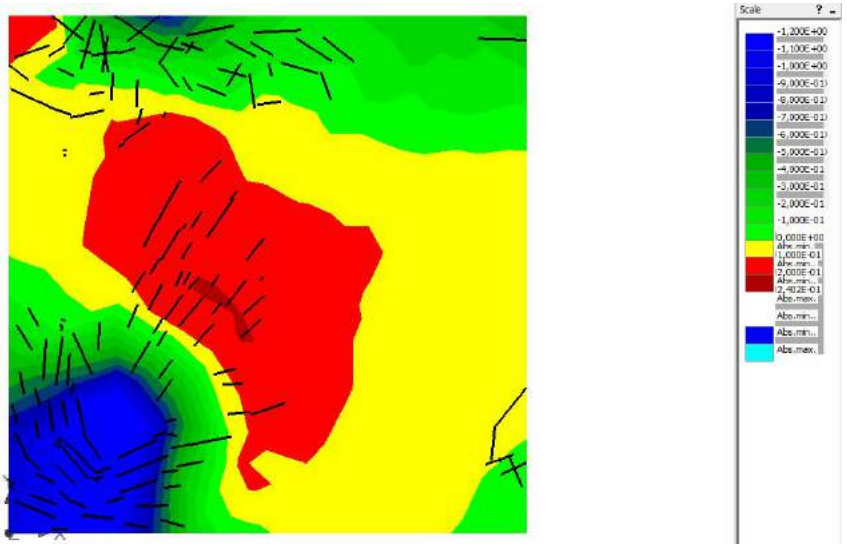

(b) Section AA, σ_{zz}

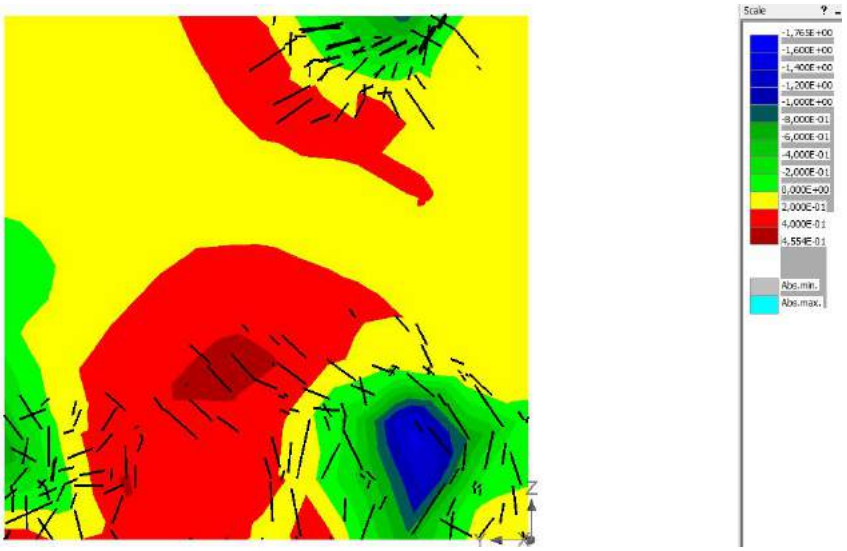

(c) Section BB', $\sigma_{principal,max}$

Figure 4.24: Results 3D model (radius = 2ϕ, spacing = 150 mm, $\alpha = 60°$)

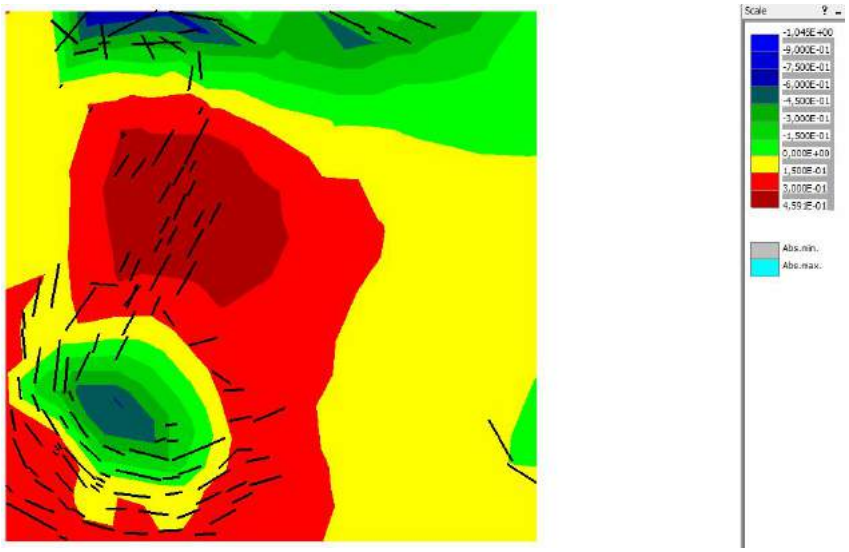

(a) Section AA', $\sigma_{principal,max}$

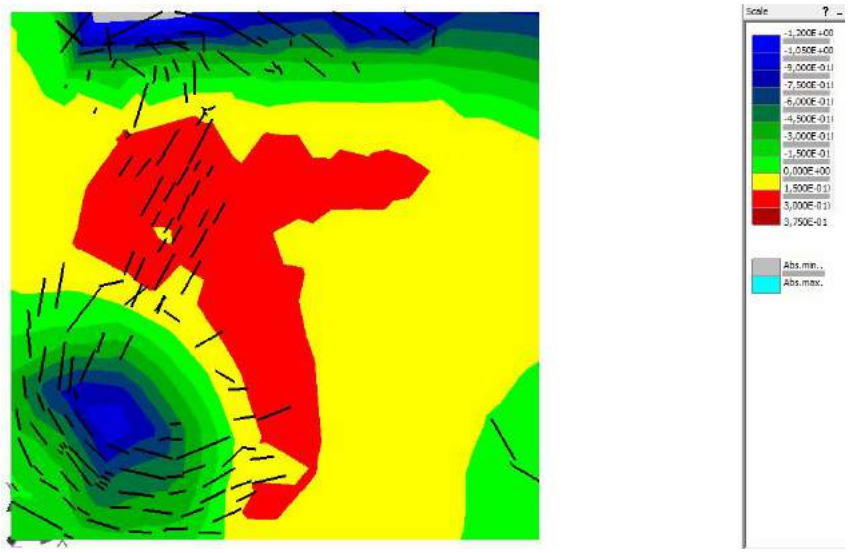

(b) Section AA, σ_{zz}

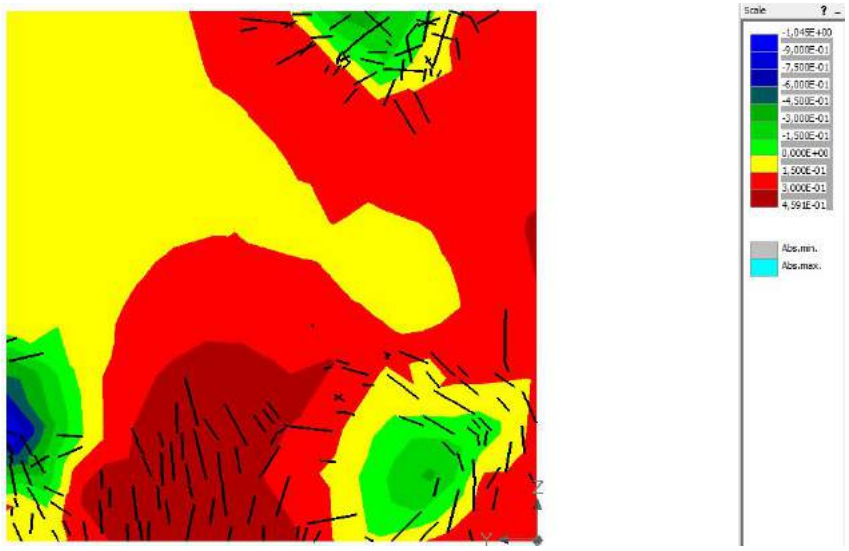

(c) Section BB', $\sigma_{principal,max}$

Figure 4.25: Results 3D model (radius = 5ϕ, spacing =50 mm, $\alpha = 60°$)

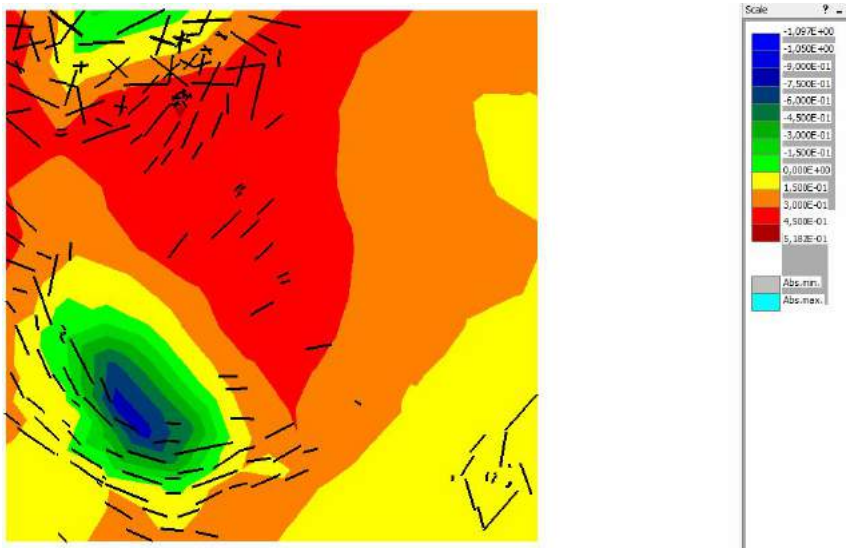

(a) Section AA', $\sigma_{principal,max}$

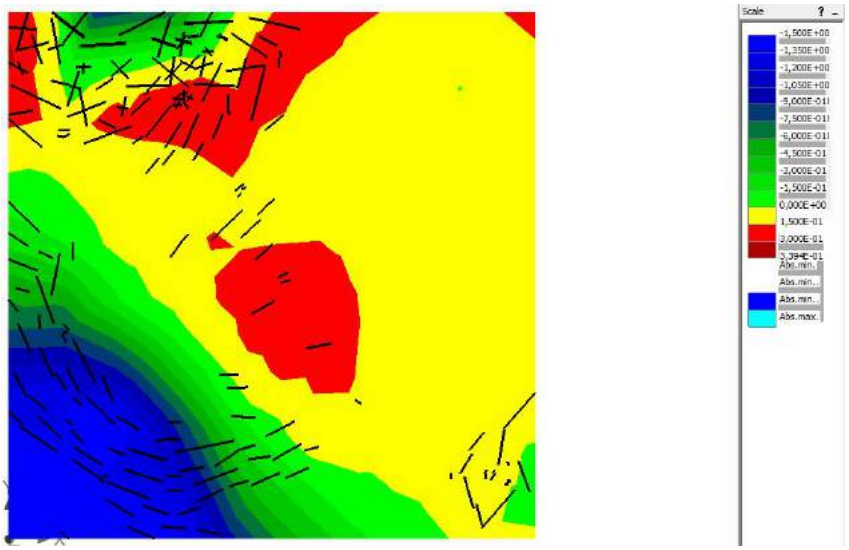

(b) Section AA, σ_{zz}

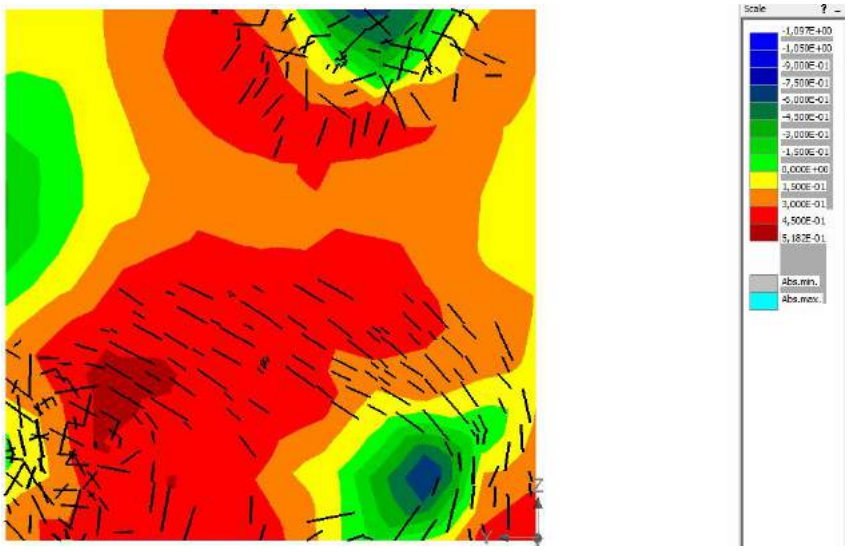

(c) Section BB', $\sigma_{principal,max}$

Figure 4.26: Results 3D model (radius = 7ϕ, spacing = 250 mm, $\alpha = 60°$)

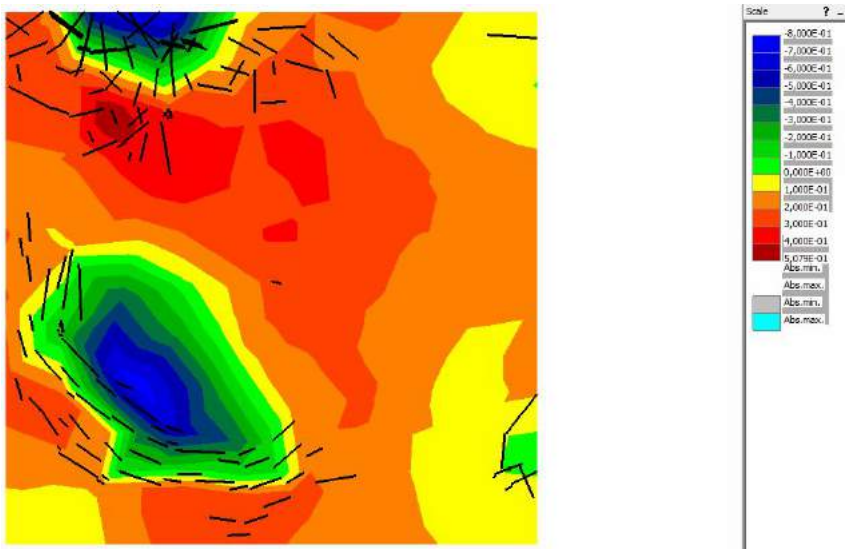

(a) Section AA', $\sigma_{principal,max}$

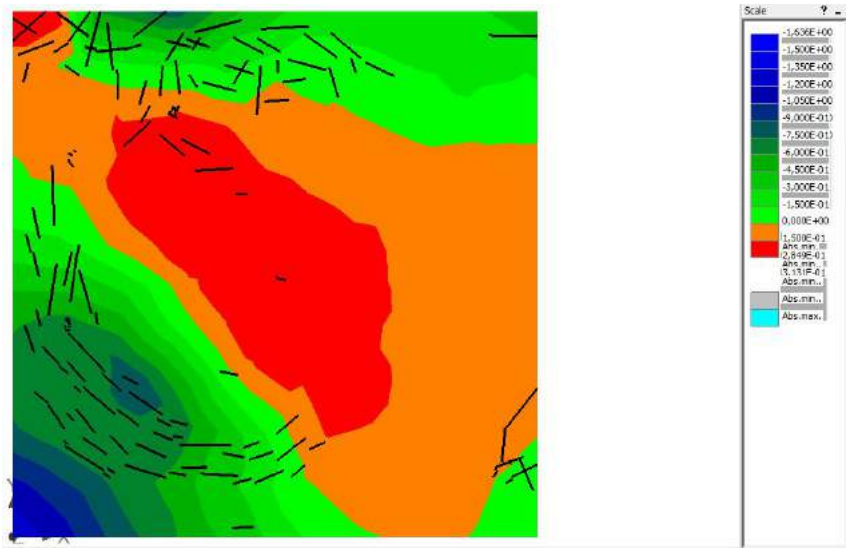

(b) Section AA, σ_{zz}

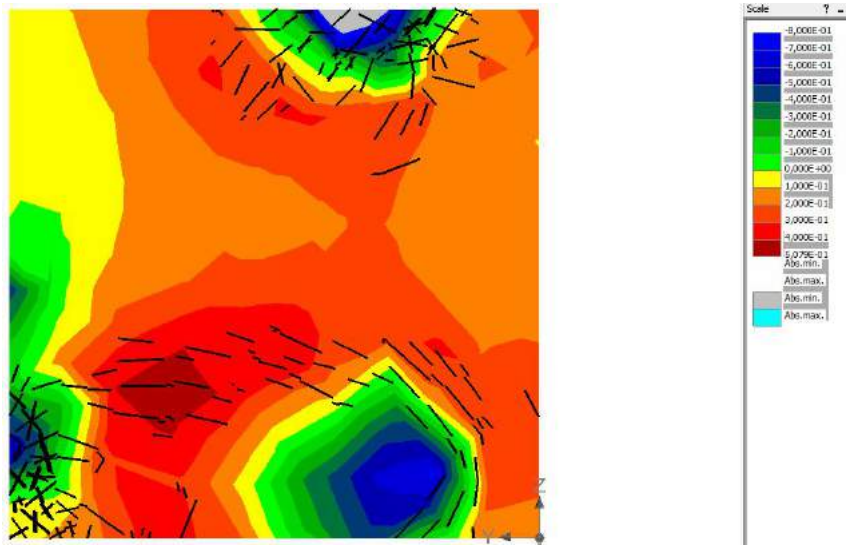

(c) Section BB', $\sigma_{principal,max}$

Figure 4.27: Results 3D model (radius = 10ϕ, spacing = 150 mm, $\alpha = 60°$)

4.4 Discussion

At first glance the results of all three models seem to be satisfactory. The failure mechanisms occurring in the 3D models correspond with a combination of both splitting failures of the 2D models. The resulting stress distribution follows the expected trajectories and the failure mechanisms are in line with the hypothesis. This is concluded from the similarities between the stress distributions in the 2D models and the corresponding cross sections of the 3D model. The location of the splitting failure depends on the geometrical properties of the detail. Based on the 2D models the detail is more sensitive to splitting failure corresponding with section BB'. The stress distribution seen in section AA' is responsible for the location of the vertical splitting failure. Both the position of the cracks and the magnitude of the failure load are dependent on the geometrical parameters of the reinforcement design. When the radius of the corner is decreased or the spacing is increased the failure load is lower.

The real question is whether or not these models actually represent reality in an accurate manner. What is the significance of the local disturbances at the entry points of the reinforcement bars? What is the cause of the cracks behind the stirrup corner? Is the model representative without taking the surrounding soil-mix in account? What is the influence of the chosen solvers? Is the magnitude of the applied loads at crack initiation and failure realistic?

The model aims to predict the stress distribution within the detail from the soil-mix to the reinforcement. When all applied forces are transferred to the reinforcement, the applied forces and the support reactions at the reinforcement bars should be in equilibrium. This implies that the reaction forces at the fictitious supports (perpendicular to the reinforcement bars in the 3D model and the 2D model of section AA'), should be (close to) zero. Unfortunately this is not the case, the perpendicular supports in both models account for approximately 20 to 25 % of the support reactions in the Y-direction. This is a significant contribution of the total force, which indicates that this disturbance is likely to have a strong influence on the total capacity of the detail. The results also show extensive cracking at these reinforcement entry points in combination with concentrated high stresses. In reality the reinforcement bars are embedded in the surrounding soil-mix. Which provides both distributed lateral support (instead of a local restriction of lateral displacements) and additional bond length. The model results lead to conclude that improvements of the current representation of the boundary conditions related to the bar reinforcement could lead to more accurate results of the actual stress distribution within the detail. The improvements could lead to a different stress distribution and less cracking at the reinforcement entry points at the edges.

The cracks behind the stirrup corner can be related to the tensile forces which developed in the reinforcement bar. These tensile stresses pull on the corner on both sides and as a result the bar tends to flatten (reduction of curvature). This flattening causes tensile stresses to develop behind the corner, which eventually leads to cracks.

The soil-mix surrounding the detail has only been taken into account partially. The soil-mix which is present below the detail has been represented by line and spring supports in respectively the model of section BB' and the 3D model. The spring properties have been based on experimental results described in chapter 3. The spring properties were chosen to be weaker than those of the material representing the detail, because the aim was to analyse the behaviour of the detail. Applying spring supports with a high stiffness would cause the stresses to concentrate at the spring supports instead of at the applied reinforcement. The springs only served the purpose of restricting excessive rotational displacements. An aspect of the surrounding soil-mix that has not been taken into account is the material above the detail. The load on the detail increases when it is further below the ground surface. Being further below ground surfaces also implies that the vertical load on the detail increases. Such a confining pressure increases the capacity of the material. Especially since the detail is prone to splitting failure, due to the low tensile strength. An additional compressive stress might have significant influence on the capacity of the detail. Whether or not the vertical stresses are relevant for the capacity of the detail is discussed in section 4.5.

Each model results in a certain capacity of the detail. The most striking result, when considering

the capacity of the detail, is the increase in strength between the 2D and the 3D models. The applied load required for the initial splitting cracks to occur in the 3D model are slightly higher than of both 2D models. This increase could be due to the presence of the longitudinal bar in the 3D model. As mentioned in the first discussion point, the lateral displacements of this segment are locally restricted as well. This restriction, unintentionally, which accounts for 20 to 25 % of the reaction forces in the Y-direction is not present in the 2D models. Also the longitudinal bar was expected account for a portion of the vertical tensile stresses which can lead to splitting cracks (failure mechanism of section BB'), which would delay the moment of cracking and increase the failure load. However, the model doesn't show any vertical reaction forces in the longitudinal reinforcement bar.

When applying a force controlled load it is recommended to use the Arc Length solver. However this did not work for the 3D model and the 2D model. The computations of these models were done with the Newton Raphson integration scheme. This method is not able to model post peak behaviour after failure. Since this research main focus was to find the maximum capacity, the post peak behaviour is not essential and the current results are sufficient.

The last discussion point on the acceptability on the magnitude of the results is also addressed in section 4.5. In this section the resulting maximum loads are translated to maximum depth of the soil-mix wall. All in relation to the details of the reinforcement design, stirrup length, spacing and radius of curvature.

4.5 Preliminary guidelines

The modelling phase provided insight in the force transfer within the reinforcement detail. This includes the likely failure mechanisms and the critical loads. These critical loads can be translated to limitations for the design of a soil-mix wall, since the loads on a soil-mix wall depend largely on the depth of the wall. A deeper wall is subject to greater soil pressures, which is directly related to higher loads on the reinforcement details.
This chapter translates the results of the modelling phase to design guidelines, which answers the last sub-question.

Is it possible to derive design guidelines from the model?

The capacity of the detail depends on the parameters used for the reinforcement design. These include the spacing between the stirrups, the length of the stirrup and the radius of the corners. Varying these parameters influences the load bearing capacity of the detail and simultaneously the allowable depth of the wall. This chapter provides an overview of recommended reinforcement design parameters for multiple specified wall depths based on the quantified results presented in chapter 4.
These guidelines however, only represent a preliminary approximation of recommended design parameters. For a conclusive set of guidelines research has to be performed on all relevant aspects, such as the bond between the reinforcement and soil-mix, heterogeneity of the soil- mix and influence of soft inclusions in the soil-mix.

4.5.1 Reinforcement design

The guidelines for the reinforcement design are based on the failure mechanisms which occurred in the models and their sensitivity to the given parameters (figure 4.28a).

- Bar diameter (ϕ)
- Stirrup length (w)
- Stirrup spacing (perpendicular to plane)
- Radius of curvature corner (r $\sim \phi$)

Determining the preferred bar diameter for the reinforcement of soil-mix walls is based on a theoretical analysis. The bond strength between soil-mix and steel is relatively low, which is related to the low

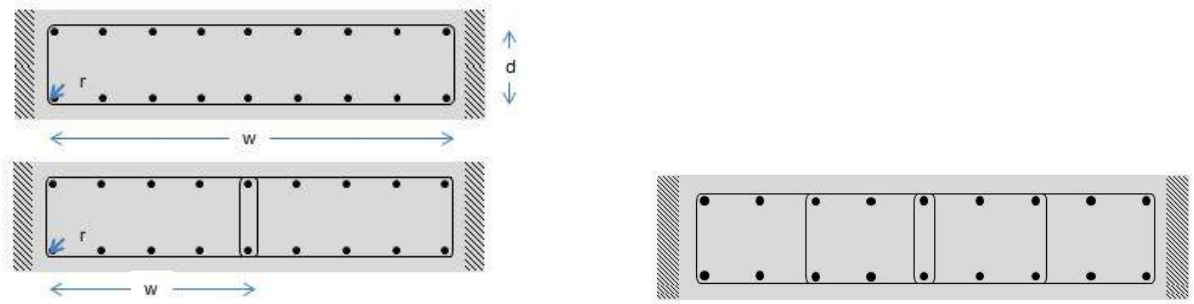

(a) Parameters stirrup design

(b) Overlapping stirrups

Figure 4.28: Stirrup reinforcement

tensile capacity of the soil-mix itself. Since cooperation between the two materials is required to achieve the optimal behaviour of the composite structure, the bond capacity is of importance. The simplest way to increase the total capacity of the connection without being able to optimize the soil-mix, is by increasing the surface area of the reinforcement. The surface area can be increased by applying multiple small reinforcement bars instead of singular large ones. Therefore, the recommendation is to apply small reinforcement bars when reinforcing soil-mix walls. The bar diameter is set at 10 mm.
The stirrup length is directly related to the orientation of the load on the detail. Applying a load with an orientation of 60° resulted in the most beneficial stress distribution in the cross section. When the load approached the detail with a steeper orientation, the horizontal section contained multiple critical zones with extreme stresses. Therefore, it is recommended to use stirrups with a length of 1100 mm, which is half of the width of a soil-mix panel. To increase the capacity of an entire panel it is possible to have overlapping stirrups as shown in figure 4.28b. Applying multiple stirrups in a horizontal slice, increases the number of details in one section. More details in one sections, means that the load can be divided amongst them and thus decreasing the load per detail.
The influence of the stirrup spacing is seen in the model results of section BB'. The failure load is roughly equal for all levels of spacing. When translating this to the capacity of an entire wall, the capacity is significantly higher with a small spacing between the stirrups. A small spacing means more stirrups per meter depth. Locally the main difference is seen in the crack propagation. With a small spacing the splitting cracks are distributed over a shorter length, as shown in table 4.6. Both results (based on capacity and crack development) indicate that it is beneficial to choose a small vertical spacing between the stirrups. The ideal spacing is dependent on the capacity required, which is related to the depth of the wall. Decreasing the spacing when the additional capacity is not required, leads to unnecessary use of steel and increased costs. An optimization between required capacity and the amount of steel (costs), leads to the ideal spacing between the stirrups.
The radius of curvature of the stirrup has to be sufficiently large, so that splitting in the horizontal plane can be avoided. The 2D model of section AA' showed that when increasing the radius of curvature up to 7ϕ there is no splitting in this plane. The 3D model partially supports this statement. The incorporation of the multi-axial stress state shows that the spacing between the stirrups also influences the type of failure mechanism. With a radius of 7ϕ diagonal splitting failure can still occur when the spacing is small (50 mm). With a larger spacing this radius is save to avoid diagonal splitting cracks. The recommended radius depends on the desired depth of the wall.

4.5.2 Maximum depth

The maximum depth of the soil-mix wall is based on the maximum capacity of the detail. The capacity of the design, which is specified as a single load (kN), is translated to a horizontal pressure on a horizontal slice of a soil-mix panel. This horizontal pressure is then used to determine the depth at which this pressure occurs, based on the chosen spacing and stirrup length. The exact calculation method is described in appendix XI.
The allowable depth can not be specified separately from the reinforcement parameters, since the detail capacity is directly related to these parameters. Therefore, the limits of the design parameters related

to the reinforcement design are quantified based on a specified minimum depth, with a range of 5 to 30 m. Currently soil-mix walls are typically constructed to a depth of 20 m. This is limited by the dimensions of the mixing equipment. The computation of these maximum depths related to the parameters is summarized in appendix XI. This resulted in a tabular set of guidelines for the design of bar reinforced soil-mix walls, table 6.3[7].
These guidelines can be consulted when designing the bar reinforcement for a soil-mix wall. It is important to realize that these guidelines only consider the capacity of the details. For a complete design a full structural analysis is necessary.

Note that these guidelines have been drafted based on the exact results from the modelling phase, without any correction. Yet there are considerations doubting acceptability of the magnitude of the results. As discussed in section 4.3 the representation of the boundary conditions related to the reinforcement bars introduce discontinuities in the stress distributions. Further research is required to quantify the influence of these discontinuities on the total capacity of the detail.

Table 4.8: Final design guidelines

Design guidelines			
Max. depth [m]	Stirrup length [mm]	Min. radius	Max. spacing [mm]
5	1100	2ϕ	150
10	1100	5ϕ	250
15	1100	5ϕ	150
20	1100	7ϕ	150
25	1100	7ϕ	100
30	1100	7ϕ	50

4.5.3 Relevance

The relevance of the research, decreasing the amount of reinforcement steel in soil-mix walls, has been described in section 1.2. Based on calculation methods commonly used for shear and bending beams, it evaluates the amount of bar reinforcement required to create equal capacity as with the profile reinforcement. The resulting quantity was used to determine the amount of steel that could be saved by applying bar reinforcement. This resulted in a reduction of steel of approximately 30 %. With the knowledge acquired from this research, these values can be evaluated to establish whether or not it is possible to reduce the amount of reinforcement steel in a soil-mix wall.
The reinforcement discussed in this research concerns the design of the stirrup reinforcement. Of the parameters discussed, the vertical spacing between the stirrups has the strongest influence on the amount of reinforcement steel in the wall. To assess the possible reduction of steel quantity, the maximum spacing form the guidelines are compared to the stirrup spacing specified in section 1.2. It shows that the spacing required for sufficient capacity (according to standard shear beam calculations) is between 70 and 160 mm. The guidelines drafted in this chapter indicate that these are acceptable spacing values concerning the capacity of the detail. Only when constructing very deep walls ($> 25m$), smaller spacing ($\approx 50mm$) is desired. This implies that the spacing required for the structural integrity of the detail, does not nullify the relevance of the research.

[7]The spacing of 100 mm for a depth of 25 m is based on an interpolation of the results for 50 and 150 m spacing.

5

Discussion

As mentioned in chapter 1 there are multiple factors which influence the possibilities and limitations of bar reinforced soil-mix walls. The aim of this project was to contribute to this research. Specifically to analyse the capacity and failure mechanism of a reinforcement detail within a soil-mix wall. At this detail the compressive forces in the soil-mix are transferred to tensile forces in the reinforcement bars. The maximum capacity of such a detail was translated to guidelines which can be consulted when designing such a structure. The research combined an experimental and numerical approach to the subject.
The research consisted of three phases, the literature study, testing phase and the modelling phase. Each phase providing relevant information for the subsequent one. This chapter elaborates on the method of each phase, along with its verification and shortcomings.

Literature study

The literature study served as the foundation of the research. The available literature on previous studies provided insight in the current knowledge on the material and was used to determine areas where knowledge was lacking. Constructing soil-mix walls for a (permanent) structural purpose is only recently up and coming. Which is also the reason for the limited research that has been conducted on the topic thus far. Articles and papers produced on the subject are written by recurring contributors. The data acquired from these articles is distributed over a wide range. Even though this is inherent to the material, it would be valuable to be able to consult multiple studies for validation of the data. The contributors of the available literature can be seen as experts in the field of soil-mix walls. Their cooperation with this research project was valuable in multiple ways. They shared their experience, knowledge and insight in the material properties, behaviour and construction technique. Which provided background information to draft a scientifically relevant research proposal and essential data for the calibration of the material model in the modelling phase. Aside from the scientific experience provided by these researchers, Dura Vermeer shared experience and design documents from their projects in which soil-mix walls were applied.

Testing phase

The data acquired from the literature study was insufficient for a complete material model in the finite element software. The properties were spread across a wide range and several parameters relevant to the material model were not specified. The main parameters that were not available from the literature were related to the stress-strain relation of the material. The testing phase was included in this research project to fill that information gap. In addition, it was thought to be valuable to gain insight in the physical properties of soil-mix from personal experience.

The tests were done on two sets of samples, which both have their own discussion points. The first set consisted of drilled cores from actual soil-mix walls, the second set were lab made samples. Given that the first set was taken from real soil-mix walls was valuable for the comparison with the lab samples. The drilled samples were all taken from the same construction site. However, the recipe used for the mixture was undisclosed. Therefore, a direct comparison between the quantified properties of the two sets would not lead to valuable conclusions. Nevertheless, the visual appearance of the samples and the overall behaviour provided valuable results for the research. The results showed the variety within the properties of samples taken from one project site, the heterogeneity of the material, the brittle behaviour of the samples and the striking visual aspects of the material.

The lab samples were made based on a recipe provided by Dura Vermeer. There were several aspects of the recipe that could not be exactly replicated with the material available at the lab. These aspects being the detailed distribution of aggregate sizes, the cement type and the moisture content of the used aggregates. Aside from the differences in construction material, the production method used for the lab samples was completely different to the actual procedure used for soil-mix walls. Due to these differences it was important to verify the acceptability of the lab samples as to be representative for actual soil-mix samples. For validating the lab samples the visual comparison with the Winmix samples was relevant. The comparison showed that the sets of samples displayed multiple similarities, small air bubbles, absence of large aggregates and a 'dusty' feel to the surface (indication of un-bonded fine particles). The findings from the visual comparison supported the acceptability of the lab samples as soil-mix samples. The one main difference between the two sets of samples was the homogeneity of the lab samples in contrast to the heterogeneity of the Winmix samples. This is due to the production method of the lab samples. The lab samples were made from certified aggregates only and mixed with a common concrete mixer. Whereas the Winmix samples were taken from an actual soil-mix wall. As explained in chapter 2 the production process of actual soil-mix walls is bound to result in a heterogeneous material.

All tests combined provided insight in the material properties and behaviour. This was incorporated in the material model, which would be used in the modelling phase.

A shortcoming of the testing phase is the quantity of the samples. A more extensive data set could be used for a detailed analysis of the material properties. This would allow for a statistical analysis

of all results, to find a more precise range (including average and deviation) of the material qualities corresponding with the used material mix.

Modelling phase

The modelling phase started with several models to calibrate the material model and simultaneously get acquainted with the software. This initial calibration was solely based on the material parameters acquired from the literature study. During the initial calibration process the lack of information on several parameters became apparent. This eventually lead to including the testing phase in the project.

After completing the testing phase and supplementing the data from the literature study to achieve a fully defined material model, the actual models were constructed. The modelling phase consisted of the analysis of 2D models of the two most critical sections (one horizontal and one vertical section) of the detail and one 3D model to analyse the influence of a multi-axial stress state. The sections which were modelled with the 2D models were chosen based on a prediction of the stress distribution within the wall. These predicted stress distributions were used to formulate the hypothesis concerning the failure mechanisms of these sections. The hypothesis was that section AA' would fail due diagonal cracks and section BB' due to splitting failure, both caused by redistribution of the stresses towards the reinforcement bars. The results of the 2D models agree with the hypothesis and both show the expected failure mechanisms. The model of the horizontal slice however, also displays significant cracking around the corner of the stirrup and at the entry points of the reinforcement bars. The cracking near the entry points of the reinforcement bars is most likely caused by a combination of a shortage of bond length and a poor representation of the boundary conditions. The cracks behind the corner of the stirrup are caused by the tensile forces which developed in the reinforcement bars. By pulling on both ends of the reinforcement the corner tends to flatten slightly (reduction of the curvature), which leads to tensile stresses and thus cracks behind the corner. In case of large tensile stresses in the reinforcement this is likely to occur in reality as well.

A failure mechanism that didn't occur in the 2D model of section AA' was vertical splitting (perpendicular to the plane, z-direction). This is due to two aspects of the model set-up. Firstly, the section is modelled with plain strain elements. These elements restrict any deformations in the z-direction. This implies that if the material wants to expand due to vertical splitting cracks, deformation is prevented and compressive stresses will occur. These compressive stresses will not cause vertical splitting of the material. Secondly, the elements had a thickness of only 50 mm. The small thickness limit the degree of vertical redistribution of the stresses. The degree of redistribution is directly related to the magnitude of vertical stresses. Since there is only limited redistribution of stresses in the z-direction, σ_{zz} is limited.

The 3D model was based on the same physical and geometrical parameters as the 2D model, with the addition of the longitudinal reinforcement segment on the inside of the reinforcement corner. As with the 2D model of the horizontal slice, this model showed extensive cracking near the entry points of the reinforcement bars and behind the corner of the stirrup corner. These cracks are explained by the same argumentation as given for the 2D model, since the geometrical set-up of the two models was similar.

The purpose of the 3D model was to analyse the influence of a multi-axial stress state on the expected failure mechanisms. Find the governing failure mechanism and analyse the influence of the reinforcement design parameters. Varying these reinforcement design parameters and analysing the corresponding crack propagation patterns resulted in the answers of those questions. Both failure mechanisms turned out to be of importance to the capacity of the detail. The model is most sensitive to vertical splitting, seen in section BB', with the exception of models based on a stirrup spacing of merely 50 mm. In all cases the horizontal stress distribution seen in section AA' influences the position and orientation of the vertical splitting cracks in the 3D model. The model is more sensitive (lower failure load) to the vertical splitting failure when the reinforcement is designed with a small radius, because the stresses are concentrated on a smaller area. These results qualitatively confirm the hypothesis.

Quantitatively the 3D model results in a slightly higher capacity of the detail than the 2D models. The strongest increase in capacity is observed when comparing the 3D model to the 2D model of section

BB'. The increase in capacity in this cross section is likely related to the presence of the longitudinal reinforcement bar in the 3D mode. The longitudinal reinforcement bar accounts for tensile stresses in the vertical direction. This component was not included in the 2D model.

The results of the 3D model agreed with the 2D models and showed similar failure mechanisms. In contrast to the 2D models the cracks which developed in the 3D model were more disperse. Whereas the splitting cracks in the 2D models were concentrated around a single line. The disperse cracking can be related to the applied mesh in the 3D model. To limit the required calculation time the 3D model was meshed with elements of 0.04 m, instead of 0.01 m like in the 2D models. A larger mesh size introduces an uncertainty in the computations, which lead to more disperse cracking.

The last discussion point related to the model concerns the used solvers. When applying force controlled load it is recommended to use the Arc Length solver. However, this did not work for the 3D model and the 2D model. The computations of these models were done with the Newton Raphson integration scheme. This method is not able to model post peak behaviour after failure. Even though the post peak behaviour is not essential, it might provide valuable information on the crack development in the material after failure.

Preliminary guidelines

The capacity of the detail has been translated to maximum depths, to be able to draft design guidelines for bar reinforced soil-mix walls. The maximum depths have been determined by calculating the depth at which the maximum load would occur on the detail. To do so a horizontal slice of the wall was considered. The capacity of the detail had to be in equilibrium with the accumulated soil and water pressure acting on the slice of the wall. In common geo-engineering practices this pressure is considered as active pressure and is multiplied with the coefficient for active soil pressure (K_A). For the calculation of the maximum depth this coefficient has been left out of the equation, to ensure a conservative conclusion. The determination of the allowable depth has been done based on a strongly simplified calculation method, but is sufficient for a rough indication of maximum depths. The resulting maximum depths vary from 2.0 to 100.0 m depending on the reinforcement design. The projects listed in section 2.2 were used to define the acceptable maximum depths and define the corresponding design guidelines. Typically soil-mix walls are constructed to a depth in the order of magnitude of 20.0 m. This is within the resulting range, but it indicates that the ultimate depths are exceeding the reasonable range. Therefore, the combination of design parameters resulting in depths exceeding 30 m are not incorporated in the design guidelines.

Another discussion point is the influence of the weight of the material above the detail. The weight will introduce an additional compressive stress, confinement stress, which might increase the capacity of the detail. The detail fails due to splitting failure and since the tensile strength of soil-mix is low, additional compressive stresses might have a significant influence of the capacity. Quantifying these stresses show that a depth of 25 m is required to reach a confinement stress of 0.50 MPa (equal to the tensile strength of the soil-mix). This indicates that the influence of the confinement stress is most likely insignificant. Additional research could lead to conclusive evidence on this matter.

Note that the maximum depths have been based on the exact capacities that resulted from the models. Since there are several discussion points on the accuracy of the model, mainly regarding the representation of the restrictions of the reinforcement. To quantify the influence of the disturbances caused by the boundary conditions additional research is required.

These are only preliminary guidelines and are not sufficient for a complete design of a bar reinforced soil-mix wall. There are multiple other aspects which influence the design parameters of the reinforcement. For examples, bond between the soil-mix and the steel, heterogeneity of the soil-mix and the risk of weak spots in the structure and more. To draft sufficiently safe design guidelines, all aspects have to be taken into consideration.

6

Conclusion

The application of soil-mix walls are upcoming and aside from temporary purpose, interest starts to grow for soil-mix walls with a permanent structural function. Currently the soil-mix walls are reinforced with steel IPE or HEA profiles. The question arose whether it would be possible to replace these massive steel elements with bar reinforcement, as commonly applied in regular concrete walls. Literature study and discussions with field experts resulted in a list of multiple factors which influence the possibilities and limitations of bar reinforced soil-mix walls. The aim of this research was to contribute to the analysis of these possibilities by focussing on one influential aspect, the capacity of the reinforcement detail in the stirrup corners. This purpose was summarized in the main research question:

What is the capacity a reinforcement detail in a bar reinforced soil-mix wall?

The question was answered by addressing several sub-questions throughout the different phases of the research. This chapter recaps on the conclusions of the performed research to answer those questions.

Literature study

Aside from acquiring the relevant knowledge on the background and previously conducted research projects to draft the research proposal, the literature study was used to answer the first of four sub-questions.

Which sections of the detail are critical for the capacity of the detail?

The question was answered by analysing the theoretical stress distribution and the corresponding failure mechanisms. Figure 6.1 shows the global stress distribution within a bar reinforced soil-mix wall along a three dimensional compression arc. Figure 6.2 shows the same stress distribution from multiple different perspectives. Visualizing the critical stress distributions. The critical detail is at the corner of the stirrup, where the compressive forces are transferred to the reinforcement.

The planes in which the most critical stress distributions were expected, were chosen to be modelled in 2D in the modelling phase. The analysis lead to two critical sections. Section AA' is a horizontal plane at the height of the reinforcement stirrup and was expected to fail due to diagonal cracking. Section BB' is a vertical cross section perpendicular to the wall. The prediction was that failure in this section would be caused by (slightly tilted[1]) vertical splitting cracks. In this case the cracks are parallel to the loading direction.

Both failure mechanisms occur due to redistribution of dispersed compressive stresses to a higher concentration of compressive stresses. To achieve equilibrium with the bent stress trajectories caused by the stress redistribution, tensile stresses will develop. When these tensile stresses reach the tensile strength, the material cracks. Figure 6.3 shows the position of the critical sections and figure 6.4 the expected stress distributions within these sections (including the corresponding cracks).

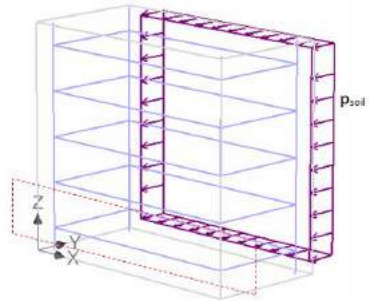

(a) Bar reinforced soil-mix wall

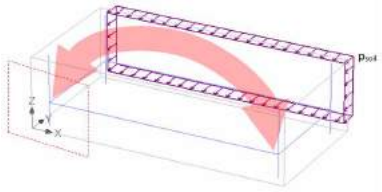

(b) 3D compression arc, single stirrup (arc not to scale)

Figure 6.1: Pressure arc from 3D perspective

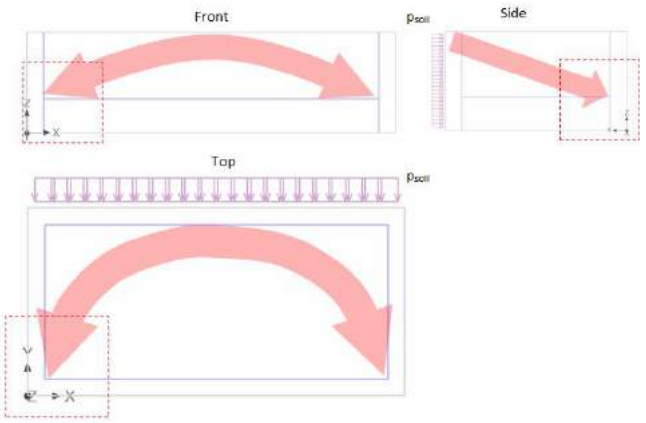

Figure 6.2: Stress distribution to bar reinforcement, 2D (arc not to scale)

[1]The actual direction of the principal stress is perpendicular to the loading direction in the vertical plane, angle β. So the principal stress direction ranges from 65° to 85° with the XY-plane

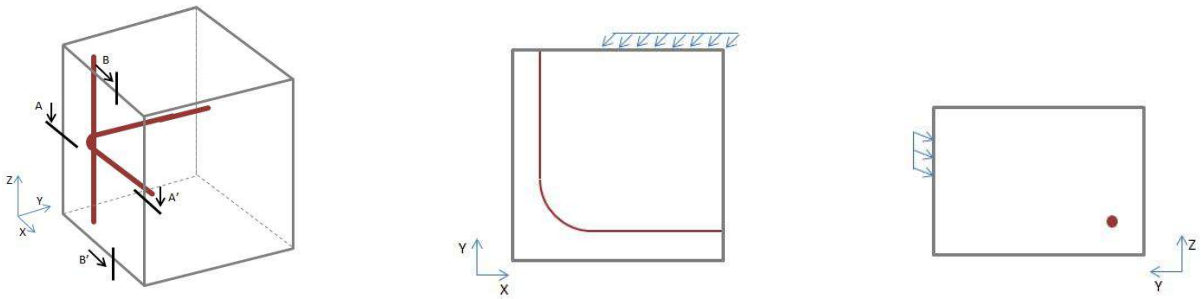

(a) Positions critical sections (b) Section AA' (horizontal) (c) Section BB' (vertical)

Figure 6.3: Critical sections

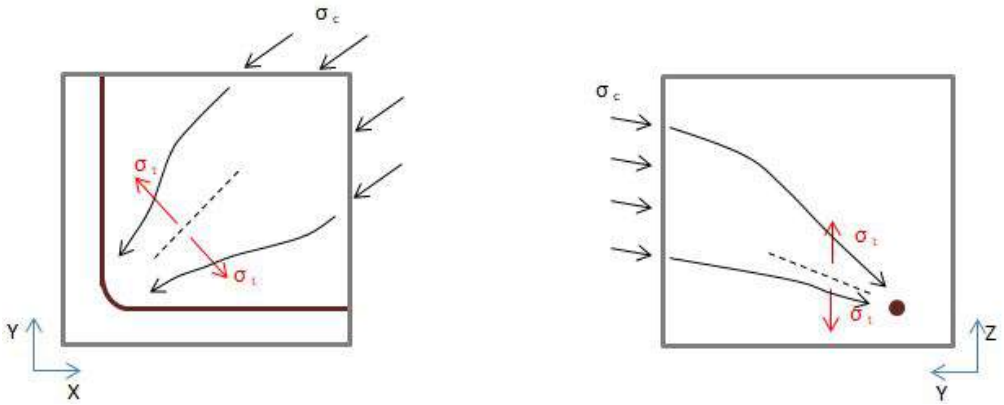

(a) Section AA' (b) Section BB'

Figure 6.4: Expected crack patterns (dashed lines represent cracks)

Testing phase

To be able to model the soil-mix material in the finite element model, a representative material model had to be defined. By combining the data from the literature study with results from the testing phase the related sub-question was answered.

What material parameters should be used to model the behaviour of soil-mix material with a finite element model?

The literature study provided insight in research performed on soil-mix samples for the purpose of mechanical characterization of the material. From the available data the main material parameters such as the compressive strength, elastic modulus, tensile strength and maximum bond strength were derived. These material parameters were based on the average strength.
Considering the deformation behaviour of the material the literature did not provide a decisive conclusion. Therefore, the literature data was supplemented with data from additional physical experiments performed solely for the purpose of this research. Parameters that could not be derived from either the literature study or the performed tests, were left to the default values which Atena defined based on the specified compressive strength. Table 6.1 provides an overview of the final material parameters and spring properties used to model the behaviour of soil-mix material in the finite element model.

Property values		
Elastic modulus (E)	5 000	MPa
Poisson's ratio (υ)	0.135	-
Specific weigth (ρ)	0.02	MN/m^3
Compressive strength (f_c)	5.0	MPa
Tensile strength (f_t)	0.5	MPa
Plastic strain at strength f_c (ϵ_{cp})	$4.3 \cdot 10^{-4}$	-
Critical compressive disp. (w)	$5.0 \cdot 10^{-4}$	m
Fracture energy (G_f)	1.754	MN/m
Reduction of f_c due to cracks (r_c)	0.8	-
Crack shear stiffness factor	20.0	-
Aggregate size	0.20	mm
Exc., Def.the shape of the failure surface	0.52	-
Direction of plastic flow (β)	0.00	-
Coefficient of thermal expansion (α)	$1.2 \cdot 10^{-5}$	$1/K$
Fixed crack model coefficient	1.00	-

(a) Properties material model soil-mix

$\sigma[MPa]$	Rel. disp [-]
0.03	$5.00 \cdot 10^{-4}$
0.00	0.00
-3.06	$-5.15 \cdot 10^{-4}$
-3.54	$-7.22 \cdot 10^{-4}$
-3.11	$-7.99 \cdot 10^{-4}$
-2.82	$-9.86 \cdot 10^{-4}$

(b) Spring properties

Table 6.1: Quantified material parameters finite element model

Modelling phase

The modelling phase combined the detail geometry and the material parameters into several finite element models, two 2D models and one 3D model. To construct these models the third sub-question had to be answered.

How can the geometry of the detail and the loading configuration on the detail be represented in a finite element model?

The geometry of the details and the loading configuration were based on knowledge acquired during the literature study, related to common wall dimensions and the expected stress distributions. The boundary conditions were specified to resemble the influence of the surrounding soil-mix material and the remaining parts of the reinforcement embedded in the soil-mix. The resulting model set-ups are shown in figure 6.5 and figure 6.6. Table 6.2 shows the quantification of the relevant geometrical parameters.
The failure mechanisms seen in the model results confirm the hypothesis of diagonal cracks in section AA' and vertical splitting cracks in section BB'. The 3D model showed that in general the vertical splitting cracks are the governing failure mechanism, unless the stirrup spacing is reduced to 50 mm.

Table 6.2: Final geometrical parameters models

Dimension	Range	No. of steps
Depth	300 mm	-
Width	300 mm	-
Height	100–300 mm	3
Coverage	50 mm	-
Width arc	250 mm	-
Height diagonal	25 – 125 mm	3
Radius	$2\phi - 10\phi$	4
α	$61° - 78°$	3
β	$6° - 26°$	3
Diameter reinforcement	10 mm	-
Thickness (AA')	50 mm	-
Thickness (BB')	20 mm	-
Mesh size 2D (brick)	0.01 m	-
Mesh size 3D (tetra)	0.04 m	-

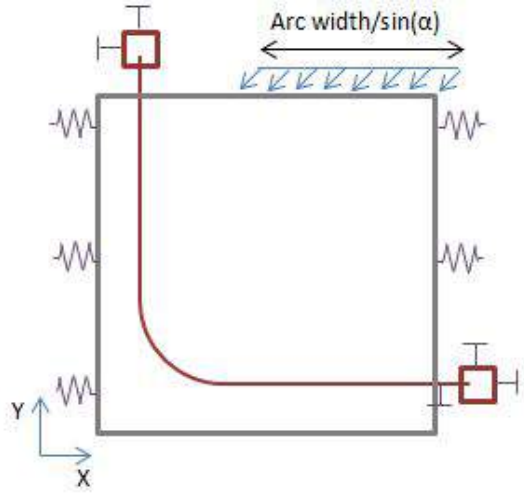

(a) Section AA'

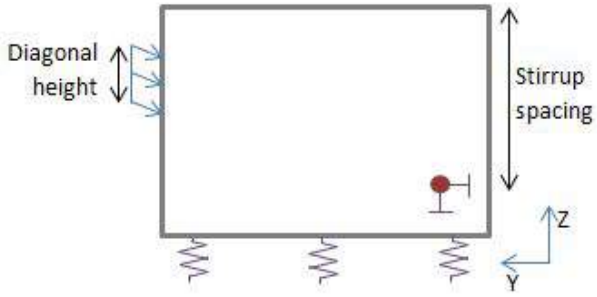

(b) Section BB'

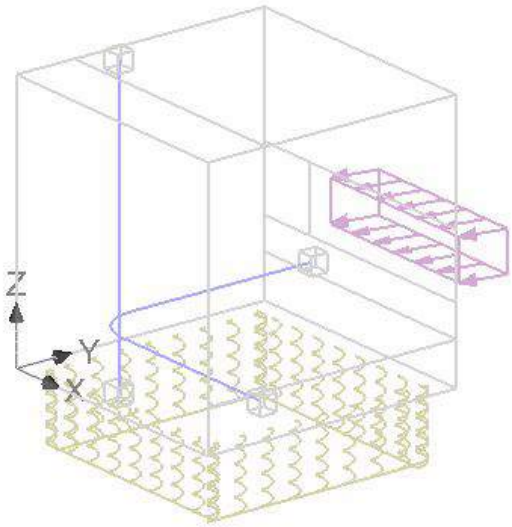

(c) 3D

Figure 6.5: Set-up of the models

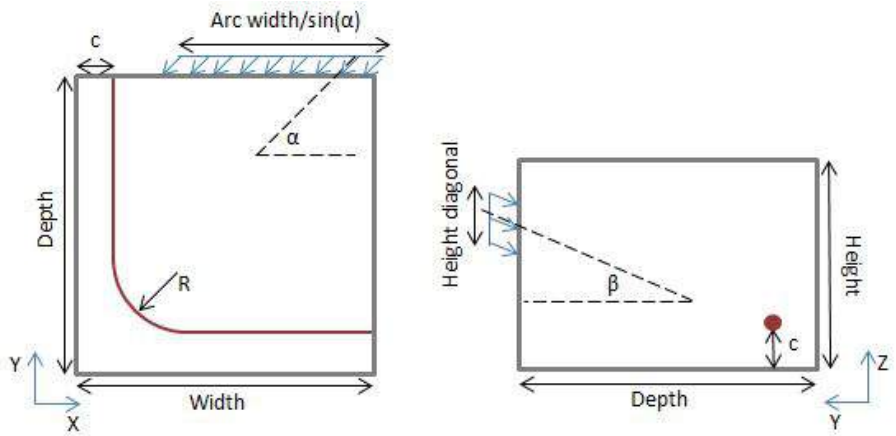

Figure 6.6: Model dimensions

Preliminary guidelines
The modelling phase resulted in a range of maximum capacities for multiple configurations of geometrical design parameters and the corresponding failure mechanisms. To answer the last sub-question, these capacities have been translated to preliminary design guidelines which can be consulted when designing a soil-mix wall with bar reinforcement.

Is it possible to derive design guidelines from the model?

To draft these preliminary guidelines the capacities of the details were directly translated to depths corresponding with the said load. Based on these transformations guidelines were specified for the design parameters related to these maximum depth. The design parameters concern the stirrup length, radius of curvature of the corner and the vertical spacing between the stirrups. The guidelines have been summarized in table 6.3.
Note: these preliminary guidelines only consider the capacity of the reinforcement detail. The reinforcement design has to be checked for the entire structural integrity of the wall considering all relevant aspects.

Table 6.3: Final design guidelines

Design guidelines			
Max. depth [m]	Stirrup length [mm]	Min. radius	Max. spacing [mm]
5	1100	2ϕ	150
10	1100	5ϕ	250
15	1100	5ϕ	150
20	1100	7ϕ	150
25	1100	7ϕ	100
30	1100	7ϕ	50

Final conclusion
All sub-questions contributed to the path which lead to answering the main research question.

What is the capacity a reinforcement detail in a bar reinforced soil-mix wall?

Based on the performed research the capacity of the soil-mix material is sufficient to resist the concentrated forces resulting from the force transfer at the details. The guidelines have been drafted for depths which can be reached with the current capacities of the equipment used for the construction of soil-mix walls. However, it is important to realize that these guidelines only consider the capacity of the detail.

To be able to provide a decisive recommendation considering all possibilities and limitations of bar reinforced soil-mix walls, more research is required. It is crucial to perform a full structural analysis of the wall to ensure the structural integrity of the entire wall. Chapter 7 elaborates on the recommendations concerning additional research on the possibilities and limitations of bar reinforced soil-mix walls.

7

Recommendations

Aside from the capacity of the detail analysed in this research, the possibilities of bar reinforced soil-mix walls are reliant on a broad range of other aspects. From executive aspects to the predictability of the soil-mix quality. The question whether or not it is actual advantageous to apply bar reinforcement instead of profile reinforced, can only be decisively answered when all of the relevant factors have been researched. This chapter gives an overview of recommendations for further research. Subjects that will support the feasibility study of the application of bar reinforcement in soil-mix walls.

Executive feasibility

Aside from a structural perspective, the feasibility of the construction is important. This includes the construction of the reinforcement cage and the positioning of the cage in the soil-mix wall. Steel profiles are heavy and during construction they slide into the wet soil-mix by their own weight. The weight and geometry of reinforcement cages is different, so lowering of the steel into the soil-mix might cause complications. Complication which might arise are hardening of the soil-mix before the cage has reached its final position, exceeding the positioning tolerances due to lack of stiffness of the cage, undesirable effects on the soil-mix due to vibrating the cage when lowering it[1]. Small scale and real-scale tests will provide insight in the executive possibilities and limitations.

Reinforcement bond

The structural integrity of an entire wall can only be ensured if the cooperation between the steel and soil-mix can be guaranteed. Therefore, it is recommended to analyse the behaviour of bar reinforced soil-mix structures to quantify the connection between the two. Quantifying the connection can be done by performing pull out tests (Denies et al., 2012a) and bending tests on reinforced elements. Such tests can be performed on small scale elements to get an indication of the degree of cooperation of the two materials. Acquiring a better definition of the bond relation between the steel and soil-mix, can also be used to improve the representation of reinforcement steel in finite element models to predict the behaviour.

To analyse the stress distribution in bar reinforced soil-mix walls and the corresponding failure mechanisms, it is recommended to perform real-scale tests on bar reinforced soil-mix elements in addition to small scale tests.

Capacity vertical splitting

The models showed that the detail is most sensitive to vertical splitting failure. The resistance of the material against this failure mechanism is influenced by the presence of longitudinal reinforcement bars and the confinement pressure exerted by the self-weight of the material above the detail. The presence of the longitudinal reinforcement bar was only considered in the 3D model. It is advised to further analyse the influence of the presence of one or more longitudinal reinforcement bars near the detail. To do so, it is important to have a better understanding of the behaviour of the bond between the reinforcement and the soil-mix.

The confinement pressure of the self-weight of the soil-mix was not taken into account in this research. However, since the tensile strength is very low ($\approx 0.5MPa$), even small additional compressive stresses can influence the resistance against vertical splitting. The influence stresses can be analysed by including additional vertical compressive stresses in both the 2D and 3D model. It is important to define a correct ratio between the compressive vertical stresses and the horizontal stresses, to get an accurate representation of the actual loading conditions.

Material quality

The main concern for soil-mix walls as permanent structural elements, is the quality of the soil-mix material and its predictability. Especially when using steel bars as reinforcement instead of profile reinforcement, since the composite strength and stiffness will strongly rely on the soil-mix properties. To ensure sufficient strength and stiffness throughout the entire wall, it is important to be able to make an accurate prediction of the material properties of the soil-mix. The soil-mix quality is reliant on multiple factors, including the soil types, the water level, the amount of additive (cement and water) and the mixing degree. The soil type and the water level are parameters inherent to the construction site and can not be altered. To predict the quality with the given soil parameters, it is recommended to research the influence of different soil types on the soil-mix properties. This can be done by creating a wide range of soil-mix mixtures with different soil types as aggregates, fine sands, coarse sands, clay, loam. Performing multiple tests on different mixture compositions can be used to find a relation between the

[1]The application of cage reinforcement in CSM walls has been done a few times in Belgium and it didn't pose any issues. For a decisive conclusion however, research on the construction process is recommended to analyse all critical aspects.

soil type and the final soil-mix parameters which are realized. Such research can be used to predict the material parameters of a soil-mix wall more accurately, based on the composition of the soil layers found in the ground at the construction site. Also the research could be used to compose guidelines for the design of mixture recipes based on the present soil layers.

Inclusions

Insufficient degree of mixing might lead to the presence of soft inclusions in the soil-mix. These spots are weaker than the properly mixed material. Weak spots might influence the structural integrity of the wall when located at critical positions. The impact of such inclusions on the stress transfer within bar reinforced soil-mix walls should be analysed, since local failure due to lack of strength is undesirable. Such an analysis should include an analysis of the impact of soft inclusions at critical positions and a risk analysis of the presence of soft inclusions, considering both position and size of the inclusions.

Durability

Compared to concrete, soil-mix is a relatively weak material and as such it is more sensitive to cracking. Cracks decrease the durability of a wall, since it might lead to leaking of the wall and corrosion of the reinforcement. Durability is a crucial aspect when analysing the possibilities of bar reinforced soil-mix walls with a permanent structural purpose. Therefore research is required on crack development in soil-mix structures. Additionally it is recommended to monitor the behaviour of realized soil-mix walls and collect the data to address the durability of the material.

Real scale

For complete certainty on the capacity of bar reinforced soil-mix walls, it is valuable to perform test on real-scale elements. Real-scale tests provide data on multiple aspects relevant to the feasibility of bar reinforced soil-mix walls, some of which mentioned above. Complications concerning the executive feasibility can be identified and the actual composite behaviour can be analysed. The real-scale tests can be compared to the small scale tests for validation and they provide insight in the actual crack development and the final failure mechanisms.

All of these recommendations aim to increase the knowledge on bar reinforced soil-mix walls and supplement the outcome of this research project. If all conclusions turn out positive and bar reinforcement proves to be advantageous compared to profile reinforcement, a profitable improvement can be made to the technique.

Bibliography

Carroll, A. C., Grubbs, A. R., Schindler, A. K., and Barnes, R. W. (2016). Effect of core geometry and size on concrete compressive strength. Project performed in cooperation with the Alabama Department of Transportation.

Cervenka, V., Jendele, L., and Cervanka, J. (2011). *ATENA Program Documentation, Part 8: User's Manual for ATENA-GiD Interface*. Cervenka consulting.

Cervenka, V., Jendele, L., and Cervanka, J. (2016). *ATENA Program Documentation, Part 1: Theory*. Cervenka consulting.

Denies, N., Huybrechts, N., de Cock, F., Lameire, B., Maertens, J., Van Lysebetten, G., and Vervoort, A. (2012a). Soil mix walls as retaining structures – mechanical characterization. *Recent Research, Advances & Execution Aspects of GROUND IMPROVEMENT WORKS*, III.

Denies, N., Huybrechts, N., de Cock, F., Lameire, B., Maertens, J., and Vervoort, A. (2012b). Mechanical characterization of deep soil mix material – procedure description. *Recent Research, Advances & Execution Aspects of GROUND IMPROVEMENT WORKS*, III.

Denies, N., Huybrechts, N., de Cock, F., Lameire, B., Maertens, J., and Vervoort, A. (2015a). Large-scale bending tests on soil mix elements.

Denies, N., Huybrechts, N., de Cock, F., Lameire, B., Maertens, J., Vervoort, A., de Leeuw, J. C. J., and Hoefsloot, F. J. M. (2015b). Design and quality control of soil mix walls afor earth and water retaining structures. *Deep foundations institute*.

Denies, N., Huybrechts, N., de Cock, F., Lameire, B., Maertens, J., Vervoort, A., de Leeuw, J. C. J., and Hoefsloot, F. J. M. (2015c). Ontwerp can soilmix-wanden voor kerende constructies. *Geotechniek*.

Denies, N., Lysebetten, G. v., Huybrechts, N., de Cock, F., Lameire, B., Maertens, J., and Vervoort, A. (2014). Real-scale tests on soil mix elements.

Dörendahl, K., Walz, B., and Pulsfort, M. (2004). Das tragverhalten von einphasen - dichtwandmassen als ausfachung von baugrubenwändenl. Bergische Universität Wuppertal Fachbereich D Abteilung Bauingenieurwesen, Bodenmechanik und Grundbau.

Eurocode2, E. N. (2011). Eurocode 2 – design of concrete structures – part 1-1: General rules and rules for buildings. Technical report. NEN-EN 1992-1-1+C2 Inclusief Nationale Bijlage (nl).

FrankiFoundations (2016). Franki foundations - soil mix: Cutter soil mix (csm) walls. [Online; accessed 5-December-2016].

Ganne, P., Huybrechts, N., de Cock, F., Lameire, B., and Maertens, J. (2010). Soilmix wanden als kerende constructies - kritische analyse van de ontwerpparameters van het materiaal. *Geotechniek*.

Huybrechts, N., Denies, N., Hannink, G., and et al (2016). *Handboek soil-mix wanden, ontwerp en uitvoering*. SBRCURnet, first edition. SBRCURnet/WTCB commissie 1794 'Soilmix wanden'.

Pryl, D. and Cervanka, J. (2016). *ATENA Program Documentation, Part 11: Troubleshooting Manual*. Cervenka consulting.

Unknown. (2010). Construction standard - testing concrete. Technical report, The Government of the Hong Kong Special Administrative Region.

van der Want, H. R. G. (2015). Rapportage laboratoriumonderzoek. Technical report, Fugro geoservices BV.

Vervoort, A., Tavallali, A., Van Lysebetten, G., Maertens, J., Denies, N., Huybrechts, N., de Cock, F., and Lameire, B. (2012). Mechanical characterization of large scale soil mix samples and the analysis of the influence of soil inclusions. *Recent Research, Advances & Execution Aspects of GROUND IMPROVEMENT WORKS*, III.

Vervoort, A. and Van Lysebetten, G. (2012). Uniaxial compression test on two large soil mix blocks and rock mechanical tests on core samples (engels plein, leuven). *Unpublished*.

Whiting, D. A. and Nagi, M. A. (1998). Control of air content in concrete. *Concrete tehcnology today*, 19.

Appendices

I Soil-mix properties - Literature results

This appendix provides the results from tests performed by Denies et al. (2012a) for the characterisation of the mechanical properties of soil-mix.

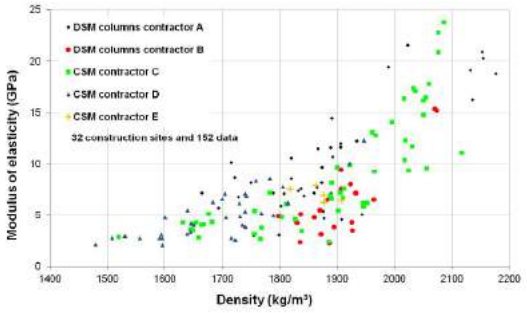

(a) Related to the density

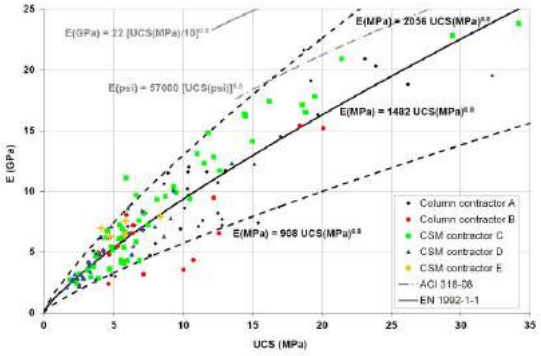

(b) Related to the ultimate compression strength

Figure I.1: Modulus of elasticity

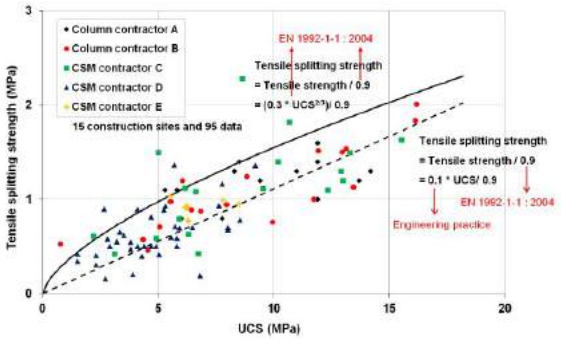

Figure I.2: Tensile strength related to the ultimate compressive strength

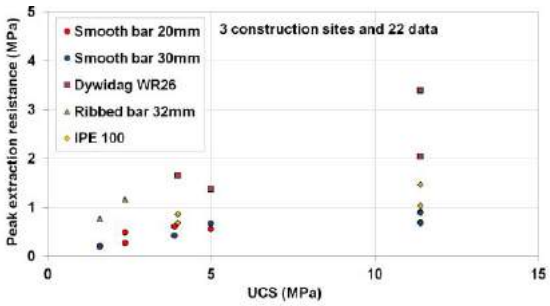

Figure I.3: Pull out strength reinforcement - bond

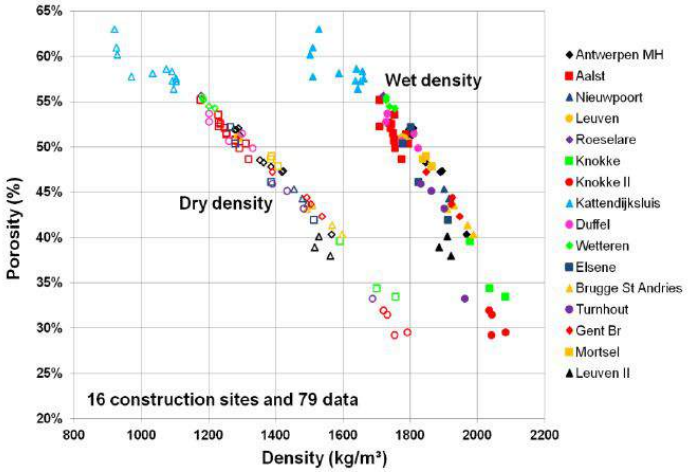

(a) Porosity related to the density

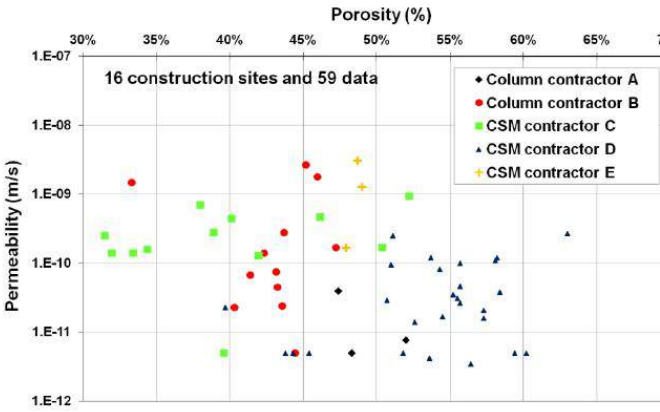

(b) Permeability related to the porosity

Figure I.4: Porosity

II Testing schedule

The tests described in chapter 3 are performed according to the schedule in table II.1.

Table II.1: Schedule of the performed test

Schedule		
When	**What**	**Notes**
25-4-2017	Deliverance of Winmix samples	
4-5-2017	Improve/check schedule, check Winmix samples for suitability	
8-5-2017	Sawing of the Winmix samples	
9-5-2017	Winmix tests	Compression and splitting test
15-5-2017	Mixing and pouring lab samples	Test workability, density and air content
16-5-2017	Remove samples from molds and move to the curing room	
22-5-2017	Tests lab samples after 7 days	Compression and splitting
29-5-2017	Tests lab samples after 14 days	Compression and splitting
2-6-2017	Displacement controlled test on Winmix samples	Compression and splitting
12-6-2017	Test lab samples after 28 days	Compression, splitting and displacement controlled
23-6-2017	Last displecement tests	Delayed due to equipment malfunction

III Production lab samples

Testing and analysing lab produced samples provided information on the material properties of soil-mix. This appendix elaborates on the production process and the determination of the mixture recipe of the lab made specimens discussed in section 3.3.

Soil

The basis of the soil-mix is the soil. For regular production of soil-mix walls the soil is an aspect which is determined by the local environment and can not be influenced. These soil conditions are governing for the determination of the mixture recipe of the soil-mix. To be able to design a recipe, the executive company performs extensive soil research. Dura Vermeer provided the soil research they performed, in collaboration with Fugro, for the purpose of the construction of soil-mix walls in The Hague (van der Want, 2015).

The research includes samples taken at different depth which have been used to determine the grain distribution in the soil layers, see table III.1. This information was used to determine the grain distribution of the available soil fraction at the TU Delft, table 3.3b. The largest share of the soil particles is found in the fraction of 0.125 mm and 0.250 mm, so the soil composition is very fine. For a definition of the degree of fineness of the soil, the fineness modulus (FM) was calculated with equation 1.

$$FM = \frac{\Sigma\, Cumulative\, sand\, fraction\, retained\, by\, specified\, sieves}{100} = 1.16 \tag{1}$$

The specified sieves are : 2.0, 1.0, 0.50, 0.250 and 0.125 mm. The fineness modulus of 1.16 is very low compared to the preferred FM for concrete mixtures. Which implies that a relative high water content is required to create a workable mix.

A significant difference between the soil and the aggregates available at the lab is the moisture content.

Table III.1: Grain distribution at different depths (van der Want, 2015)

	Grain size distribution			
	0.7 - 5.0m -GL	*5.0 - 6.7m -GL*	*6.7 - 12.0m -GL*	*Average*
16 mm < ...	1.3%	0.0%	0.0%	0.5%
8 mm < ... < 16 mm	2.1%	0.0%	0.1%	0.8%
4 mm < ... < 8 mm	1.7%	0.0%	0.0%	0.6%
2 mm < ... < 4 mm	1.2%	0.0%	0.1%	0.5%
1 mm < ... < 2 mm	0.7%	0.1%	0.1%	0.3%
0.5 mm < ... < 1 mm	0.9%	0.6%	1.1%	0.9%
0.250 mm < ... < 0.50 mm	14.7%	15.1%	15.5%	15.1%
0.125 mm < ... < 0.250 mm	69.4%	79.4%	66.4%	69.5%
0.063 mm < ... < 0.125 mm	3.2%	3.7%	13.3%	8.0%
0.02 mm < ... < 0.063 mm	1.3%	0.1%	1.6%	1.3%
0.002 mm < ... < 0.02 mm	1.6%	0.6%	0.5%	0.9%
... < 0.002 mm	1.9%	0.4%	1.3%	1.4%
Total	**100.0%**	**100.0%**	**100.0%**	**100.0%**

The soil found at the construction site is saturated, where the sands in the lab are entirely dry. To create a similar mixture in the lab, water has to be added to the lab sands to replicate the actual soil. The estimated amount of water required for saturation is based on the $2kN/m^3$ difference between the dry and wet weight specified in the (undisclosed) design document of Dura Vermeer. This lead to a volume of 10L of water required to saturate 70L of sand. This amount was used to determine the remaining material quantities for the mixture recipe, the cement and water.

The nature of the soil present at the project site in The Hague is that of dune sands, which are round particles. The sands available at the lab are round as well, therefore the influence of the difference in shape is not taken into account.

Mixing

Before starting the mixing procedure (15-05-2017), all material quantities are weighed and prepared for the process. The mixing process is divided into three steps.

1. Homogenizing sands
2. Saturating sands (replicating soil)
3. Adding cement and water

To start with the sand fractions are mixed together to create a homogeneous mix. Figure III.1 shows the dry sand fractions before and during mixing. After the sands are sufficiently mixed, water is added to

(a) Dry sand fractions

(b) Mixing of the dry sand fractions

Figure III.1: Mixing step 1: Homogenizing dry sand fractions

replicate saturated soil. Water is added gradually, until the saturation point is reached. The amount of water estimated previously is used as a reference point, but the decisive factor is the visual appearance and physical feel of the mixture. Saturation was reached after adding 12 L of water. Figure III.2 shows the saturated soil.

Last, the cement and water are added to the soil. When constructing real soil-mix walls, the cement

Figure III.2: Mixing step 2: saturating sands (replicating soil)

Figure III.3: Mixing step 3: adding cement and water

and water are added as a mixed suspension. In this case, water and cement are added to the soil in

small quantities and in an alternate order. By doing so the consistency of the mixture can be monitored throughout the mixing process. Figure III.3 shows the final mixture.

Mixture tests
The wet mixture was used for several tests to determine the density, workability and air content. These characteristics can be linked to material properties.

Density
To determine the density of the mixture a bucket was filled with eight litres of compacted soil-mix. The corresponding weight determined the density of the mixture (figure III.7).
Eight litres of the soil-mix weighed 16.250 kg, which results in a density of 2031.25 kg/m^3. Compared to the density of the Winmix samples this is relatively high, those densities averaged at 1753 kg/m^3.

Workability
The workability of a mixture is influenced by the following main factors.

- Water content
- Amount and type of cement
- Grain distribution aggregates
- Nature of the soil (shape, size, roughness of the particles etc.)

The water content of the mixture was high, which tends to lead to a more workable mix. However, the fineness modulus of the soil is very low. Which resulted in more surface area to absorb the water. Both aspects made it difficult to predict the workability before mixing.
The workability of the mixture was analysed by performing a slump test. The wet mixture was put into a cone. When the cone mould was removed, the soil-mix will deform, figure III.4. The measured slump defined the workability of the mixture. Figure III.5 shows the tool used for the test and the deformed soil-mix after the cone has been removed. The mixture shows true slump behaviour, with a slump of 20 mm (figure III.5c). This slump value corresponds with consistency level S1, which is considered as a (semi-)dry mixture.

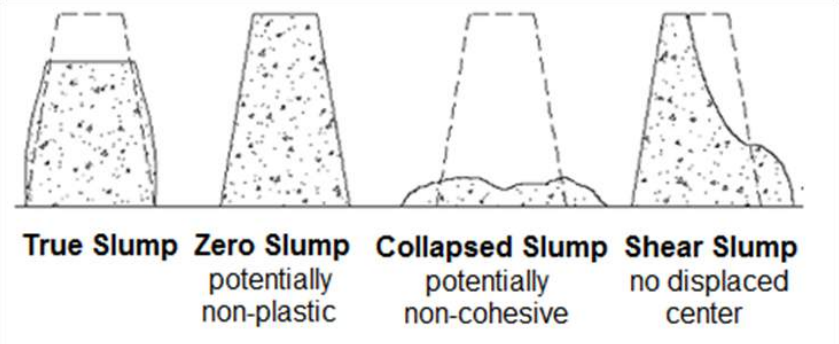

Figure III.4: Different types of deformation with slump test

(a) Slump tool

(b) Soil-mix slump

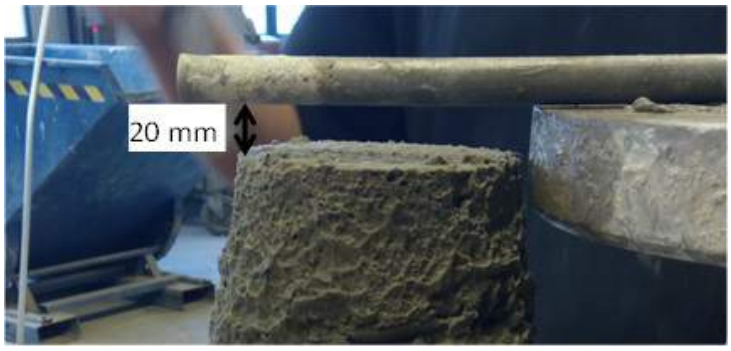

(c) Slump measurement

Figure III.5: Workability test soil-mix

Table III.2: Consistency classes (according to NEN-EN 206)

Slump class	**Slump (mm)**
S1 Dry (Kerb backing, dry fill and sloping slabs etc.)	10 – 40
S2 Standard (Foundations, Slabs and other general structures)	50 – 90
S3 Wet (Foundations, slabs, Pumping concrete)	100 – 150
S4 Very Wet (Foundations, slabs, Pumping and Piling concretes)	160 - 210
S5 Self Levelling (Foundations, slabs, Pumping and Piling concretes)	$\geq$ 220

Air content

The bucket used for determining the density of the soil-mix belongs to a tool which was also used to determine the air content of the mixture. The bucket was closed, the remaining empty volume is filled with water and finally the enclosed environment was pressurized (figure III.8). The required pressure determines the air content of the mixture as a volume percentage.

The air content of the mixture was 3%. For a mixture with small aggregates this is a low air content, even when considering the mild to moderate conditions to which soil-mix walls are exposed (figure III.6). The air content is relevant for the durability of the material, especially when it is exposed to freeze-thaw cycles.

Nominal maximum aggregate size, mm (in.)	Air content, percent*		
	Severe exposure**	Moderate exposure†	Mild exposure††
9.5 (3/8)	7-1/2	6	4-1/2
12.5 (1/2)	7	5-1/2	4
19.0 (3/4)	6	5	3-1/2
25.0 (1)	6	4-1/2	3

* Project specifications often allow the air content of the concrete to be within –1 to +2 percentage points of the table target values.
** Concrete exposed to wet-freeze-thaw conditions, deicers, or other aggressive agents.
† Concrete exposed to freezing but not continually moist, and not in contact with deicers or aggressive chemicals.
†† Concrete not exposed to freezing conditions, deicers, or aggressive agents.

Figure III.6: Recommended air content for regular concrete (Whiting and Nagi, 1998)

Figure III.7: Measuring of the density

Figure III.8: Measuring of the air content

Casting and curing

Casting of the specimens was done manually by scooping the mixture into the moulds. The specimens where compacted slightly to smooth the surface. During the actual construction process the material is not fully compacted, but is subjected to the movement of the production of the equipment and the positioning of the reinforcement. Therefore slight compaction of the lab samples is acceptable.
After casting the specimens are set to rest, until they are ready for de-moulding. De-moulding was possible after 24 hours of resting (16-05-2017). Directly after de-moulding the specimens were put in a warm and humid curing room until testing.

Figure III.9: Several casted specimens

Visual remarks

Aside from the measured test results, the visual and physical appearance of the material also provided valuable information . Whether the appearance was in line with the expectations or if there were unexpected features to the material can give insight in related properties.

The first interesting aspect was the low workability of the mixture. Even though the water content and water cement ratio were both high, the slump test resulted in the lowest workability class. So the fineness of the soil in the mixture compensated for the large volumes of water added to the mixture.

The structure of the material after removing the slump cone looked similar to the structure seen in the cores provided by Winmix BV. This was a positive result, since it implies that the lab made mixture is similar to the actual material.

The last aspect of the lab mixture was the excessive bleeding of the specimens. After slightly compacting the specimens and some resting time, all samples had water on the top surface (figure III.11).

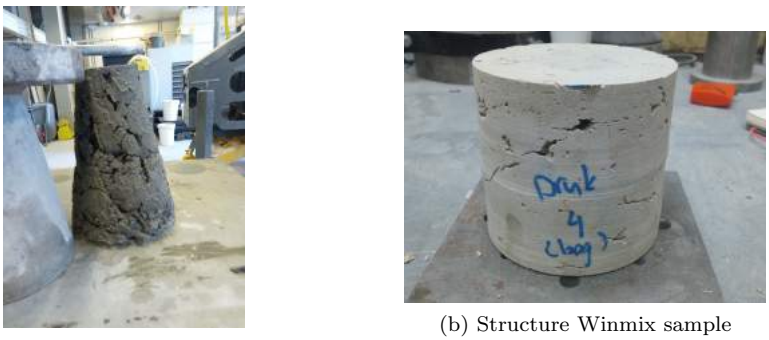

(a) Stucture lab mixture

(b) Structure Winmix sample

Figure III.10: Structure of lab mixture and Winmix core

Bleeding of the material was also seen during construction of the parking garage in The Hague. Drainage channels were dug around the mixing shafts to control the flow of excessive fluids. However, the bleeding was heavy to such extend that the channels were insufficient to transport all the liquid and the construction site was covered in soil-mix residue. Obviously the lab samples are not constructed in a similar way as on a construction site, but the fact that they show heavy bleeding supports the assumption of a representable mixture.

Interesting is that the mixture seemed to be quite dry and was very stiff when testing the workability. Thus indicating that water was well absorbed. This is contradictory with the excessive bleeding, since that usually means that the water content is too high and the water is not completely absorbed.

Figure III.11: Bleeding of a specimen after casting

IV Experimental set up: Tonibank

Figure IV.1 shows the set up used for the displacement controlled tests for the Winmix samples.

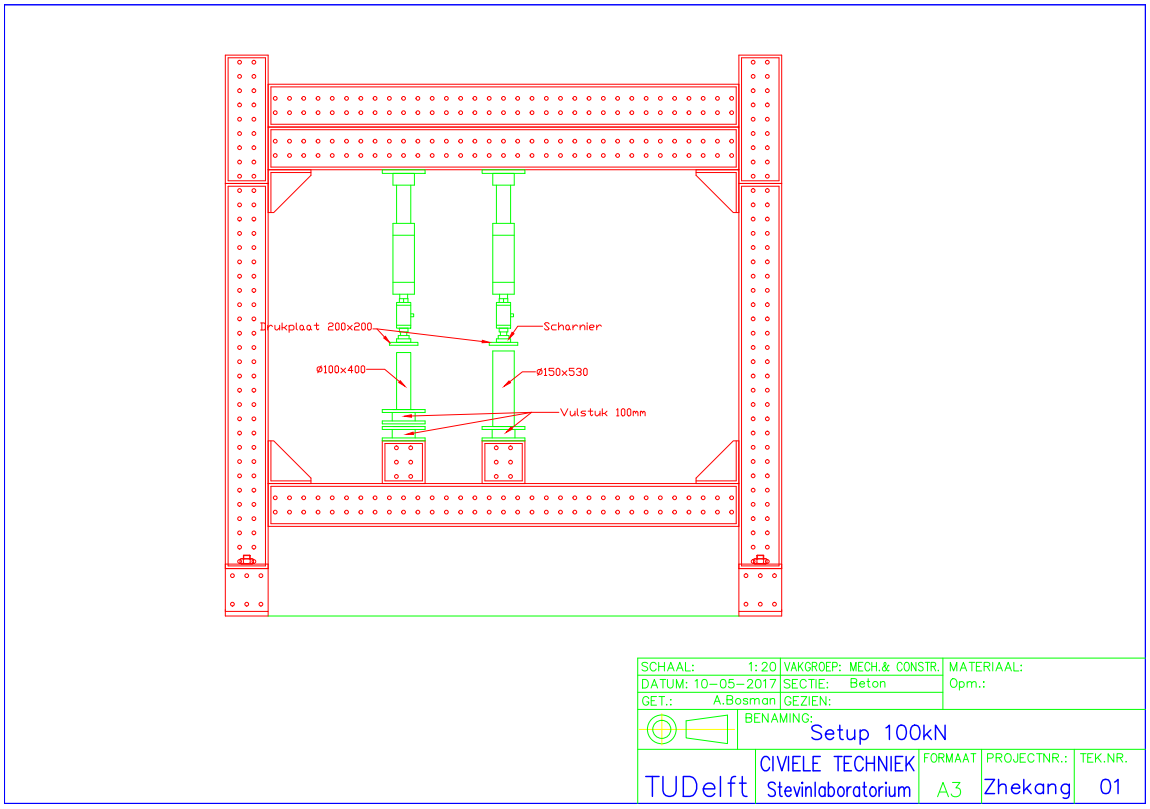

Figure IV.1: Visual representation of the experimental set up for the displacement controlled tests on the Winmix samples

V Testing results

V.1 Testing report Winmix samples

The first batch that was tested were drilled cores provided by Winmix BV. These cores were drilled from a cutter soil-mix walls realised in one of Winmix' projects. Unfortunately specifics on the project could not be shared. Which means there are no details available on the composition of the soil-mix. The information acquired from these tests could therefore not be used for relating material properties to the mixture composition.
The cores were drilled for quality control test by TNO. The samples used in this research were leftovers and have not been tested by TNO. The batch contained 13 cores of different diameters and lengths. These were sawn to adjust the dimension in such a way that they are suitable for the compression, splitting and displacement tests. Two of the samples had sufficient length to be used for the displacement controlled test. The other samples were used to create the compression and splitting specimens. For compression tests the ideal height to diameter ratio is 2, however the options are limited by the length of the available cores and the required length of the samples for the splitting tests. Based on previous research (Denies et al., 2012a) the tensile strength of the material is expected to be very low (in the order of magnitude of $0.5 - 2.0\,MPa$). Increasing the length of specimens used for these splitting tests will consequently increase the loading capacity and thus delay the moment of failure. Since the expected tensile capacity of the material has a wide range of low strengths this is valuable, because it decreases the risk of instant failure. The preferred length of the splitting samples is chosen to be 200 mm. This leaves a save margin for extremely weak spots in the material. As a result $H/D = 2$ could not be realised for the compression samples, for these samples the minimum of $H/D = 1$ was used. With these boundary conditions the following samples were created (table V.1).
Figures V.1 to V.3 show the samples after testing. The results of the all tests are listed in section 3.3. In addition to these values figure V.4 shows the stress-strain relation measurements from all LVDT's attached to the specimens.

Table V.1: Dimensions of specimens sawn from the cores provided by Winmix BV

Compression samples			
Sample	$\phi\,[mm]$	$h\,[mm]$	$mass\,[g]$
1	94	100	1064
2	93	98	1048
3	94	100	1048
4	104	100	1443
5	104	97	1621
6	104	100	1665

Splitting samples			
Sample	$\phi\,[mm]$	$h\,[mm]$	$mass\,[g]$
1	93	246	2762
2	104	200	3213
3	104	168	2675
4	104	200	3297
5	94	178	2009
6	104	200	2988
7	104	150	2303

Displacement samples			
Sample	$\phi\,[mm]$	$h\,[mm]$	$mass\,[g]$
1	145	530	14345
2	93	400	4263

(a) Sample 2

(b) Sample 3

(c) Sample 4

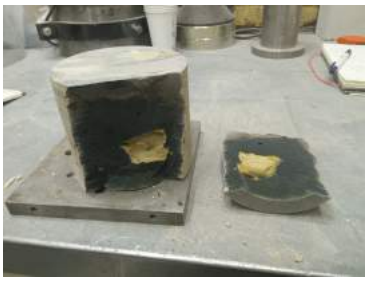

(d) Sample 5

(e) Sample 6

Figure V.1: Compression test samples after testing

(a) Sample 2

(b) Sample 3

(c) Sample 3 (sideview)

(d) Sample 4

(e) Sample 6

Figure V.2: Splitting test samples after testing

(a) Sample 1

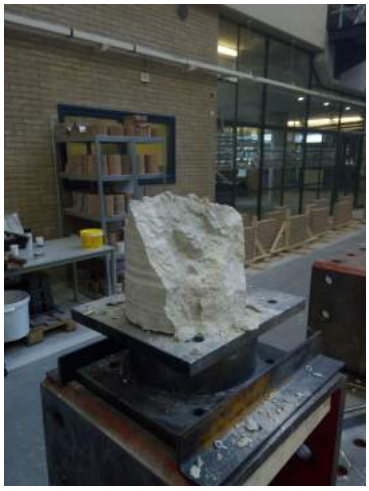

(b) Sample 1, failed

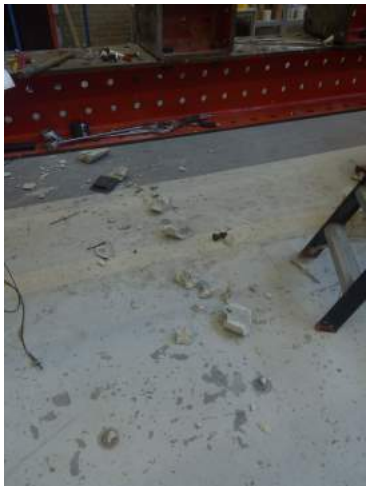

(c) Sample 1, explosive failure

(d) Sample 2

(e) Sample 2, failed

Figure V.3: Displacement test samples before and after testing

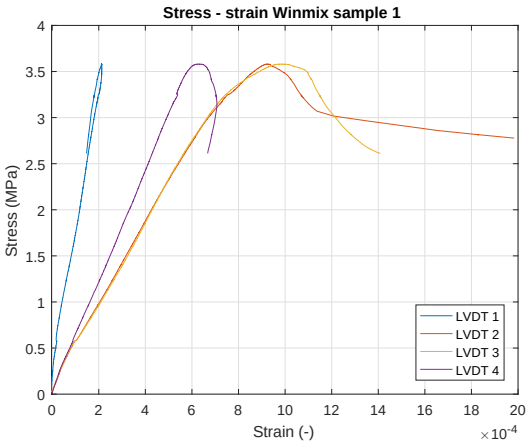

(a) Sample 1

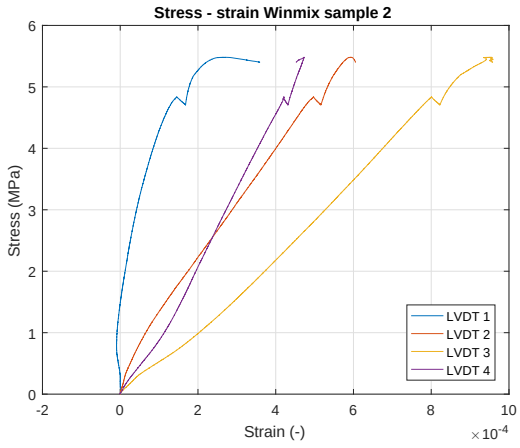

(b) Sample 2

Figure V.4: Stress-strain relation Winmix samples

V.2 Testing report 7 days

After 7 days of hardening (22-05-207) six samples were taken from the curing room to test for the tensile and compressive strength. Both the compression as the splitting test was done in threefold. The results of these tests are presented in table V.2. Figure V.5 shows one sample of each test.

(a) Compression sample 3

(b) Compression sample 3, failed

(c) Splitting sample 3

(d) Splitting sample 3, failed

Figure V.5: Selection of lab samples tested after 7 days of hardening

Table V.2: Results of tests after 7 days of hardening

7 Days tests					
Compression test					
Sample	$\boldsymbol{Mass[kg]}$	$\boldsymbol{h[mm]}$	$\boldsymbol{\rho[kg/m^3]}$	$\boldsymbol{F_{fail}[kN]}$	$\boldsymbol{\sigma_{fail}[MPa]}$
1	6,520	14,30	2026,4	65,5	2,9
2	6,700	14,50	2053,6	83,7	3,7
3	6,795	14,70	2054,4	70,9	3,2
Splitting test					
Sample	$\boldsymbol{Mass[kg]}$	$\boldsymbol{h[mm]}$	$\boldsymbol{\rho[kg/m^3]}$	$\boldsymbol{F_{fail}[kN]}$	$\boldsymbol{\sigma_{fail}[MPa]}$
1	6,650	14,45	2045,4	16,4	0,482
2	6,700	14,50	2053,6	18,6	0,544
3	6,600	14,15	2073,0	16,4	0,492

V.3 Testing report 14 days

After 14 days (29-05-2017) of hardening the same testing procedure was followed as after 7 days of hardening. Resulting in the values found below in table V.3.

(a) Compression sample 3, at maximum load

(b) Compression sample 3, failed

(c) Splitting sample 3

(d) Positioning of loading application element

Figure V.6: Selection of lab samples tested after 14 days of hardening

Table V.3: Results of tests after 14 days of hardening

14 Days tests					
Compression test					
Sample	$\boldsymbol{Mass[kg]}$	$\boldsymbol{h[mm]}$	$\boldsymbol{\rho[kg/m^3]}$	$\boldsymbol{F_{max}[kN]}$	$\boldsymbol{\sigma_{max}[MPa]}$
1	6,605	14,15	2074,6	98	4,36
2	6,675	14,50	2046,0	100,9	4,48
3	6,670	14,45	2051,5	109,6	4,87
Splitting test					
Sample	$\boldsymbol{Mass[kg]}$	$\boldsymbol{h[mm]}$	$\boldsymbol{\rho[kg/m^3]}$	$\boldsymbol{F_{max}[kN]}$	$\boldsymbol{\sigma_{max}[MPa]}$
1	6,640	14,65	2014,4	21,9	0,634
2	6,755	14,60	2056,3	11,0	0,320
3	6,730	14,75	2027,9	19,7	0,567

V.4 Testing report 28 days

After 28 days of hardening (12-06-2017) the compression and splitting tests were performed for the last time. The results are listed in table V.4. During the first compression test the measurement settings were incorrect, which lead to a test without results. Therefore there is no strength data available for the first specimen. In addition to the compression and splitting test the displacement tests were started on the same day. However the equipment malfunctioned during the first test, therefore the last 2 displacement tests were performed after an additional 10 days of hardening, on the 23-06-2017.

Table V.4: Results of tests after 28 days of hardening

28 Days tests					
Compression test					
Sample	$\boldsymbol{Mass[kg]}$	$\boldsymbol{h[mm]}$	$\boldsymbol{\rho[kg/m^3]}$	$\boldsymbol{F_{max}[kN]}$	$\boldsymbol{\sigma_{max}[MPa]}$
1	6,665	14,65	2022,0	-	-
2	6,670	14,65	2023,5	111,2	4,94
3	6,655	14,60	2025,9	140	6,22
Splitting test					
Sample	$\boldsymbol{Mass[kg]}$	$\boldsymbol{h[mm]}$	$\boldsymbol{\rho[kg/m^3]}$	$\boldsymbol{F_{max}[kN]}$	$\boldsymbol{\sigma_{max}[MPa]}$
1	6,645	14,65	2015,9	23,5	0,681
2	6,720	14,75	2024,9	22,8	0,656
3	6,660	14,60	2027,4	23,3	0,677

Displacement tests

Each of the cuboid specimens was equipped with four longitudinal LVDT's and four transversal LVDT's. Figure V.7 shows the method used to attach the LVDT's. The LVDT's were attached to the specimens using clamps which were glued to the soil-mix. High accuracy was required to ensure all LVDT's were centric aligned and suitable for the measurements. Measurements deviated too much from the others were excluded from the data used to determine the average behaviour. Figures V.8 to V.10 show all measured strains on the lab samples during the displacement controlled tests.

Figure V.7: Attaching the LVDT's

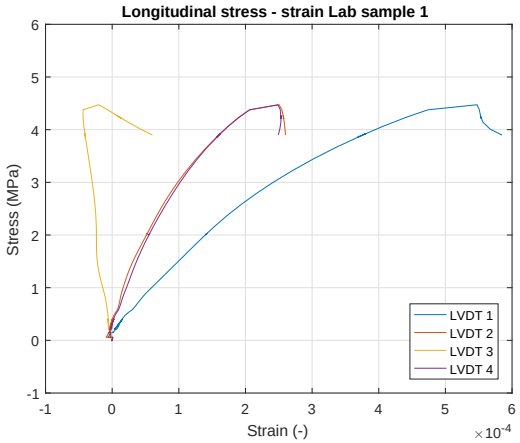

(a) Longtidunal strains

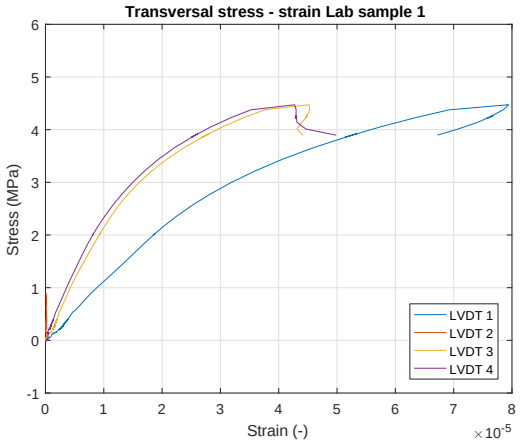

(b) Transversal strains

Figure V.8: Stress-strain relation lab sample 1

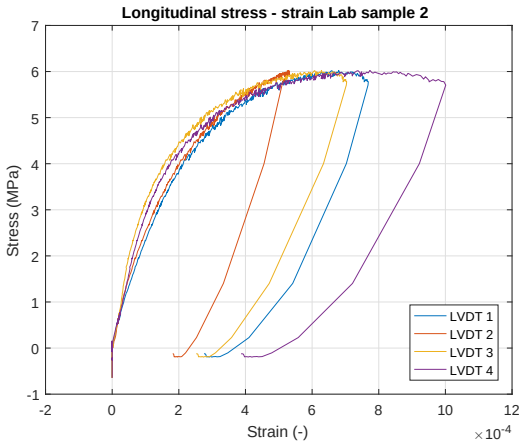

(a) Longtidunal strains

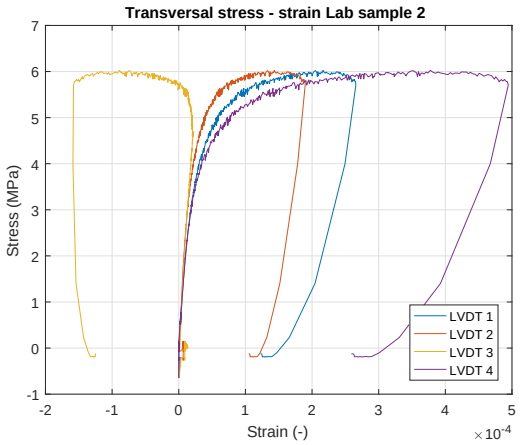

(b) Transversal strains

Figure V.9: Stress-strain relation lab sample 3

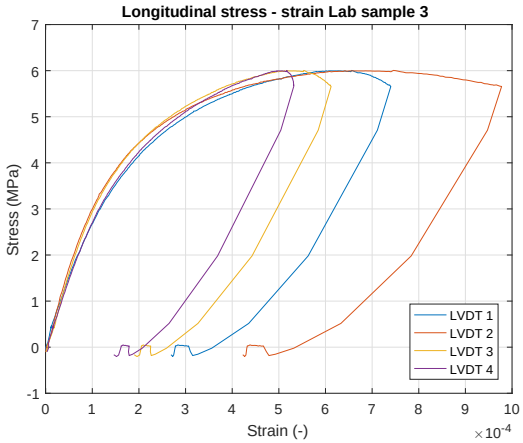

(a) Longtidunal strains

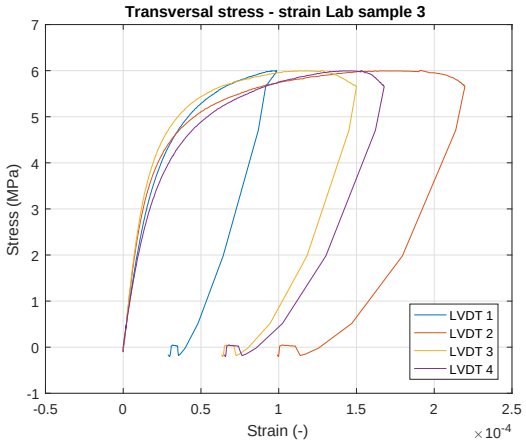

(b) Transversal strains

Figure V.10: Stress-strain relation lab sample 3

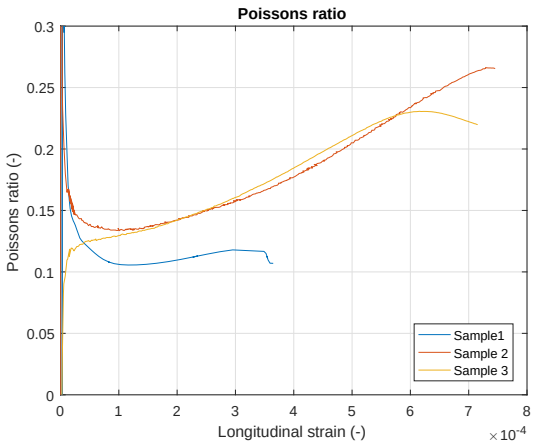

Figure V.11: Poisson ratio related to longitudinal strain

VI Initial model calibration

Thus far soil-mix material has never been modelled in a 3D finite element model (FEM) based on structural mechanics. The single FEM that has been made and used in a publication, is a 2D model built in Plaxis (Huybrechts et al., 2016). Plaxis is a software program based on geo-technical models for the analysis of soil behaviour. In this model the soil-mix was represented with soil parameters, like cohesion, the internal friction angle and the corresponding characteristics.
In Atena however, material cannot be specified with soil characteristics (Cervenka et al., 2016). Therefore it is necessary to calibrate the material parameters of the model and provide proof that the model can accurately represent the behaviour of the (reinforced) soil-mix.
The calibration process described in this appendix serves as supporting information for the final material model used in the modelling phase. The final model is complemented with data acquired from the testing phase. Another purpose of this calibration process is to get acquinted with the abilities and restrictions of the software.

VI.1 Method

The model was calibrated with the experimental results of large scale bending tests acquired by Denies et al. (2014) and Denies et al. (2015a). As an additional test of the acceptability of the model, the calibration results are compared to theoretically expected values.
The bending tests used for the calibration have been performed on soil-mix elements (dimensions 1.2m x 0.6m x 4.3m) with centric reinforcement of one steel HEA240 profile. This implies that there are three material models that influence the performance of the model being the representation of the soil-mix, the steel and the interface connection. To get independent results for the performance each of these materials, the behaviour of the soil-mix and the steel elements are analysed separately. These models are compared to the theoretical response expected for the applied load configuration.

- Analyse steel and soil-mix model separately
  - Comparison with theory
    - $\sigma = \frac{M}{W}$
    - $w = \frac{1}{48}\frac{Fl^3}{EI}$
    - $M_{cr} = f_t \cdot W$
- Analyse combined structure
  - Compare model response to experimental results
    - M, u - diagram
    - Steel stresses (force distribution steel and soil-mix)
  - Analyse influence of the interface connection
  - Compare to theoretical behaviour (combined stiffness, homogeneous material)

VI.2 Results

This section presents the calibrated results from the model. The soil-mix and steel model are discussed first, subsequently the interface is addressed. For the purpose of this research the calibration of the soil-mix material is the most relevant. The aim of this research is to analyse the possibilities of bar reinforcement in soil-mix. In contrary to regular steel, bar reinforcement is a standard element implemented in the Atena software with a corresponding simple bond-slip connection to the surrounding material. Therefore the final model with bar reinforcement does not contain a separate material definition for steel and the interface connection.

Soil-mix

The soil-mix material model was based on a model meant for rock and concrete like materials (NonLinCementious2). The behaviour of soil-mix is similar to that of a weak concrete, low tensile strength and with a brittle failure mechanism. This model is based on the following parameters.

- Elastic Modulus (MPa)
- Compressive strength (MPa)
- Tensile strength (MPa)
- Fracture energy (MN/m)
- Critical compressive displacement (m)
- Reduction f_c due to cracks (-)
- Plastic strain at compressive strength (-)
- Eccentricity of the failure surface (-)

Each of these parameters was determined by Atena based on the specified compressive strength, but can be altered manually to create the desired material characteristics.
Denies et al. (2012a) researched the main characteristics of soil-mix material created from multiple soil types. This resulted in a relation between the compressive strength with both the elastic modulus of the material ($E = 1000 f_c$) and the tensile strength ($f_t = 0.1 f_c$). These results, combined with the characteristics found by Denies et al. (2014) are the foundation for the material model of the soil-mix. The additional parameters are initially kept to the automatic values created by Atena based on the specified compressive strength.
The material model was tested by creating a displacement controlled three point bending test and monitoring the occurring stresses and the cracking load. The values resulting from the model analysis are then compared to the expected values from the theory. Figure VI.1 shows the set-up of the model. The geometry (4.3 x 1.2 x 0.6 [m]) was meshed with brick elements with a dimension of approximately 0.1 [m]. The model was loaded with a displacement of $5 \cdot 10^{-4}[m]$ every step. The loading was increased

(a) Schematic model (b) Model geometry: Atena

Figure VI.1: Model set-up for the soil-mix calibration

step by step, until the element failed. The stresses during the loading steps, as well as the failure load can be estimated with the following formulas.

$$\sigma_{max} = \frac{M}{W} \qquad [MPa] \tag{2}$$

$$w = \frac{1}{48}\frac{Fl^3}{EI} \qquad [m] \tag{3}$$

$$F_{cr} = 4 f_t W l \qquad [N] \tag{4}$$

With:

σ	Stress in the ultimate fibre [MPa]
M	Maximal bending moment [kNm]

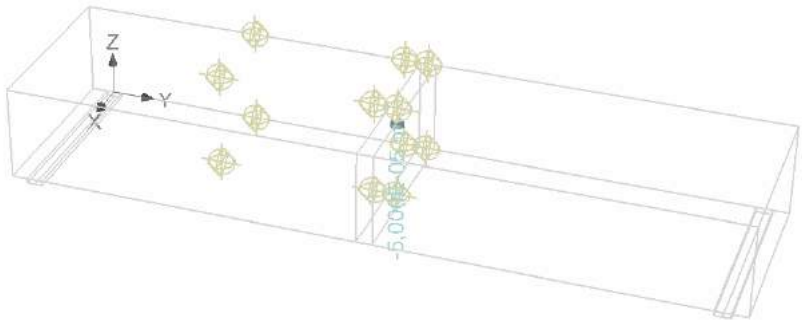

Figure VI.2: Monitoring points for σ_{yy}

W	Section modulus $[mm^3]$
w	Vertical deflection [mm]
F	Applied load [kN]
l	Span length [mm]
E	Elastic modulus [MPa]
I	Moment of inertia $[mm^4]$
F_{cr}	Crack load [kN]
f_t	Tensile strength [MPa]

To analyse whether the modelled values correspond with the theory, the model was equipped with multiple monitoring points. These monitors measure σ_{yy} at each load step. The position of the monitor points is shown in figure VI.2. When the stresses reach the tensile- or compressive strength the model should show a failure mechanism. Since the tensile strength of soil-mix is significantly lower than the compressive strength, it was inevitable that the tensile limit was reached first and the element cracked. After cracking of the element there is no tensile strength remaining, which lead to brittle failure of the entire element. The model is executed for multiple soil-mix characteristics, to get a valid image of the performance of the model related to theoretical behaviour of the soil-mix material. A detailed overview of the input parameters per material model can be found in appendix VII.

- Soil-mix Aalst (Denies et al., 2014)
  - Core characteristics
  - Average characteristics
  - Block characteristics
- Soil-mix theoretical characteristics based on f_c (Denies et al., 2012a)
  - $f_c = 2 \quad [MPa]$
  - $f_c = 5 \quad [MPa]$
  - $f_c = 10 \quad [MPa]$

Stresses in a beam subject to a three point bending test are expected to be linearly distributed along the height of the cross section. Unfortunately the model shows discontinuity in the stress distribution at midspan, where the loading is introduced in the element. This discontinuity is decreased by applying a surface load instead of a point load, but nevertheless is still noticeable. Therefore this part of the beam is not representative for the actual stress distribution within the beam and is not considered for the comparison with the theory. Instead a point just outside of the disturbed area (2 meter from the support) and point at 1 meter from the support are chosen for the comparison.
The comparison between the modelled and theoretical stresses are shown in figure VI.3 and VI.4. These figures show that the modelled stresses are within a close range of the theoretical values. To support the graphs table VI.1 provides numerical evidence of the validity of the model. The table provides a

comparison between the theoretical values of the displacement, applied force and the maximum stress[2] when the first crack appears to the modelled values corresponding to the first crack.
Note that the capacity (F_{cr}) seems to be higher than the theoretical capacity of the beam. This can be explained by considering the fracture energy, energy required to open a unit area of a crack. This implies that when the first crack occurs, the stress is redistributed within the cross section, creating a more plastic behaviour and thus increasing the capacity of the element.

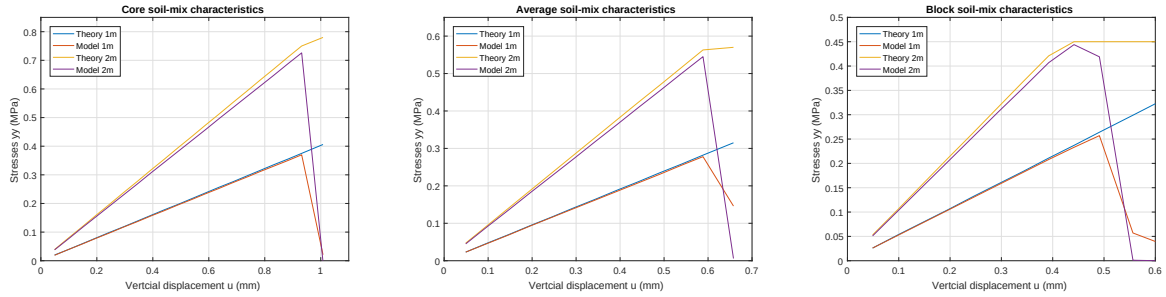

Figure VI.3: Theoretical stresses (expected for the load on the model by the given displacement) compared to the model results of soil-mix with characteristics from Denies et al. (2014).

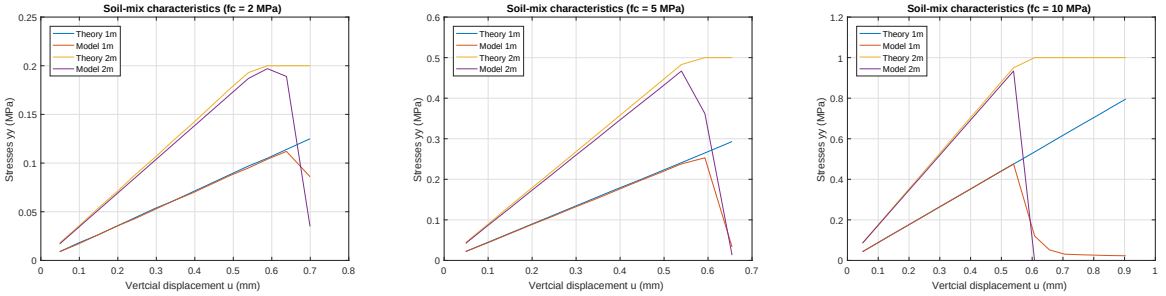

Figure VI.4: Theoretical stresses (expected for the load on the model by the given displacement) compared to the model results of soil-mix with characteristics from Denies et al. (2012a).

Table VI.1: Numerical comparison between theoretical and modelled values at cracking

	$w_{crack}[mm]$			$F_{cr}[kN]$			$\sigma_{cr}[kN]$		
	Theory	**Model**	**Ratio**	**Theory**	**Model**	**Ratio**	**Theory**	**Model**	**Ratio**
Core	0,89	0,93	*104%*	52,24	54,03	*103%*	0,75	0,75	*99%*
Average	0,55	0,59	*108%*	38,18	40,56	*106%*	0,56	0,56	*99%*
Block	0,39	0,44	*115%*	30,14	34,54	*115%*	0,48	0,44	*92%*
$f_c = 2MPa$	0,51	0,54	*105%*	13,40	13,90	*104%*	0,19	0,19	*99%*
$f_c = 5MPa$	0,51	0,54	*105%*	33,49	34,76	*104%*	0,48	0,48	*99%*
$f_c = 10MPa$	0,51	0,54	*105%*	66,98	68,40	*102%*	0,95	0,96	*101%*

Additional parameters

With the additional parameters left to the default values, the behaviour of the soil-mix material model is acceptable. However, it is valuable to check the influence of these additional parameters when they are varied. Several simulations with multiple combinations of the parameters showed that there is no observable influence when adjusting the additional parameters within a reasonable range (see table VI.2). Therefore in further use of the soil-mix material model in this calibration, the additional parameters will

[2]The stresses are extracted outside the disturbed area at midspan, therefore these values are slightly lower than f_t. This f_t is the regular tensile strength, since the flexural tensile strength of th material is unknown.

be left to the default values created by Atena. In a later stage these were changed to values based on the experimental results.

Table VI.2: Range additional parameters

	Range
Critical compressive displacement (m)	$1 \cdot 10^{-4} - 1 \cdot 10^{-3}$
Reduction f_c due to cracks (-)	$0.5 - 0.8$
Plastic strain at compressive strength (-)	$3 \cdot 10^{-4} - 6 \cdot 10^{-4}$
Eccentricity of the failure surface (-)	$0.52 - 1.0$

Discussion

A repetitive process was followed to find an acceptable model. When issues were encountered the model was analysed and altered to increase its accurateness. The set-up of the model was quite simple, therefore using a method of trial and error was sufficient to lead to an acceptable calibration. Aspects that were tweaked during the process are listed below.

- Force introduction
  - Displacement controlled instead of force controlled
  - Without additional loading (steel) element - to avoid additional capacity
  - Applied as surface load - for less discontinuity in the stress distribution at midspan
- Elements
  - Brick elements
  - Element size limited by computer memory (especially relevant for the steel profile) - for higher accuracy

The final model results do not exactly match with the values expected from a theoretical approach. The main issue is that the reaction force given by the model as a response to an applied displacement does not correspond with $\frac{1}{48}\frac{Fl^3}{EI}$. The reaction force turns out to be lower than would be expected from the applied displacement. The stresses and the moment of failure computed by the model do correspond with the reaction force on the model, but are not as expected when taken the applied displacement as origin for the calculations. This implies that there is a error within the translation of applied displacement to required force for the specified displacement.
To a certain extend a smaller mesh leads to a more accurate result. The mesh used for simulation in the calibration phase has elements of 0.1 [m]. This means that there are six elements along the height of the soil-mix element. Fewer elements means a larger error band for the results, since the values are integrated and averaged over a relative large area. Therefore it is likely that a higher accuracy can be achieved in the results when using a smaller mesh. Nevertheless results with the current mesh size are acceptable for calibration purposes.
As explained in chapter 2 soil-mix is a heterogeneous material. Not only due to varying soil qualities present in a single wall, but also due to the uncertainty of the mixture degree. Since the material is made in an uncontrolled environment (underground) chances of soft inclusions in the material are high. The calibration did not include these phenomena. When choosing a quality of soil-mix for a model, it is wise to go with the lowest quality expected to be present in the mixture and thus eliminating the risk of overestimating the strength of the structure. Accounting for extreme local weaknesses is a whole other story. To do so would require a risk analysis on the presence of such inclusions and the chances of them being at high risk locations. Vervoort et al. (2012) took a numerical approach to the risk of inclusions in soil-mix elements. The aspect of soft inclusions is not included in this research.

Steel

The steel material model was based on the 3D Bilinear steel von Mises model, which has been developed for modelling steel elements. It models a linear relation between stress and strain until the yield strength

is reached. At that point the stress stays constant (with the hardening modulus set to zero) as the strain keeps increasing, see figure VI.5a. The input required by the model are all commonly known properties of steel. For the calibration steel type S235 HEA profile, figure VI.5b, is used.

Figure VI.6 shows the calibration results, for the observed displacement and corresponding stresses.

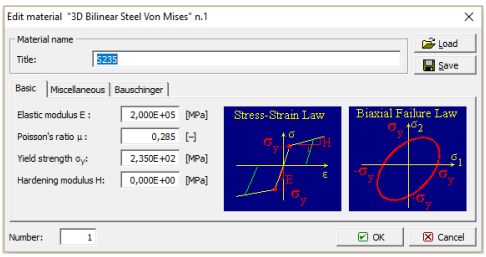

(a) 3D Bilinear steel Von Mises model Atena

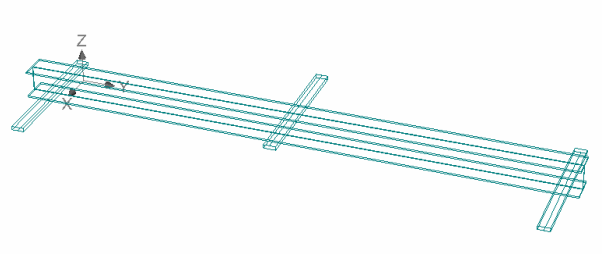

(b) Geometry steel profile

Figure VI.5: Calibration steel input parameters and geometry

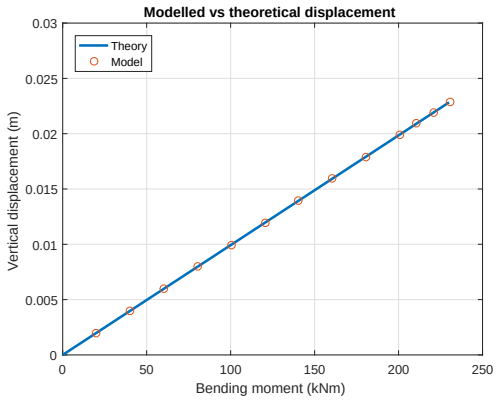

(a) Displacement

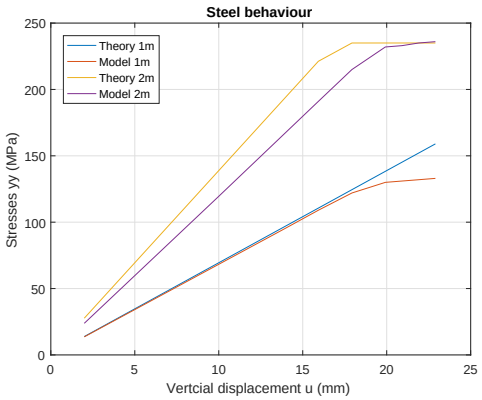

(b) Stresses

Figure VI.6: Behaviour of the modelled steel profile compared to theoretical response

The displacements exactly coincide with the response that is expected based on theoretical calculations (Figure VI.6a). Unfortunately the modelled result differ from the theoretical stress values with approximately 10% close to midspan and 2% at one meter from the support (figure VI.6b). The deviation at midspan is exceptionally large and is not acceptable. Closer to the support however, the model is more accurate. Figure VI.7 provides insight in the explanations for the large deviation around midspan. As can be seen the stress distribution along the height is not linear around midspan. There is a discontinuity in the distribution which is caused by the transfer of the locally introduced forces. Outside of the disturbed area the modelled stresses can directly be confirmed with the theoretical values.

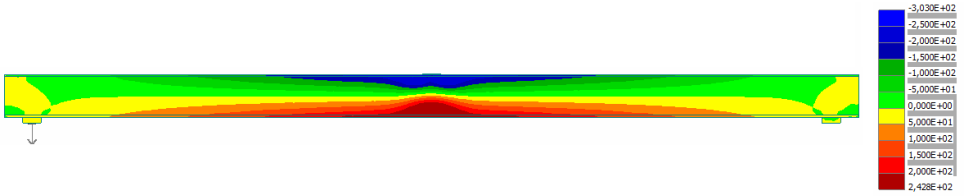

Figure VI.7: Stress distribution, $\sigma_{yy}[MPa]$

Discussion

Complications that arose with the calibration of the steel are related to the geometry of the element and the mesh used to model it. An HEA240 profile consists of three thin elements with the order of magnitude of 10 [mm] and has a height of only 240 [mm]. Initially the model was run with elements sized 100 [mm]. This resulted in stresses deviating from the theoretical values with approximately 25%. Obviously an element size which is larger than a third of the total structure height the results are inaccurate. With a reduction of the element size to 25 [mm] the calibration came to acceptable results.
However the required element size might cause some complications when calibrating the soil-mix reinforced with the steel profile. Since the capacity necessary to calculate both the steel and the soil-mix with such small elements is not available. Additionally it is not possible to use larger elements for the soil-mix than for the steel profile, because the interface connection requires similar element sizes for both adjacent materials.

Interface

The contact areas between the soil-mix and the steel have to be defined by a 3D interface model. Pull out tests done by Denies et al. (2012a) prove that there is a simple bond-slip relation which can describe the adherence between the steel and the soil-mix corresponding with the Bigay relation used in Atena, see figure VI.8a. The research also shows that there is no difference between the bond relation of smooth steel profiles or ribbed bars to the soil-mix. The only difference can be found in the capacity of the connections, figure VI.8b.

Yet the material model required for modelling the thin interface between the steel profile and the

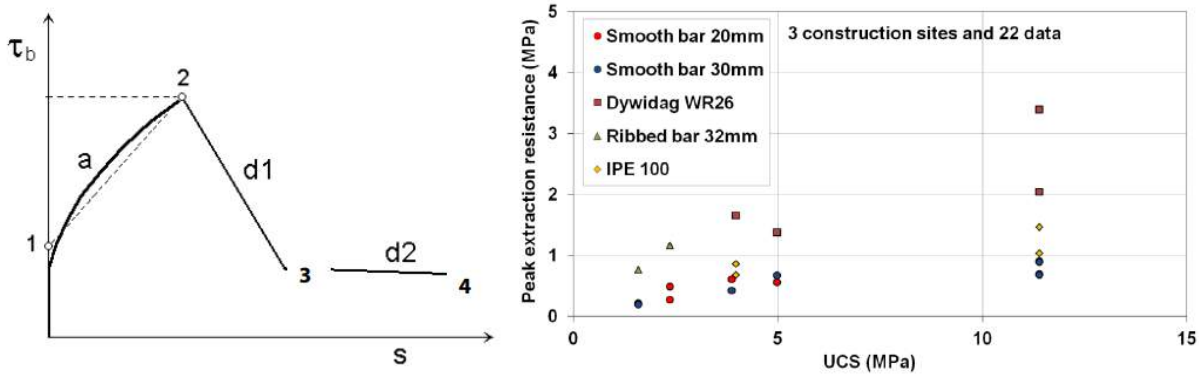

(a) Bond law by Bigay (Cervenka et al., 2016)

(b) Peak pull-out resistance of steel elements in function of the UCS of cored soil-mix material (Denies et al., 2012a)

Figure VI.8: Steel adherence in soil-mix

soil-mix is more complex than the previously mentioned bond-slip model. As can be seen in figure VI.9 the material model for the interface requires both a normal and a tangential stiffness. This is in contrary with the regular bond slip model, which only concerns the tangential behaviour and asks to specify the tensile strength, the cohesion and the friction coefficient. Theoretically the cohesion corresponds with the pull out strength found by Denies et al. (2012a). The other parameters have not been researched and are thus unknown.

Pryl and Cervanka (2016) provides a basic formula which can be used to determine the stiffness of the interface. The formula is based on the elastic modulus of the surrounding material, in this case the soil-mix.

$$K = \frac{E_{soil-mix}[MPa]}{elementsize[m]} * 10 \quad [MN/m^3] \tag{5}$$

Pryl and Cervanka (2016) advises to set the cohesion at 1-2 times the tensile strength. The friction coefficient is not discussed in the mentioned document. However the Eurocode 2 states that the friction coefficient between concrete and a smooth steel element is typically 0.15. These guidelines combined with the maximum pull-out strength (set as the cohesion) found by Denies et al. (2012a) lead to the

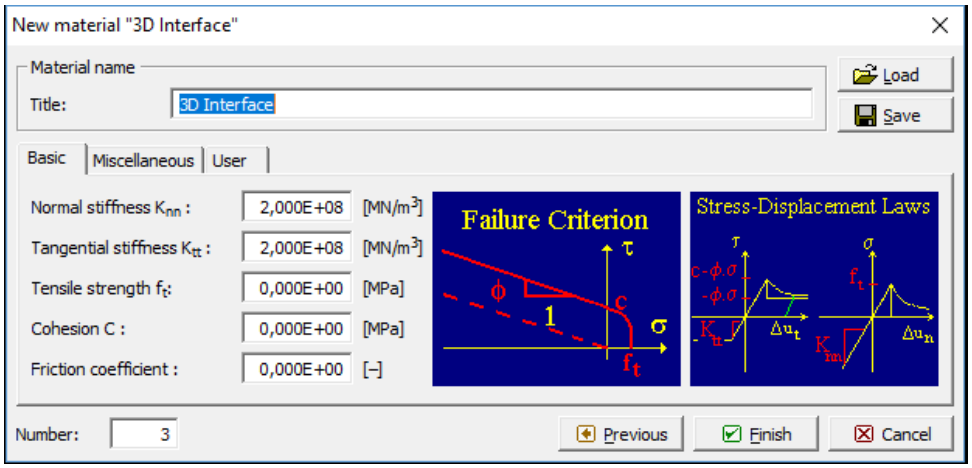

Figure VI.9: Atena model for interface material

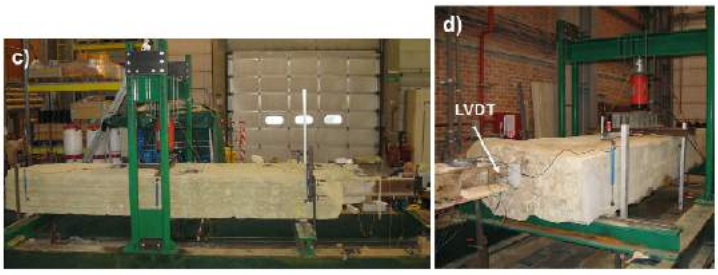

(a) Real scale test set-up (Denies et al., 2014)

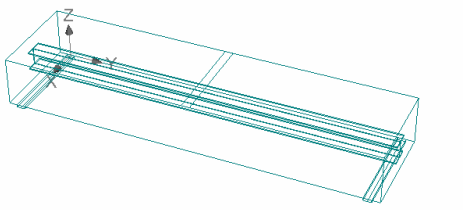

(b) Model geometry

Figure VI.10: Real scale tests, physical and modelled

most sensible parameter values for the interface material.

The geometry of the model is shown in figure VI.10b. The steel profile is embedded in the soil-mix element and the contact surfaces between the two material types have been given the specifications discussed above. The model replicates a real scale test of which the set-up can be seen in figure VI.10a. Several units were measured during the real scale testing, two of which will be used the verify the results from the model.

- Bending moment versus the vertical displacement at midspan
- Bending moment versus the maximum steel stresses at midspan

Figure VI.11 shows the result of the model compared to the real scale tests. Even though it is indisputable to state that the model results differ significantly from the values measured during the real scale tests, the outcome is quite satisfying.
Up to a load of 100 [kNm] the values found by the model for both vertical displacement and the maximum steel stresses correspond with the values measured in the tests. However at that point the model shows unexpected behaviour, more displacement and a higher level of stress at the top of the steel element. This might be caused by premature failure of the interface, which ceases the cooperation between the steel and soil-mix and thus decreases the stiffness of the element. Whenever the interface fails the stiffness is determined by the steel profile. Which explains why the displacement curve does show the correct shape, even after the discontinuity at 100 [kNm]. Unfortunately this does not apply for the stress curves. The stresses measured at the bottom of the element (tensile stresses) seem to correspond quite accurately till the model reaches the yielding strength ($f_y = \frac{235}{1.15}[MPa]$). The measured stresses in the real scale test exceed the yielding strength and keep increasing as the load increases. This could be caused by the method used for measuring these stresses. The measurements are based on strains measured by strain gauges attached to the steel profile. It seems like these strains are linearly transformed to

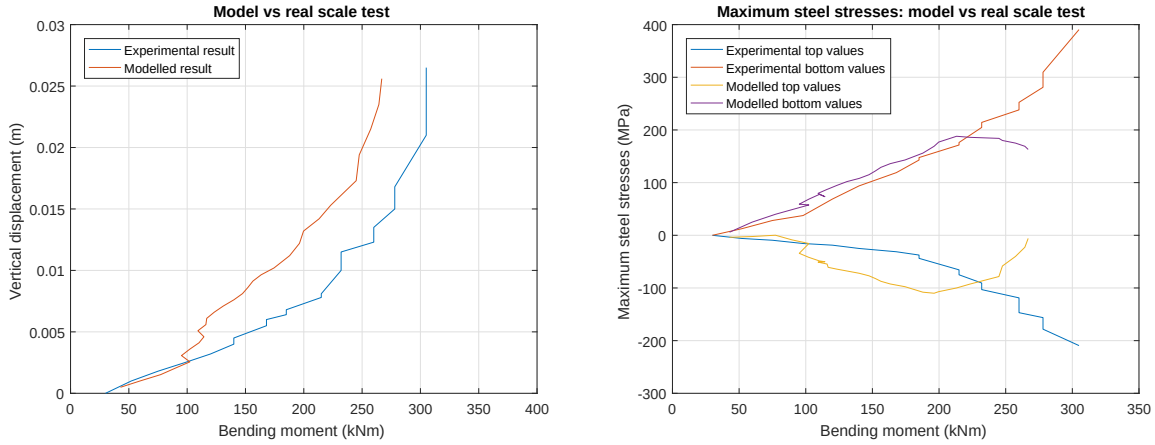

(a) Moment - displacement

(b) Moment - maximum steel stresses

Figure VI.11: Calibration results profile reinforced soil-mix element

stresses, without considering the yielding behaviour of steel. The model does show yielding as would be expected from a steel material model. The stress measured at the top of the steel element (compressive stresses) during the testing follows a concave curve, whereas the modelled stresses form a convex curve. At the end of the loading cycle the contribution of stresses in the steel is significantly less than measured during the experiment. Which implies that the compressive capacity of the modelled soil-mix material is larger than the actual capacity. For more insight in this difference, it is interesting to analyse the compressive behaviour of the soil-mix material by performing a simulation of a uni-axial compression test.

Discussion

The behaviour of the profile reinforced structure is not entirely as desired, but shows a similar displacement response and an explicable distribution of stresses between the two materials. The result can be optimized by slightly altering the parameters of the interface material till a more satisfying result is found. Considering the goal of this research, modelling bar reinforced soil-mix walls, the interface material is no longer required for the research aside from the calibration phase. Therefore the calibration of the interface material is accepted nor declined. After comparing the experimental results and the modelled results for the reinforced soil-mix element, it became evident that the compressive behaviour of the soil-mix in the tests does not coincide. Therefore the compressive behaviour of the soil-mix requires a more detailed analysis.

VI.3 Conclusion

The calibration process focussed on three different elements.
Each element posed its own complications during the process. The calibration of the soil-mix dealt with multiple properties of the material and focused on the influence of additional parameters that had not yet been defined by previous research. Additionally the geometry used for the application of the force lead to some unexpected issues. It can be concluded from the calibration that the most accurate results are acquired when the soil-mix parameters are derived from the compressive strength, according to Denies et al. (2012a), since those qualities give the most precise and constant results.

The calibration of the steel element was complicated by the slender geometry of the profile, which required very small elements to get acceptable results. Similar to the calibration of the soil-mix, the force introduction was an issue as well due to the discontinuities in stress distribution it caused.

The interface was the most complex element to calibrate. It required multiple parameters that were not readily available. Extensive knowledge on the theory behind the model was necessary to successfully define these parameters. Eventually the modelled reinforced structure gave results with a similar

behaviour to that of the real scale tests (Denies et al., 2014), but with a margin on the capacity and force distribution.

VII Soil-mix properties

For the final calibration series of the soil mix material six different material qualities where used. For more detail on the material model, this appendix gives an overview of the material parameters used for each quality.

- Soil-mix Aalst (Denies et al., 2014)
  - Core characteristics
  - Average characteristics
  - Block characteristics
- Soil-mix theoretical characteristics based on f_c (Denies et al., 2012a)
  - $f_c = 2 \quad [MPa]$
  - $f_c = 5 \quad [MPa]$
  - $f_c = 10 \quad [MPa]$

Table VII.1: Overview of the final material parameters used for the validation of the calibrated material model

	Soil-mix Aalst (Denies et al., 2014)			**Compressive strength based (Denies et al., 2012a)**		
	Core	Average	Block	$f_c = 2$ [MPa]	$f_c = 5$ [MPa]	$f_c = 10$ [MPa]
Material type	*CC3DNonLinCementious2*					
Elastic modulus $E[MPa]$	$4{,}500{\cdot}10^{3}$	$5{,}350{\cdot}10^{3}$	$6{,}000{\cdot}10^{3}$	$2{,}000{\cdot}10^{3}$	$5{,}000{\cdot}10^{3}$	$1{,}000{\cdot}10^{4}$
Poissons ratio $\mu[-]$	0,350	0,350	0,350	0,350	0,350	0,350
Tensile strength $f_t[MPa]$	0,780	0,570	0,450	0,200	0,500	1,000
Compressive strength $f_c[MPa]$	-7,800	-5,700	-4,500	-2,000	-5,000	-10,000
Specific fracture energy $G_f[MN/m]$	$2{,}360{\cdot}10^{-5}$	$1{,}915{\cdot}10^{-5}$	$1{,}635{\cdot}10^{-5}$	$9{,}524{\cdot}10^{-6}$	$1{,}754{\cdot}10^{-5}$	$2{,}785{\cdot}10^{-5}$
Critical compressive displacement $w_d[m]$	$-5{,}000{\cdot}10^{-4}$	$-5{,}000{\cdot}10^{-4}$	$-5{,}000{\cdot}10^{-4}$	$-5{,}000{\cdot}10^{-4}$	$-5{,}000{\cdot}10^{-4}$	$-5{,}000{\cdot}10^{-4}$
Plastic strain at compressive strength $\epsilon_{cp}[-]$	$-4{,}035{\cdot}10^{-4}$	$-3{,}433{\cdot}10^{-4}$	$-3{,}041{\cdot}10^{-4}$	$-2{,}014{\cdot}10^{-4}$	$-3{,}209{\cdot}10^{-4}$	$-4{,}599{\cdot}10^{-4}$
Reduction of f_c due to cracks $r_{c,lim}[-]$	0,8	0,8	0,8	0,8	0,8	0,8
Crack shear stiffness factor $S_f[-]$	20	20	20	20	20	20
Aggregate size $[m]$	0,020	0,020	0,020	0,020	0,020	0,020
Failure surface eccentricity [-]	1,000	1,000	1,000	1,000	1,000	1,000
Multiplier for plastic flow direction β [-]	0,000	0,000	0,000	0,000	0,000	0,000
Specific weight $\rho[MN/m^3]$	$1{,}850{\cdot}10^{-2}$	$1{,}850{\cdot}10^{-2}$	$1{,}850{\cdot}10^{-2}$	$1{,}850{\cdot}10^{-2}$	$1{,}850{\cdot}10^{-2}$	$1{,}850{\cdot}10^{-2}$
Coefficient for thermal expansion $\alpha[1/K]$	$1{,}200{\cdot}10^{-5}$	$1{,}200{\cdot}10^{-5}$	$1{,}200{\cdot}10^{-5}$	$1{,}200{\cdot}10^{-5}$	$1{,}200{\cdot}10^{-5}$	$1{,}200{\cdot}10^{-5}$
Fixed crack model coefficient [-]	1,000	1,000	1,000	1,000	1,000	1,000

VIII MatrixFrame

MatrixFrame is a software model which is used for structural calculations of simplified structures. It is able to perform calculations on beams, 2D and 3D frameworks, floors and walls. With geometry, supports, loads and material properties as input the program returns the resulting bending moments, normal and shear forces in the separate elements.
This research used MatrixFrame to get an indication of the force distribution with a CSM wall. This was done by creating multiple frameworks which could resemble the tensile reinforcement bars and compression zones in the wall. The best option had no tension in the element representing the soil-mix zones. Tension in the elements representing soil-mxi material is unrealistic, since the tensile strength of the material is low. This configuration is presented in chapter 4. Other configuration which have been tried are presented in figure VIII.1.

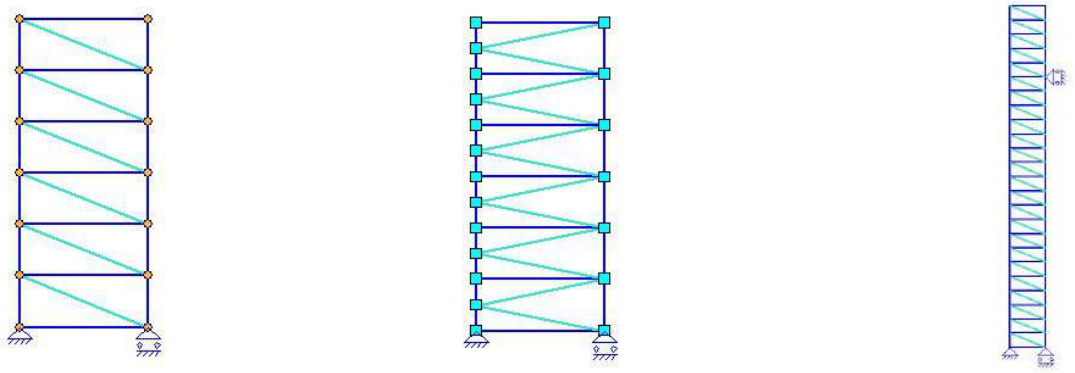

Figure VIII.1: Unfavourable MatrixFrame configurations

IX Trigonometry simplification

The following code was used to determine the ratio between the compressive forces and the tensile force found in the simplified strut and tie model of 2D section BB', which has been introduced in section 4.3.
For section BB'

```
% Script to determine tensile force in the simplified strut and tie model
% Resulting rt is the value of the tensile force relative to the concentrated
% applied compression forces at the nodes of the compressive rods.

l=245; %horizontal distance from edge section to reinforcement
spacing=linspace(50,250,3);
s=spacing;
 for i=1:3
     if s(i)==50;
        beta(i)=5; %orientation of the applied load
     elseif s(i)==150;
         beta(i) = 15;
     else
         beta(i)=25;
     end

h(i)=s(i)-s(i)/4-5;
h1(i)=2*l/3*tand(beta(i));
h2(i)=h(i)-h1(i);
beta2(i)=atand(h2(i)/(l/3));
alpha(i)=beta2(i)-beta(i);

rt(i)=tand(alpha(i)); %ft=rt*fc
rt
 end
```

X 3D failure plane

Figure X.1 gives a rough visual representation of the failure plane in the 3D model.

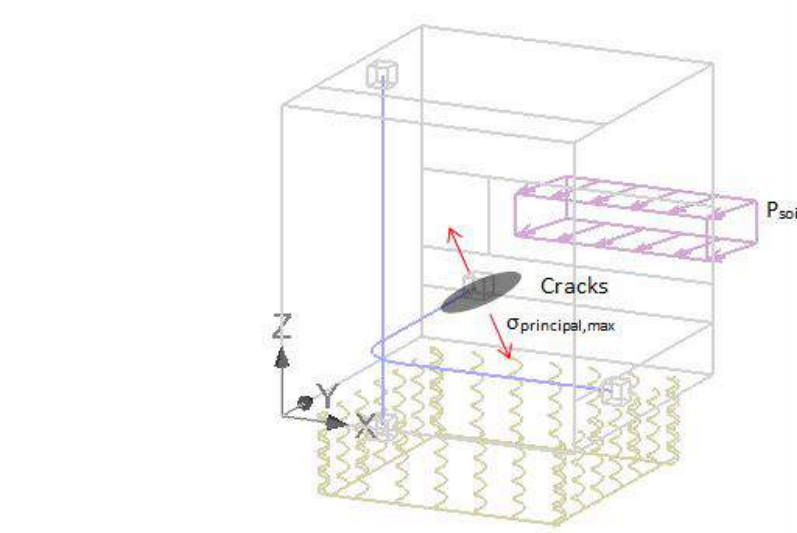

(a) 3D perspective

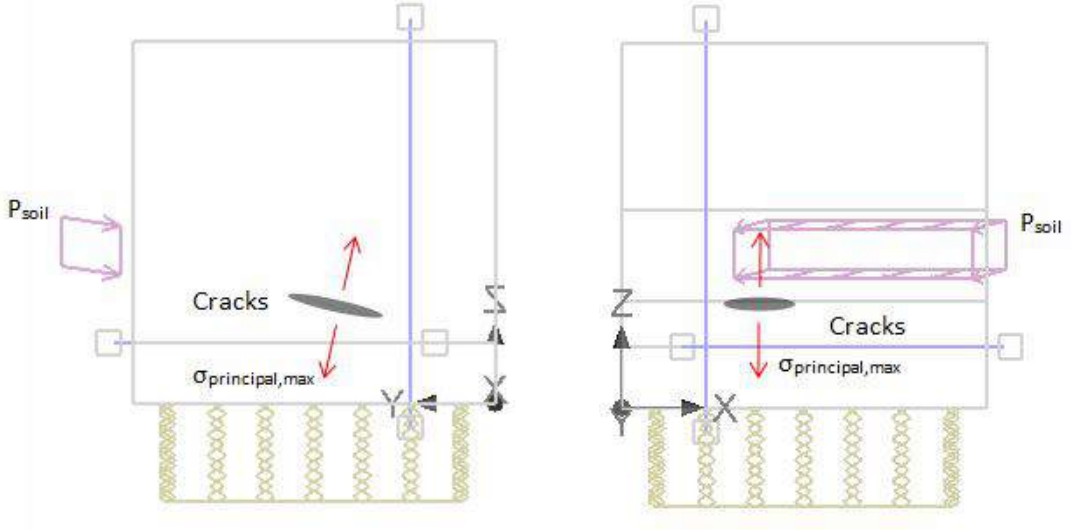

(b) YZ-plane perspective

(c) XZ-plane perspective

Figure X.1: Visualization of the 3D failure plane in the 3D model

XI Maximum depths soil-mix wall

A soil-mix wall with greater depth, means higher loads on the structure and an increase of load on the detail. Since the capacity of the detail is limited, so is the allowable depth of the soil-mix wall. This was introduced in chapter 4.5. To translate the maximum capacity of a detail to a maximum depth a horizontal slice of the wall with a thickness equal to the spacing between the stirrups is considered. The maximum load on the slice is limited by the capacity of two corner details, when considering a horizontally orientated load perpendicular to the wall. These calculations were done with the results of both 2D models and the 3D model.

$$\rho g h \cdot w \cdot spacing = 2F_H$$
$$p_h = F_H \cdot 2 \cdot /(w \cdot spacing)$$
$$h_{max} = p_h/\rho \cdot g$$

With:

F_H	Component of the applied load in the horizontal plane perpendicular to the wall [kN]
α	Load orientation in the horizontal plane [°]
β	Load orientation in the vertical plane [°]
p_h	Soil pressure at depth h [MPa]
w	Length of the stirrup [mm]
$spacing$	Vertical spacing between the stirrups [mm]
$\rho \cdot g$	Unit weight of soil ($20kN/m^3$)

To perform those calculations the total load on the detail is required, which is horizontally oriented and perpendicular to the wall . For section AA' this is done by summation of all the external load vectors. This summation is then multiplied by $\sin\alpha$, in which α is the horizontal orientation of the load.

$$F_{H,AA'} = \sin\alpha \cdot \Sigma F_{applied}$$

For section BB' this is slightly more complicated, since the section only represents a thin slice out of the detail and the vertically oriented forces are present over a wider area, the effective width. The effective width represents the area at where the stresses are concentrated around the reinforcement. Therefore a accumulation of all external load vectors is insufficient and a multiplication with $\cos\beta$ (in which β is the vertical orientation of the load). The total force has to be multiplied by a factor related to the effective width.

$$F_{H,BB'} = \cos\beta \cdot \Sigma F_{applied} \cdot \frac{w_{eff}}{t_{BB'}}$$

The effective width is smaller when the stirrup reinforcement has a smaller radius. The effective width has been determined based on the stress distribution from the models of section AA'. Figure XI.1 shows a sketch of the concept behind the effective width. Table XI.1 provides the final effective widths for each radius.

Table XI.2a shows the depths limitations based on the 2D models related to all parameters relevant to the reinforcement design. These results were used to determine the most relevant 3D models and later on the design guidelines. To determine the total force on the 3D model the orientation in both the

Table XI.1: Effective widths for section BB' based on radius sizes

Effective width [mm]	
2ϕ	2.16
5ϕ	5.40
7ϕ	8.64
10ϕ	12.96

horizontal and the vertical plane had to be considered. This resulted in the following formula:

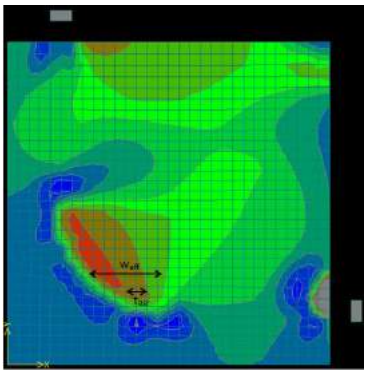

Figure XI.1: Visualization effective width section BB'

$$F_H = \sin\alpha \cos\beta \cdot \Sigma F_{applied}$$

The resulting depth limitation are presented in table XI.2b.

Table XI.2: Depth limitations based on modelled results

(a) 2D models of section AA' and BB'

Section AA'											
Model specifications		*Critical loads*		*Spacing [mm]*	250	150	50		250	150	50
Radius	**Load orientation**	F_{cr} [kN]	F_{fail} [kN]	σ_{crack} [MPa]	h_{crack} [m]	h_{crack} [m]	h_{crack} [m]	σ_{fail} [MPa]	h_{fail} [m]	h_{fail} [m]	h_{fail} [m]
2ϕ	60°	23,8	35,7	1,65	8,7	14,4	43,3	2,47	13,0	21,6	64,9
	70°	19,4	39,5	1,46	7,1	11,8	35,3	2,97	14,4	23,9	71,8
	80°	16,6	41,9	1,31	6,0	10,1	30,2	3,30	15,2	25,4	76,2
5ϕ	60°	40,1	58,5	2,78	14,6	24,3	72,9	4,05	21,3	35,5	106,4
	70°	32,4	53	2,44	11,8	19,6	58,9	3,98	19,3	32,1	96,4
	80°	30,3	54,6	2,39	11,0	18,4	55,1	4,30	19,9	33,1	99,3
7ϕ	60°	No diagonal cracks	54,5	No diagonal cracks				3,78	19,8	33,0	99,1
	70°		55,5					4,17	20,2	33,6	100,9
	80°		55,7					4,39	20,3	33,8	101,3
10ϕ	60°		59,7					4,14	21,7	36,2	108,5
	70°		55,6					4,18	20,2	33,7	101,1
	80°		57,3					4,51	20,8	34,7	104,2

Section BB'										
	Radius		2ϕ		5ϕ		7ϕ		10ϕ	
Spacing [mm]	$F_{max,BB'}$ [kN]	$\sigma_{h,max}$ [MPa]	F_{max} [kN]	h_{max} [m]	F_{max} [kN]	h_{max} [m]	F_{max} [kN]	h_{max} [m]	F_{max} [kN]	h_{max} [m]
50	4,6	9,16	4,9	9,0	12,4	22,5	19,8	36,0	29,7	54,0
150	6,6	6,38	10,3	6,3	25,8	15,6	41,3	25,0	62,0	37,6
250	5,5	1,99	5,4	2,0	13,5	4,9	21,5	7,8	32,3	11,7

(b) 3D model

Radius	**2ϕ**			**5ϕ**			**7ϕ**			**10ϕ**		
Spacing [mm]	**50**	**150**	**250**	**50**	**150**	**250**	**50**	**150**	**250**	**50**	**150**	**250**
$F_{in}[kN]$	32,3	38,8	32,2	41,4	47,4	44,0	53,7	55,4	44,0	37,4	43,1	44,0
$F_{cr}[kN]$	50,0	58,6	44,0	58,6	70,7	52,0	74,4	71,5	55,8	73,3	63,8	47,0
$F_{fail}[kN]$	77,3	89,7	64,6	80,5	86,0	76,3	83,6	89,7	82,6	73,3	88,9	69,9
$h_{max}[m]$	**51**	**20**	**9**	**65**	**24**	**13**	**84**	**28**	**13**	**59**	**22**	**13**